秋田県立大学大学院博士学位論文

Construction and Performance Investigation of Conductive Polymer-Based Flexible Supercapacitor

（導電性高分子によるフレキシブルスーパーキャパシタの創製と性能評価）

劉　啓凡

2022年 3月

Abstract

Electronic devices are developing in the direction of thinness, flexibility, and wearability. To realize the requirements of visualization products such as flexibility, slimness, and lightness, and portability, their energy supply components also need to be flexible and high-performance. Therefore, flexible energy storage devices, which are energy supply systems for flexible electronic products, have emerged. As an important member of flexible energy storage devices, flexible supercapacitors are gradually showing their potential market value due to their excellent electrochemical performance and much higher safety than traditional energy storage devices. However, flexible supercapacitors still have problems such as low energy density, poor mechanical stability, and specific capacitance attenuation under high deformation. The essential to solving these problems is to avoid delamination of the flexible substrate with the electroactive material under high deformation and to balance mechanical durability and electrochemical properties. In this thesis, from the perspective of flexible electrode structure design, flexible electrodes with excellent electrochemical properties are obtained by utilizing or preparing a variety of flexible substrates with high electrical conductivity and growing on the surface of the flexible substrates or filling the inside with electroactive materials to prepare flexible supercapacitors with excellent electrochemical and mechanical properties. The main contents and conclusions of the paper are as follows:

(1) In chapter 3, a flexible supercapacitor was designed and fabricated using a two-step polymerization method based on fiberglass cloth and the unique morphology of polypyrrole (PPy). In this extraordinary nanostructure, not only do PPy tentacles provide high-speed channels for the transfer of electrons and ions, but they also create a larger specific surface area, thus enhancing energy storage. The fabricated PPy/CFC supercapacitor possesses an excellent area-specific capacitance of 549.6 mF cm^{-2} and a remarkable energy density of 48.85 μWh cm^{-2}. Besides, it achieves the high capacitance retention of 92.4% after 10 000 charge and discharge cycles and 96.08% after 1000 bending cycles. Furthermore, it is demonstrated that the PPy/CFC supercapacitor is capable of ensuring a stable power supply for practical applications by driving an LCD

electronic watch. The fiberglass cloth-based supercapacitors with PPy tentacles provide a new approach to the practical applications of wearable power supplies.

(2) In chapter 4, a lightweight and compressible all-in-one flexible supercapacitor that can easily extend voltage window was fabricated based on melamine foam (MF) and PPy by the one-step polymerization method. The MF serves as the substrate for depositing PPy and the separator to avoid a short circuit. In addition, the MF can sufficiently absorb and lock in the electrolyte to make the electroactive material fully contact the electrolyte. This device exhibits superior electrochemical performance with a volumetric specific capacitance of 2.86 F cm^{-3} and a volumetric energy density of 0.18 mWh cm^{-3}, outstanding mechanical stability which can work stably under different compressive strains. With the novel design, the output voltage of this device can be adjusted handily by a simple cutting method without connecting several supercapacitors in series. This novel strategy may potentially guide the development of all-in-one supercapacitors for portable and wearable electronics.

(3) In chapter 5, a hybrid polyvinyl alcohol/poly(3,4-ethylenedioxythiophene): polystyrene sulfonate (PVA/PEDOT:PSS) hydrogel electrode with 3D interpenetrated network structure is prepared by the freeze-thaw crosslinking and solution immersion method. Due to the strong intermolecular force between PVA and PEDOT:PSS, coupling with the use of liquid phase mixing, this hybrid hydrogel electrode shows uniform interconnectivity and robust mechanical properties. The all-gel-state flexible supercapacitor based on the PVA/PEDOT:PSS hydrogel is fabricated to demonstrate its excellent mechanical durability of which capacitance retention retains 98.1% after 1000 bending cycles as well as excellent electrochemical performance whose areal specific capacitance is 128.9 mF cm^{-2} and energy density is up to 11.46 μWh cm^{-2}. Moreover, it can continuously power the LCD watch in bending, compression, and low-temperature environments. The outstanding comprehensive performance of this supercapacitor indicates that it has the potential to be used in a new generation of flexible energy storage devices.

(4) In chapter 6, an all-gel-state integrated asymmetric flexible supercapacitor based on poly(3,4-ethylenedioxythiophene): polystyrene sulfonate (PEDOT:PSS) and polypyrrole (PPy) composite hydrogel electrodes with an interchangeable positive and negative electrode was fabricated. The device has robust flexibility and mechanical durability, with an elongation at break of 286% at a tensile strength of 22.3 MPa and a

capacitance retention rate of 98% after 1000 bending cycles, as well as fascinating electrochemical properties, with an energy density of 397.99 μWh cm^{-3} and a capacitance retention rate of 88.1% for 10,000 charges/discharge cycles. Moreover, the positive and negative electrodes of this asymmetric device can be used interchangeably, and it can power the light-emitting diodes (LEDs) without distinguishing between positive and negative. This design concept will perhaps open a new trend in the design of high-energy-density flexible supercapacitors.

Contents

Chapter 1 Introduction

1.1 Background

In recent years, with the rapid development of electronic technology, more and more consumer electronic products are developing in the direction of lightness, thinness, and flexibility.[1-3] Foldable and bendable electronic products have gradually realized commercialization, such as radio frequency identification tags, wearable sensors, implantable medical devices, bracelets, watches, and even mobile phones.[4, 5] And with the booming development of these consumer electronics, the form of wearable electronic devices is becoming more diverse and humane.[4, 6] The new generation of flexible electronics is like the human body's "skin", can be a perfect fit with human tissue and organs in contact, not only to enhance the way to interact with the surrounding environment, and even create a new way of communication. This puts forward higher flexibility requirements for flexible electronic products, that is, fully flexible electronic devices. For flexible electronics, except for a very few self-powered, battery-free wearable/implantable systems, the vast majority require power systems. To achieve fully flexible electronics, their energy supply components also need to be highly flexible. However, only flexible and foldable display components and circuits have been commercialized, and thin and flexible energy storage devices that can be compatible with them remain a great challenge.[7] Flexible energy storage devices (FESDs) need to ensure a continuous and stable energy supply to electronic products under extreme conditions such as mechanical deformation and even dynamic deformation caused by external forces, and must also have high safety and stability, high power density, and energy density as well as long cycle life and other basic properties to meet the application of flexible electronics in different situations.[8]

1.2 Flexible energy storage devices

Traditional energy storage devices such as lead batteries, dry batteries, and lithium batteries are rigid, and when bent and folded, they can cause the electrode material and collector fluid to separate, affecting the electrochemical performance and even leading

to short circuits, causing serious safety problems. Currently commercialized flexible bendable, foldable screen electronic products, their energy storage devices are still rigid, which greatly limits their development. To accommodate the development of next-generation flexible electronic devices, FESDs have become one of the most popular research fields.[9, 10] FESDs currently under study mainly include flexible supercapacitors (FSCs)[11] and flexible lithium-ion batteries (FLIBs)[12] of the electrochemical energy storage type, and flexible photovoltaic cells[13] of the non-electrochemical energy storage type. Among these FESDs, photovoltaic cells can only be used in special applications because of their energy storage characteristics, which require sunlight. The FESDs that can be widely used are electrochemical energy storage devices such as FLIBs and FSCs. Since the concept of FESDs was proposed, FSCs and FLIBs have been studied for more than a decade, as shown in **Fig. 1.1**.[14] FLIBs have a high energy density, good cycling performance, and good stability, which makes them an ideal candidate for FESDs.[15, 16] Compared to FLIBs, FSCs have excellent properties such as high-power density, fast charging and discharging with high current density, and long service life, which can make up for the shortcomings of FLIBs.[17] FLIBs can only use organic electrolytes, they must be assembled in an inert gas environment, and the requirements for packaging technology are relatively high. However, FSCs using water-based electrolytes do not require an inert gas atmosphere and can be assembled in the air at a lower cost.[18] In addition, since FSCs can use water-based electrolytes, the safety level is much higher than that of FLIBs, which can only use organic electrolytes. **Table 1.1** lists the performance and basic parameters of FLIBs and FSCs.[19] As can be seen, FSCs have several advantages, and given these advantages, FSCs are expected to become the most competitive FESDs.

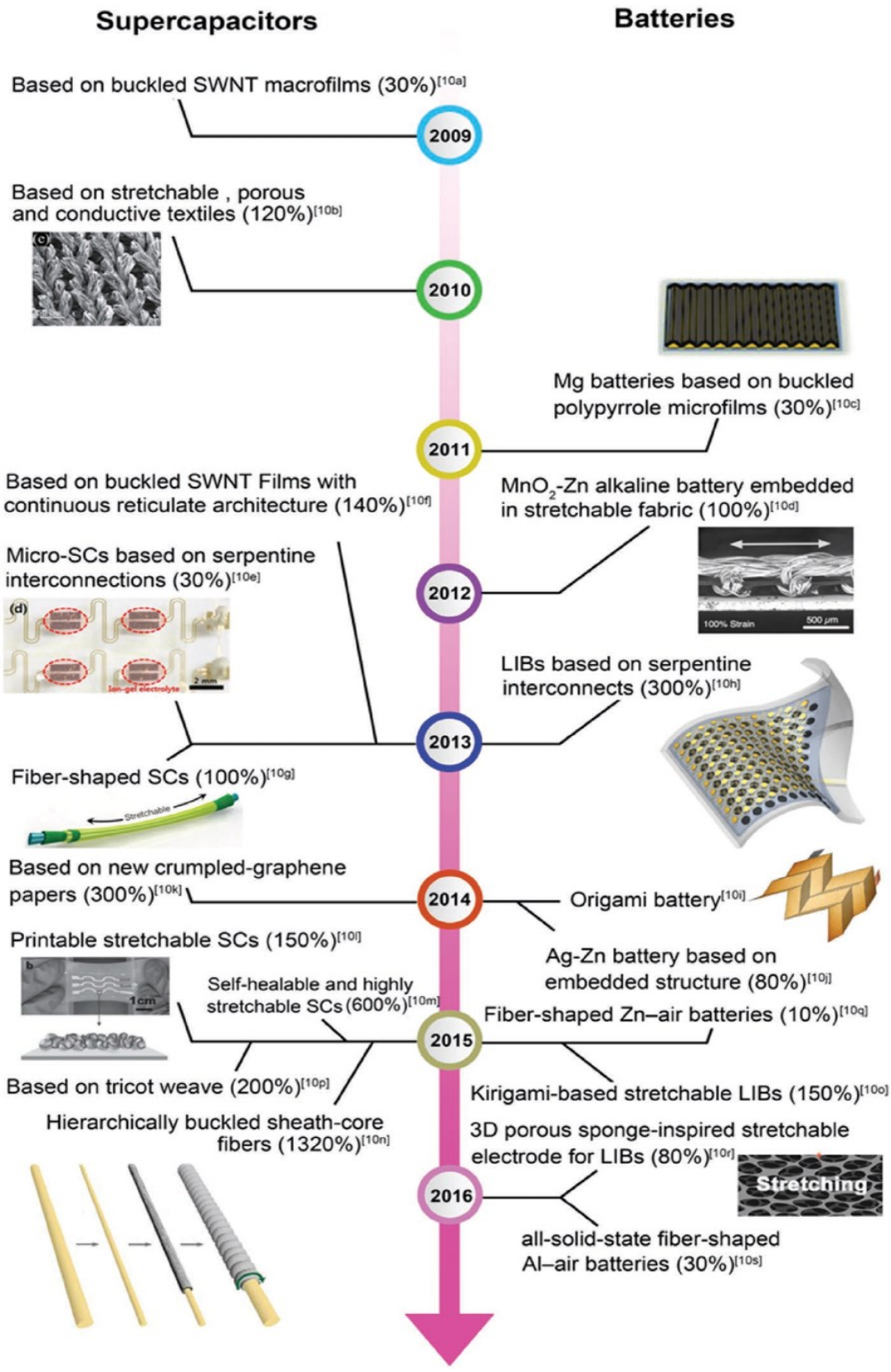

Fig. 1.1 A brief chronology of the development of flexible energy storage systems.[14]

Table 1.1 Performance comparison between supercapacitors and lithium-ion batteries.[19]

Feature	Supercapacitors	Lithium-ion batteries
Power density (W/kg)	3000~40,000	1500
Gravimetric energy (Wh/kg)	4~10	100~265
Volumetric energy (Wh/L)	4~14	220~400
Efficiency (%)	97~98	75~90
Lifetime	>10 k cycles	150 to 1500 cycles
Charge time	1~10 s	10~60 min
Risk of thermal runaway	No	Yes
Risk of explosion	No	Yes
Operating voltage (V)	0.8~1.23	1.2~4.2
Operating temperature (°C)	−40 to 85	−20 to 65

1.3 Flexible Supercapacitors

1.3.1 Structure and composition of flexible supercapacitors

FSCs is a new concept in response to the demand for energy storage devices for flexible electronic devices, as the name implies, it is a supercapacitor with flexibility. Supercapacitors, also known as electrochemical capacitors, are a new type of energy storage device between secondary batteries and conventional capacitors.[20, 21] It has the fast charge/discharge characteristics of a capacitor and the energy storage characteristics of a battery. Currently, supercapacitors are widely used in industrial instrumentation, uninterruptible power supply, hybrid and electric vehicles, rail transportation, wind power generation, grid equipment, grid energy storage, ports, and heavy machinery. It can be used as the power source for small instruments and devices, the main power source for public transportation and rail transportation, startup power source, backup power source, power compensation device, energy recovery device and voltage control device, etc. **Fig. 1.2** illustrates the structure of a typical supercapacitor. The internal structure of supercapacitor mainly consists of positive and negative electrode materials, electrolyte and diaphragm; the external structure is a bare metal

collector and a flexible soft pack or rigid aluminum case wrapped by aluminum plastic film.

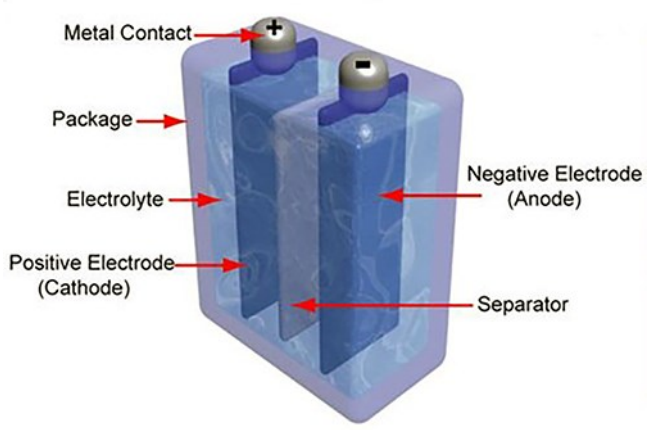

Fig. 1.2 The structure diagram of supercapacitor.[22]

Electrodes are the core components of supercapacitors and play a decisive role in the electrochemical performance of the devices. Electrodes are generally prepared by coating process by coating electroactive materials on the surface of the conductive current collector. Electroactive materials are generally solid powders such as activated carbon, carbon nanotubes, metal oxides, metal hydroxides, conductive polymers, etc. Another widely used technique is the use of vapor deposition, chemical polymerization, and electrochemical polymerization to coating the electroactive material on the collector surface, which raises the threshold of the electroactive material, but has the advantage of avoiding the influence of the binder on the electrode performance. In addition, there are integrated self-supporting electrodes that do not require a current collector, such as reduced graphene oxide film electrodes, conductive polymer hydrogel electrodes, which are both conductive current collectors and electroactive materials themselves.

The electrolyte is located between the positive and negative electrodes and its role is to provide a dielectric channel for ion/solventilized ion transport. Electrolytes are also an important factor in the electrochemical performance of supercapacitors. The wettability of the electrode in the electrolyte determines the utilization of the electroactive material and thus affects the specific capacitance of the device. Different types of electrolytes have different potential intervals, and the electrolyte affects the voltage window of the supercapacitor. According to the energy density equation of

supercapacitor $E = 1/2CU^2$, the capacitance and operating voltage of the device determine the energy density of the device. In addition, the ionic conductivity of the electrolyte largely determines the equivalent series resistance (ESR), which is one of the key factors affecting the power density of the device. The viscosity, boiling point, and freezing point of the electrolyte affect the thermal stability of the device, which in turn determines the operating temperature range of the device. Therefore, the ideal electrolyte should have a wide potential window, high ionic conductivity, high chemical and electrochemical stability, high chemical and electrochemical inertness to the device components, wide operating temperature range, good compatibility with electrode materials, low volatility, low flammability, environmental friendliness, and low cost.

The diaphragm is located in the electrolyte between the positive and negative electrodes, and the function is to avoid short-circuiting the contact between the positive and negative electrodes while allowing the electrolyte to pass ions quickly. Therefore, the diaphragm needs to have good electrochemical stability, high thermal stability, high porosity, and electrochemical inertness. In quasi-solid-state supercapacitors, there is no need for a separator because the gel electrolyte is semi-fluid and has viscosity, which effectively separates the two electrodes and acts as a separator while satisfying ion transport.

Compared with traditional supercapacitors, FSCs not only have the characteristics of traditional supercapacitors but also have good mechanical flexibility.[23] It can still work properly and ensure continuous energy output even when it is deformed by external forces. Therefore, the entire components on the FSCs must have excellent flexibility. FSCs are mainly composed of flexible electrodes, flexible encapsulation materials, separators, and electrolytes (**Fig. 1.3**), which is similar to conventional supercapacitors. To realize that FSC devices can continue to provide stable energy output under repeated bending and folding, the development of flexible components, such as electrodes, separators, electrolytes, and housings, is essential. The key to supercapacitor flexibility is to find suitable flexible electrode materials, so researchers in the field of FSCs have focused their research mainly on the preparation of high-performance flexible electrode materials.

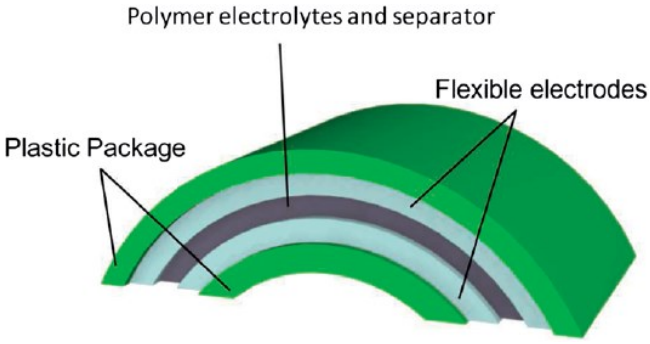

Fig. 1.3 Schematic illustration of flexible supercapacitors.[24]

1.3.2 Flexible electrode materials

Flexible electrodes can be classified structurally into two types, one is the substrate-type and the other is the self-supporting-type.[25] The substrate-type flexible electrode uses a flexible conductive substrate as the current collector to realize electronic conduction between the electroactive material and the current collector while ensuring that the electrode has sufficient mechanical strength and flexibility. Commonly used conductive substrate materials are carbon materials, metallic materials, or non-conductive elastomers with metal surface modifications.[26-28] The electroactive material is deposited on the surface of the flexible collector by hydrothermal, vapor-phase deposition, or electrodeposition.[29] The relatively strong intermolecular forces or chemical bonds between the electroactive material and the collector fluid ensure that the electroactive material does not fall off easily during the deformation of the flexible electrode. The self-supporting flexible electrode is designed and assembled so that a single material or composite material itself exhibits sufficient electrochemical and mechanical properties without the need for additional flexible substrate materials. Common self-supporting flexible electrodes are directly used as working electrodes in the form of films or fibers. Such as graphene or carbon nanotube film flexible electrodes, carbon fiber flexible electrodes, etc.[30-34]

1.3.3 Electrolyte for flexible supercapacitor

Flexible supercapacitor electrolytes can be classified into liquid electrolytes and solid/quasi-solid electrolytes. Liquid electrolytes can be categorized into aqueous

electrolytes, organic electrolytes, and ionic liquid electrolytes.[35-38] **Table 1.2** shows the comparison of the advantages and disadvantages of different systems of electrolytes. In acidic or alkaline aqueous electrolytes, the voltage of supercapacitors is limited to 1.23 V; in neutral aqueous electrolytes, the voltage of the device can be increased to 2.2 V,[39] but it is also lower than that of organic electrode liquids (2.5~2.7 V) and ionic liquids (3~6 V). Although organic and ionic liquid electrolytes have a high voltage window, the ionic conductivity of aqueous electrolytes is at least an order of magnitude higher than that of organic and ionic liquid electrolytes. The low ionic conductivity of the electrolyte results in a relatively large ESR of the device, which results in a relatively low specific capacity. According to the energy density calculation formula, the energy density of supercapacitors is proportional to the specific capacity and proportional to the square of the voltage, so increasing the operating voltage is more effective in increasing the energy density of the device than increasing the specific capacity. However, liquid organic electrolytes have disadvantages such as leakage, flammability, and toxicity, while ionic liquids also have the problem of high cost. On balance, environmentally friendly and inexpensive aqueous electrolytes are preferred. However, aqueous liquid electrolytes are more demanding for device packaging and are prone to leakage during device deformation. More and more researches have been conducted to prepare flexible supercapacitors using quasi-solid aqueous electrolytes.

Table 1.2 Comparison of the properties of electrolyte

Feature	aqueous electrolytes	organic electrolytes	ionic liquid electrolytes
Voltage window (V)	≤2.2	2.5~2.7	3~6
Ionic conductivity	High	Low	Very low
Viscosity	Low	Medium/High	High
Costs	Low	Medium/High	Very high
Assembly environment	Air	Inert gas	Inert gas
Toxicity	Low	Medium/High	Low

Solid/quasi-solid electrolytes can be classified as solid polymer electrolytes, hydrogel polymer electrolytes, and inorganic electrolytes.[40-42] The most commonly used solid electrolyte for FSCs is hydrogel polymer electrolytes.[43] Compared to the dry solid polymer electrolytes (10^{-8} to 10^{-7} S cm^{-1}), the hydrogel polymer electrolytes exhibit higher ionic conductivity at room temperature of approximately 10^{-4} to 10^{-3} S cm^{-1}.[24, 44] The hydrogel electrolyte consists mainly of the polymer network of the main body, deionized water as a solvent, and a solute to provide ions. The aqueous electrolyte is dispersed between polymers in which the ions are transported with the assistance of water, so the ionic conductivity is high compared to other solid electrolytes. The main polymers commonly used for the preparation of hydrogel electrolytes are polyacrylate (PAA), polyethylene oxide (PEO), polyvinyl alcohol (PVA), polyacrylonitrile (PAN), etc., while the solutes include acidic (e.g. H_2SO_4, H_3PO_4), neutral (e.g. Na_2SO_4, KC1, LiCl) and alkaline inorganic salts (e.g. KOH, NaOH).[45] Therefore, aqueous hydrogel electrolytes can be classified as acidic hydrogel electrolytes, salt hydrogel electrolytes, and alkaline hydrogel electrolytes. PVA is not only easy to process, easy to form films, and low in price, but also has excellent flexibility. Therefore, it is an ideal polymer host in the field of hydrogel electrolytes.[46] Currently, different types of PVA-based gel electrolytes have been developed extensively for different use environments, such as PVA/H_3PO_4 [47], PVA/H_2SO_4 [48], PVA/KOH [49], PVA/LiOH [50], PVA/Na_2SO_4 [51], PVA/KNO_3 [52], PVA/KCl [53], PVA/LiCl [54] etc. These hydrogel electrolytes have been widely used in different types of FSCs, such as carbon material-based FSCs, transition metal oxide-based FSCs, and conductive polymer-based FSCs. In addition, hydrogel electrolytes have also been shown to help improve the cycling stability of supercapacitors.[55]

1.3.4 Classification of flexible supercapacitors

The classification standards of FSCs are not very clear, and the concepts currently reported in the literature include the concepts of bendable,[56] twistable,[57] stretchable[58], and compressible.[59] Therefore, FSCs can be divided into bendable, stretchable, and compressible types according to the expression of flexibility. To satisfy the application requirements of different scenarios, devices with different geometries have been developed successively. Hence, FSCs can be classified into two-dimensional

stacked supercapacitors (sandwich structure),[60] miniature supercapacitors (coplanar forked finger electrode structure)[61] and one-dimensional wire supercapacitors[62] according to their geometries. Another broader classification is by the type of electroactive material. In the past decades, electrode materials for supercapacitors have been extensively studied, and there are three main types of electrode materials, namely carbon-based materials, transition metal oxides (MOx), and conductive polymer materials (CPs).[63, 64] Carbon-based high surface area materials such as activated carbon (AC),[65] CNTs,[66] graphene,[67] graphene oxide (GO),[68], and carbon fibers (CFs)[69] are common double-layer capacitors (EDLC) electroactive materials, while CPs (polyaniline, polypyrrole, and polythiophene) and metal oxides (RuO_2, MnO_2, V_2O_5, and Fe_2O_3, etc.)[70] are often successfully used as faraday style pseudocapacitors electroactive materials. According to this classification, flexible supercapacitors are classified as carbon-based FSCs, Transition metal oxide-based FSCs and CPs-based FSCs.

Of course, the above various classification methods have certain limitations, and with the continuous development of flexible supercapacitors, some flexible supercapacitors with composite functions have been developed. For example, flexible supercapacitors that can be stretched, bent, and compressed at the same time;[71-74] asymmetric hybrid flexible supercapacitors that combine multiple energy storage mechanisms, etc.[75-77]

1.4 Research progress of flexible supercapacitors

With the development of new technologies in the fields of wearable devices, portable consumer electronics, and electronic skin, the design and development of flexible electrochemical energy storage devices are receiving increasing attention. FSCs are considered as an ideal flexible energy storage device due to their high power density, good cycling stability, and excellent mechanical durability, and are now widely used as energy storage devices for flexible electronic products. In the past few years, researchers have invested a lot of effort to investigate different types of flexible supercapacitors to meet the market demand. Based on the energy storage mechanism, supercapacitors are classified into electrical double-layer capacitors (EDLCs), pseudocapacitors, and hybrid capacitors, whose electrode materials are all based on carbon-based materials, transition metal oxide materials, and conductive polymer

materials. Next, the current status of the development of FSCs based on various electroactive materials will be briefly introduced by way of the classification of electrode materials.

1.4.1 Carbon-based flexible supercapacitors

Activated carbon particles have rich pores and large specific surface areas, which are commonly used as electrode materials for conventional supercapacitors, but cannot be directly used in flexible supercapacitors. Commercially available carbon materials such as carbon cloth and carbon nanofiber paper not only have high electrical conductivity but also exhibit fairly good flexibility and can be used directly as electrodes in flexible supercapacitors, but their specific capacity is very low. Advanced carbon materials, such as carbon nanotube, graphene, and their composites, possess unprecedented physical/chemical properties and exhibit great potential for use in FSCs. As shown in **Fig. 1.4**, they can be prepared into different shapes of flexible electrodes, and FSCs based on these flexible electrodes show excellent electrochemical performance and good application prospects.

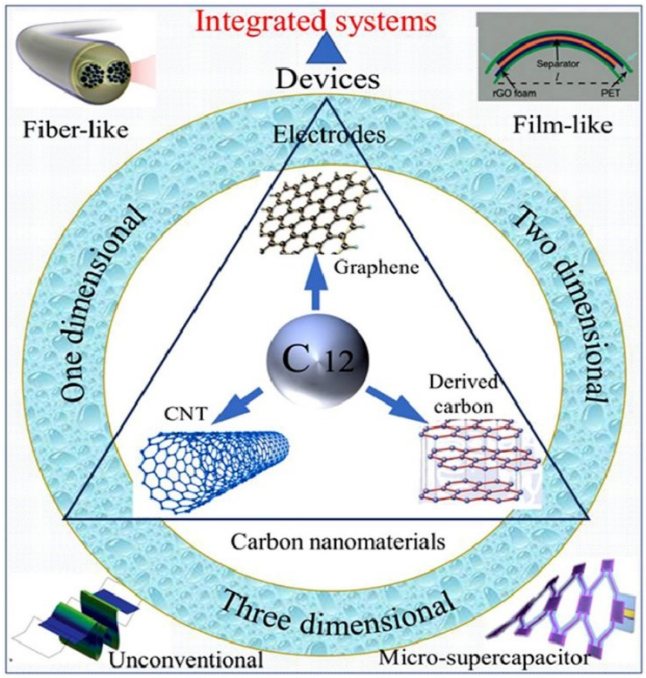

Fig. 1.4 Demonstration of flexible electrodes based on carbon materials for flexible supercapacitors. [78]

Carbon nanotubes (CNTs) are hollow cylinders made of carbon sheets rolled into a typical one-dimensional (1D) structured carbon. It has a very large aspect ratio, good mechanical flexibility, metallic conductivity and large specific surface area, and is widely used in flexible supercapacitors. Since CNTs possess a unique 1D nanostructure, they can be easily assembled into fibrous macroscopic structures. For example, CNTs yarns can be easily obtained by wet or dry spinning. The flexible CNT-based electrodes have shown great advantages in bendability, stretchability, and/or compressibility, as well as long cycle life.

Shang et.al report a substrate-free, self-stretchable carbon nanotube (CNT) yarn supercapacitor utilizing the helical loop structure incorporated into the CNT yarns, as shown in **Fig. 1.5**. [79] These helical CNT yarn supercapacitors can work stably under many extreme deformation conditions such as super-elongation (tensile strain up to 150%), arbitrary shape change (entangling), and high frequency stretching (up to 10 Hz over 10000 cycles). This fibrous supercapacitor with a specific yarn structure has extremely high potential applications in portable, wearable, and body-integrated energy storage devices.

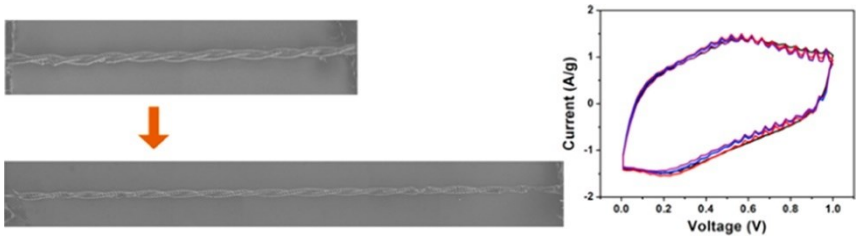

Fig. 1.5 Self-stretchable, helical carbon nanotube yarn supercapacitors with stable performance under extreme deformation conditions.[79]

Jesse Smithyman et al. fabricated a flexible supercapacitor with a yarn-like geometry using coaxially aligned electrodes, as shown in **Fig. 1.6**.[80] The CNT network electrodes allow the electronic conductors and active materials of each electrode to be integrated into a single assembly. The CNT yarn is used as the inner electrode to provide the support structure of the device. The integration strategy of these components eliminates the need for inactive materials, resulting in devices with the highest reported volumetric energy and power density for flexible carbon-based EDLCs. At a current density of 333 mA $g^{-1}$the energy and power density was 0.71 Wh $kg^{-1}$and

1.4 kW kg^{-1}. In addition, the coaxial yarn cell design provides a robust structure that can withstand bending deformation with minimal impact on energy storage performance. Over 95% of the energy density and 99% of the power density are retained when wound on an 11 cm diameter cylinder.

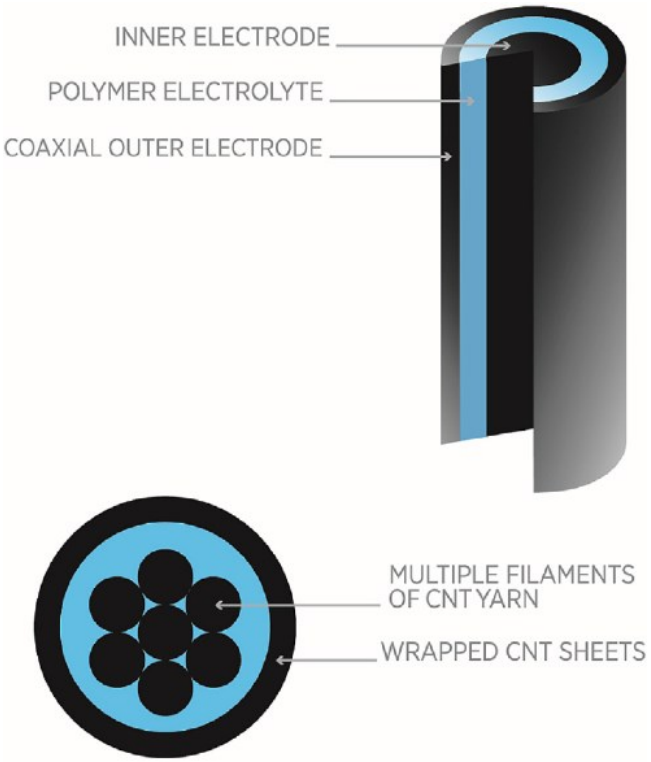

Fig. 1.6 Top: Schematic of the coaxial electrode design for flexible electrochemical cells. Bottom: Cross-section of the multifilament CNT yarn cells fabricated in this report.[80]

1.4.2 Transition metal oxide-based flexible supercapacitors

Transition metal oxides (MOx) are typical pseudocapacitive materials that can store several times more electrical energy than carbon materials using a rapid electrochemical redox mechanism at or near the surface, but the cycling performance of the materials is relatively poor.[81] In addition, the conductivity of transition metal oxides is usually poor, making the prepared devices exhibit electrochemical properties much lower than the theoretical values. Despite this, MOx is also widely used in electrode materials, the most well-known Fe_2O_3, MnO_2, ZnO, NiCo layered-double-hydroxide (LDH), CoAl

LDH, Co_3O_4, and their composites have been widely studied.[82] The main reason should be looked for in the special characteristics of MOx, including challengeable valence, which is a charge of pseudocapacitance allowing the intercalation of ions and electrons into the lattice of the metallic compounds and their considerable inherent stability.[82-86] MOx can be easily deposited on the surface of conductive flexible substrates, so it is widely used in flexible supercapacitors.

Zhong et al. constructed petal-shaped Ni-doped MnO_2 nano-array electrode materials based on a flexible carbon cloth with strong adhesion using a simple and environmentally friendly hydrothermal reaction, and assembled a flexible quasi-solid-state supercapacitor with PVA/Na_2SO_4 gel electrolytes, as shown in **Fig. 1.7**.[87] The voltage window of Ni-doped MnO_2 nano-array@CC electrode materials could reach 1.2 V, especially the area-specific capacitance was up to 1398.8 mF cm^{-2}. As an assembled device, the voltage window could reach 2.2 V, the volumetric capacitance was as high as 1022.08 mF cm^{-3}, the energy density could reach 0.6871 mWh·cm^{-3}, and the power density could be achieved as 31.43 mW cm^{-3}, demonstrating good prospect in applications for the flexible energy storage device.

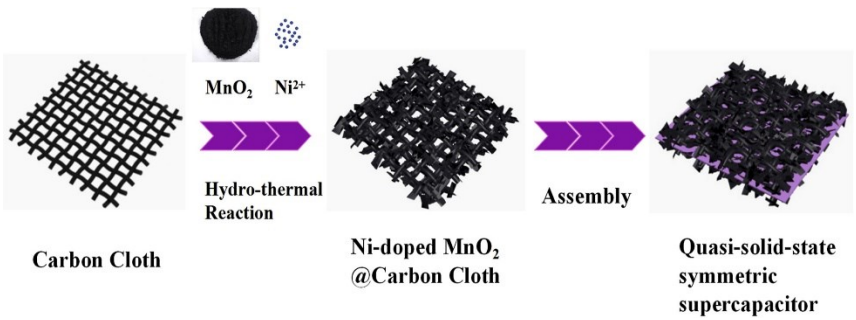

Fig. 1.7 Schematic illustration of formation progress of the Ni-doped MnO_2 nano-array@CC and the quasi-solid-state symmetric supercapacitor after assembly.[87]

Ma et al. reported a flexible hybrid paper consisting of Fe_2O_3 nanoparticles (NPs) anchored on Ti_3C_2Tx (Fe_2O_3 NPs@MX) via electrostatic self-assembly and annealing treatments. (**Fig. 1.8**)[88] The interlayer spacing of Ti_3C_2Tx nanoflakes is effectively enlarged through the incorporation of Fe_2O_3 NPs, allowing more electrochemical active sites to store charge. Meanwhile, Ti_3C_2Tx nanoflakes form a continuous metallic skeleton and inhibit the volume expansion of Fe_2O_3 NPs during the

charging/discharging process, enhancing the cycling stability. The flexible, ultrathin (4.1 μm) Fe_2O_3 NPs@MX hybrid paper shows considerably improved electrochemical performances compared to those of pure Ti_3C_2Tx and Fe_2O_3, including a wide potential window of 1 V, an ultrahigh volumetric capacitance of ~2607 F cm^{-3} (584 F g^{-1}), and excellent capacitance retention after 13,000 cycles. Besides, the as-assembled symmetric solid-state supercapacitor exhibits an energy density of 29.7 Wh L^{-1} and excellent mechanical flexibility. This design of decorating nanoparticles in a two-dimensional metal network has universal applicability and can be used to manufacture high-efficiency composite materials for advanced energy storage devices.

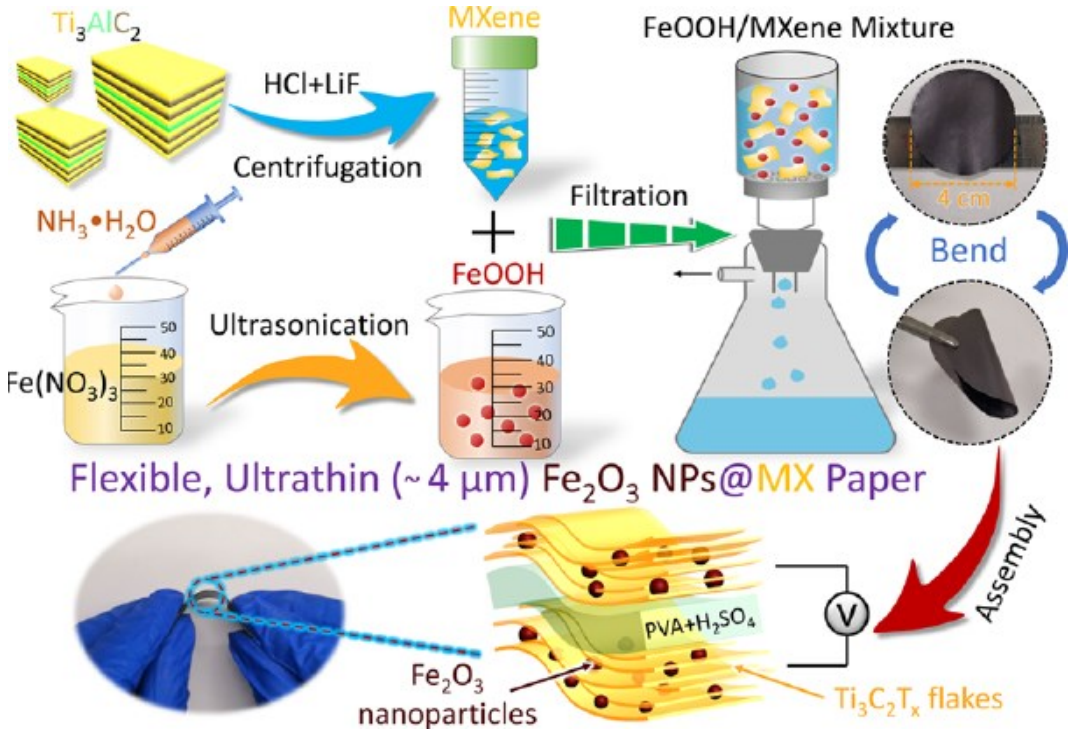

Fig. 1.8 Schematic illustration of the fabrication process of Fe_2O_3 NPs@MX-based flexible supercapacitors.[88]

Zhai et al. prepared a new flexible electrode composed of porous carbonized cotton, ZnO nanoparticles, and CuS microspheres by a two-step method. (**Fig. 1.9**)[89] The porous carbonized cotton/ZnO/CuS composite (pCcZC) electrode exhibits excellent specific capacitance (1830 mF cm^{-2} at 2 mA cm^{-2}), high rate performance (74% retention with current density increasing from 2 to 10 mA cm^{-2}), and outstanding cycle stability, owing to the synergistic effect of electrochemical double-layer capacitance and

pseudo capacitance (14.8% loss of initial capacitance after 5000 cycles). The electrode is binder-free, flexible, and wearable thanks to the flexible and lightweight carbonized cotton used as a current collector. Furthermore, the flexible symmetrical supercapacitor with pCcZC electrodes obtains a higher energy density of 0.27 Wh cm^{-2} at 4.26 W cm^{-2}.

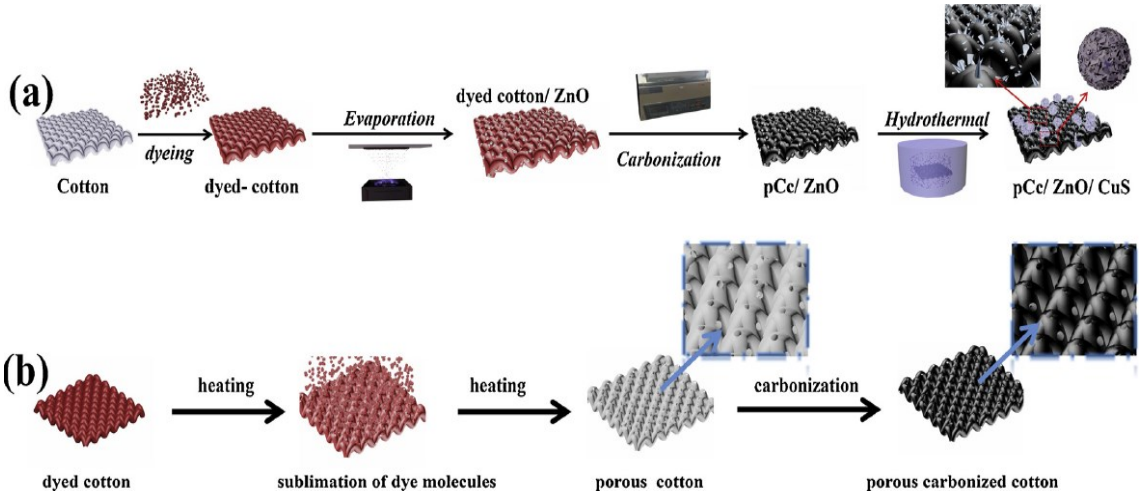

Fig. 1.9 (a) Schematic diagram of the synthesis process of pCcZC; (b) Carbonation process of dyed cotton.[89]

1.4.3 Conductive polymer-based flexible supercapacitors

Conductive polymers (CPs) are electroactive materials with pseudo-capacitance characteristics. Commonly used CPs include polyaniline (PANI), polypyrrole (PPy), polythiophene (PTh), and poly(3,4-ethylenedioxythiophene) (PEDOT), and the structure is shown in **Fig. 1.10**.[90, 91] By adjusting the doping level, the conductivity of CPs can reach a change of more than ten orders of magnitude. The reverse doping-dedoping characteristic of CPs has been exploited for a variety of smart applications in advanced electronic devices, batteries, supercapacitors, and sensors. CPs can be synthesized by oxidative polymerization using common oxidants such as ammonium persulfate, Fe^{3+}, or by electrochemical polymerization. Compared to the other common electroactive materials, CPs are most promising due to their inherent flexible polymeric nature suitable for flexible supercapacitor applications.[92] By changing the conditions of electrochemical polymerization, CPs can be polymerized into different forms, including powders and films. In addition, various forms of CPs, such as nanofibers,

nanotubes, nanorods, nanoarrays, nanowires, etc., can be obtained by different synthesis or processing methods, such as hard-template, soft-template, electrochemical, interfacial polymerization, and post-synthesis electrospinning.[93-97] These different morphologies of CPs provide more maneuverability for the fabrication of flexible supercapacitors based on CPs.

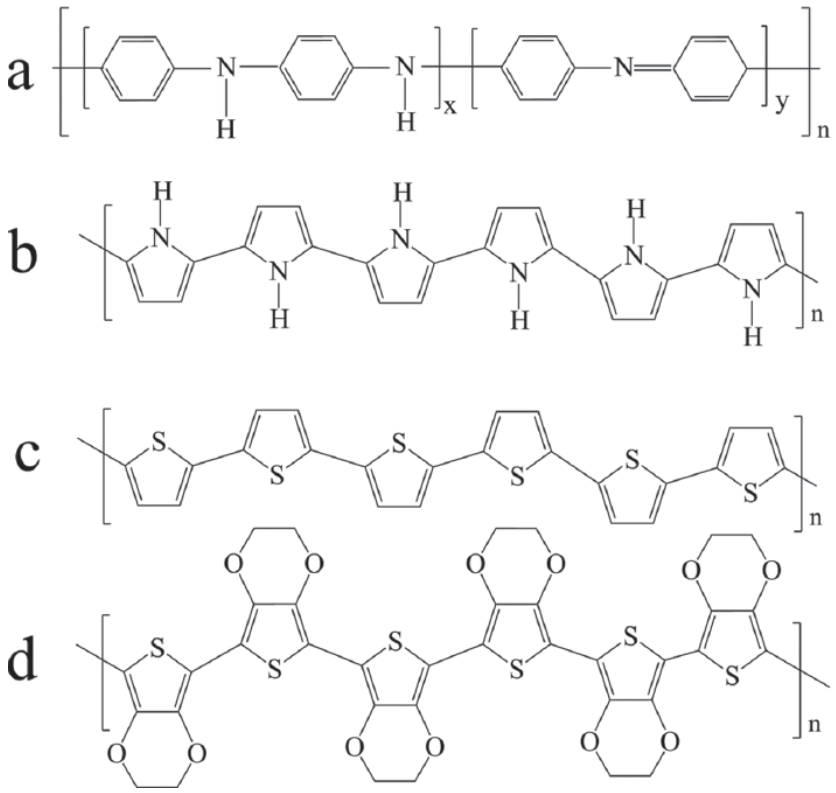

Fig. 1.10 Chemical structure of a) PANI (x + y = 1), b) PPy, c) PTh, and d) PEDOT.[90]

The most traditional method for manufacturing CPs-based FSCs is to prepare a slurry of chemically or electrochemically polymerized CPs and coat it with adhesives and additives on a flexible conductive substrate to fabricate flexible electrodes and then assemble them into FSCs. However, the performance of the FSC fabricated by this process is not satisfactory because the high interfacial resistance and the inherent resistance of the binder material slow down the ion transport of the electrode during the redox reaction. To overcome such effects, a direct growth method has been devised for growing CPs directly on a conductive flexible substrate. For example, Liu et al. used electrochemical polymerization to polymerize a microconical structure of PPy on the surface of a stainless steel yarn, which was then assembled into an all-solid-state fiber-

like flexible supercapacitor (ASSFS). **(Fig. 1.11)**[98] The microcone arrays and interconnected network structure of PPy could increase the transport path for ions/electrons and enlarge the real contact area between PPy and electrolyte, leading to superior specific capacitance. The resultant ASSFS exhibits a maximum specific capacitance of 42.7 F cm^{-3}, an energy density of 3.8 mWh $cm^{-3,}$ and a power density of 388 Mw cm^{-3}. The specific capacitance maintains 100% at different bending angles and 93.5% of its initial value after 1000 bending cycles.

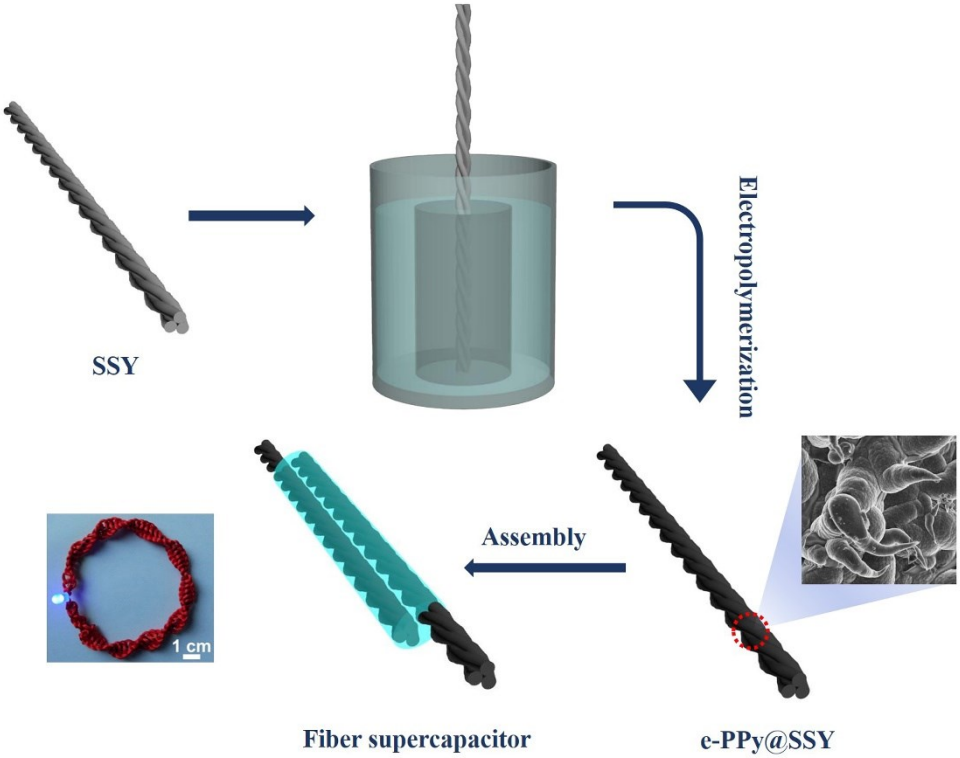

Fig. 1.11 Schematic representation of preparation process of the symmetric all-solid-state fiber supercapacitor.[98]

The direct growth of CPs on flexible conducting substrates is certainly a good method, however, since conducting polymers are inherently very conductive as well as somewhat flexible, the design of self-supporting CPs flexible electrodes without additional flexible substrates has also been proposed. For example, yang et al. integrated two types of conducting polymers, polyaniline (PANI) and PEDOT, through a molecular bridge provided by phytic acid.[99] The acid replaced part of the PSS and facilitated the conversion of the PEDOT chain from a benzoic structure to a quinone structure. The

resulting hydrogel consists of a three-dimensional network of PEDOT sheets in which PANI is embedded; it has highly improved mechanical properties compared to PEDOT hydrogels due to molecular interactions between PANI and PEDOT. (**Fig. 1.12**) The flexible solid-state supercapacitor based on PEDOT/PANI hydrogel delivered a high volumetric energy density of 0.25 mWh cm^{-3} at a power density of 107.14 mW cm^{-3}. This device exhibits excellent electrochemical performance and mechanical elasticity, which points out a new direction for the development of conductive polymer composite hydrogels.

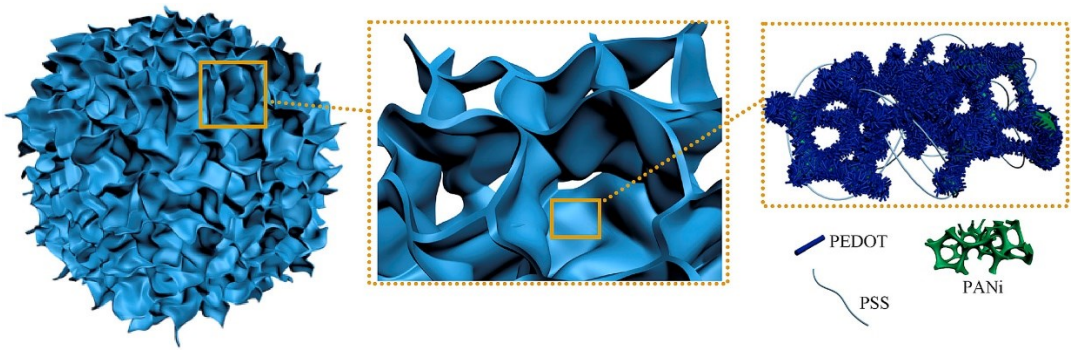

Fig. 1.12 Schematic of hydrogel skeleton, porous network, and PEDOT sheets containing PANI.[99]

Li et al. used a supramolecular strategy to prepare conductive hydrogels with excellent mechanical and electrochemical properties and fabricated flexible solid-state supercapacitors with high performance. The supramolecular assembly of polyaniline and polyvinyl alcohol through dynamic borate bonds produces polyaniline-polyvinyl alcohol hydrogel (PPH). (**Fig. 1.13**)[100] The PPH showed significant tensile strength (5.3 MPa) and electrochemical capacitance (928 F g^{-1}). PPH-based flexible solid supercapacitors have a large capacitance (306 mF cm^{-2} and 153 F g^{-1}) and a high energy density (13.6 Wh kg^{-1}) and show good stability. After 1000 folding cycles, the capacitance retention rate is 100%, and after 1000 charge-discharge cycles, the capacitance retention rate is 90%. The high activity and robustness enable the PPH-based supercapacitor as a promising power device for flexible electronics.

Zang et al. used a gas-phase polymerization method to embed polypyrrole into a chemically cross-linked PVA hydrogel film to prepare a conductive polymer hydrogel with an interpenetrating network structure of PPy and PVA interpenetration (PPy/CPH).

(Fig. 1.14)[101]

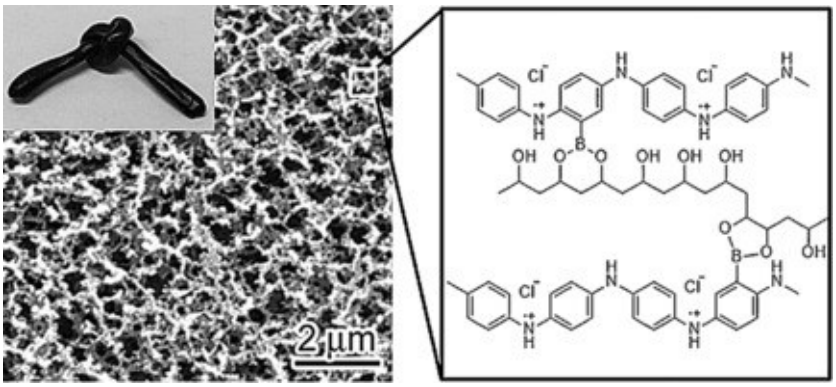

Fig. 1.13 Schematic molecular structure of PPH showing the crosslink between PANI and PVA.[100]

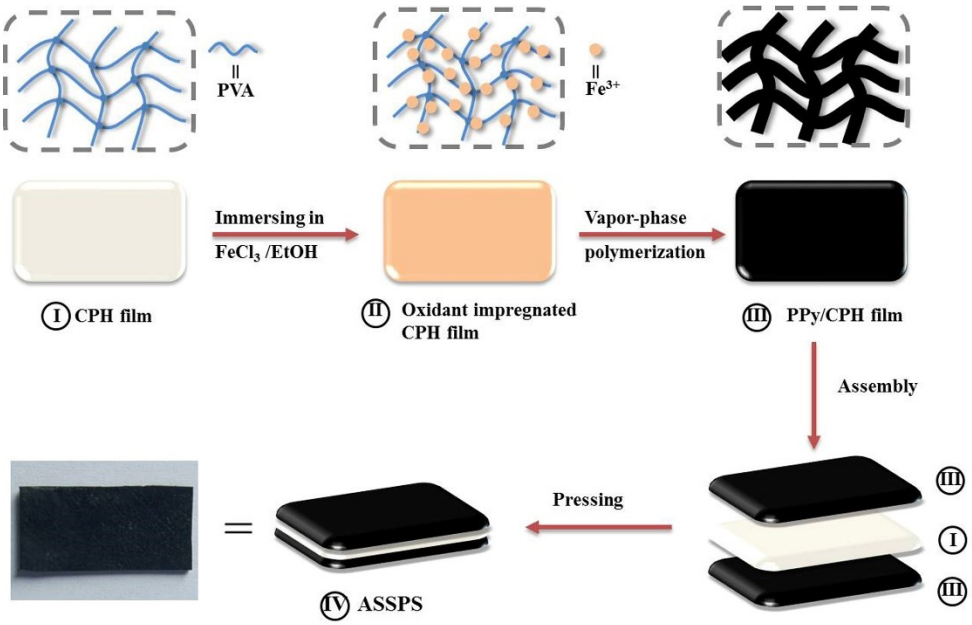

Fig. 1.14 Schematic representation of preparation process of the flexible all-solid-state polymer supercapacitor.[101]

The PPy/CPH was then prepared as an all-solid-state polymeric flexible supercapacitor (ASSPS). Due to the strong hydrogen bonding interaction between the electrode and electrolyte layers and the high mechanical properties of PPy/CPH, ASSPS exhibits extremely excellent mechanical properties with a tensile strength of 20.83 MPa and an elongation at a break of 377%. It also exhibits excellent electrochemical properties with

a maximum volume specification capacitance of 13.06 F cm^{-3} and an energy density of 1160.9 μWh cm^{-3}. After 10,000 folding cycles and 10,000 charge/discharge cycles, its electric capacity was maintained at 97.9% and 86.3% of the initial value, respectively.

1.5 Current issues and future trend

In summary, flexible supercapacitors have made significant developments in recent years. The optimized use of various electrode materials has improved the specific capacity and energy density of the device; the development of wire-shaped flexible supercapacitors has provided more options for selecting energy storage devices for micro and wearable devices; the development of stretchable and compressible hydrogel supercapacitors has broadened the application scenarios of flexible supercapacitors, improved the adaptability of the devices to the environment, and reduced the maintenance cost of the devices. However, flexible supercapacitors still face many problems. As flexible electronics technology is counter-progressing, the requirements for flexible energy storage devices are getting higher and higher. The primary goal is to continue to improve the electrochemical performance of flexible supercapacitors. Secondly, to make the devices easily integrated and modular, to improve the integration with other devices, to reduce the number of components, mass, and volume of the devices, to make the devices more functional, smaller in size, lighter in mass, and more adaptable to the environment. In addition, the functionalization of flexible supercapacitors should not be left behind, such as low-temperature resistance characteristics, which will affect their application scope.

Although stretchable and compressible supercapacitors have attracted a lot of attention, there are still some problems to be solved in the research of flexible supercapacitors that can be bent or twisted. 1) The energy density of flexible supercapacitors is relatively low compared with that of ordinary supercapacitors, which is mainly due to the trade-off between electrochemical and mechanical properties to achieve better flexibility, so the active material loading is low, which often makes the volume-specific capacity and energy density of the device very limited. Therefore, there is a need to develop flexible supercapacitors with higher volume utilization. 2) Lack of device structure optimization and dynamic research on the mechanical stability of the

device for flexible supercapacitors. The structure of flexible supercapacitors determines the mechanical and electrochemical stability of the devices under dynamic deformation, and the study of dynamic stability can examine the stability of flexible supercapacitors in practical applications, which is important for both evaluating and improving the devices. Therefore, the structural design of supercapacitors also appears to be crucial. A reasonable structural design can avoid the delamination of the flexible substrate and electroactive materials under high deformation and balance the mechanical durability and electrochemical performance.

1.6 Contribution from this dissertation

As an important energy storage device, supercapacitors have the advantages of high power density, ultra-fast charging and discharging speed, ultra-long cycle life, and safety, which play an important role in the development and application of mobile electronic devices. Wearable devices have gradually become a hot spot for mobile electronic devices, and energy storage components such as supercapacitors are required to have the characteristics of good flexibility, small size, light weight, and high energy density. The preparation of flexible quasi-solid supercapacitors with high energy density, good mechanical flexibility and stability, small size, and light weight has become one of the important directions of current research on supercapacitors. Flexible two-dimensional laminates, miniature, and one-dimensional wire supercapacitors have been developed successively, all of which have made great progress, but there are still some problems. Although electrodes based on nanostructured active materials exhibit high mass-specific capacity, the use of inactive substrates and the limited mass of active materials on the substrate results in low capacitance and energy density of the electrodes and devices. The preparation of flexible supercapacitors currently has problems such as complex processes, high cost, and degradation of electrochemical properties during deformation. There is a lack of quantitative research on the electrochemical stability of flexible supercapacitors during dynamic deformation, etc., and it is impossible to accurately evaluate the structural stability of flexible devices. This thesis addresses these problems in flexible supercapacitors and identifies the development of high-performance flexible electrodes based on conductive polymers, taking into account the overall design of flexible devices, and the preparation of new flexible supercapacitors, aiming at

improving the electrochemical and mechanical properties of flexible supercapacitors, simplifying the preparation method, and studying the electrochemical properties of the devices under dynamic deformation, etc. The main contents of the thesis include:

(1) In chapter 3, the conductive glass fiber fabric is prepared by gas-phase polymerization, and then PPy with special morphology is deposited on the surface of the conductive glass fiber fabric by controlling the conditions of electrochemical polymerization to prepare a fabric electrode with high flexibility and high electrochemical performance. Then, a flexible solid-state supercapacitor was constructed based on this fabric electrode. The effects of different electrochemical polymerization conditions on PPy micromorphology were investigated, and the electrochemical properties of the devices were studied under different deformations. The gas-phase polymerization of PPy for the preparation of conductive glass fiber cloth proposed in this study is a general strategy that can be extended and applied to different non-conductive flexible substrates to obtain electrical conductivity. The fiberglass cloth-based supercapacitors provide a new approach to the practical applications of wearable power supplies.

(2) In chapter 4, a lightweight and compressible all-in-one flexible supercapacitor that can easily extend voltage window was fabricated based on melamine foam (MF) and PPy by the one-step polymerization method. The MF serves as the substrate for depositing PPy and the separator to avoid a short circuit. In addition, the MF can sufficiently absorb and lock in the electrolyte to make the electroactive material fully contact the electrolyte. This device exhibits superior electrochemical performance and outstanding mechanical stability which can work stably under different compressive strains. The output voltage of this device can be adjusted handily by a simple cutting method without connecting several supercapacitors in series. The concept of adjusting the device output voltage by cutting is proposed in this work, which may provide a new idea for the development of integrated flexible supercapacitors.

(3) In chapter 5, a hybrid polyvinyl alcohol/poly(3,4-ethylenedioxythiophene): polystyrene sulfonate (PVA/PEDOT:PSS) hydrogel electrode with 3D interpenetrated network structure is prepared by the freeze-thaw crosslinking and solution immersion method. Due to the strong intermolecular force between PVA and PEDOT:PSS, coupling with the use of liquid phase mixing, this hybrid hydrogel electrode shows

uniform interconnectivity and robust mechanical properties. The all-gel-state flexible supercapacitor based on the PVA/PEDOT:PSS hydrogel demonstrates excellent mechanical durability as well as excellent electrochemical performance, and also has good frost resistance, capable of stable power supply at -25°C. The all-gel integrated design eliminates the problem of slippage between electrolyte and electrode during deformation, providing a new direction for the design of flexible supercapacitors.

(4) In chapter 6, an all-gel-state integrated asymmetric flexible supercapacitor based on poly(3,4-ethylenedioxythiophene): polystyrene sulfonate (PEDOT:PSS) and polypyrrole (PPy) composite hydrogel electrodes with an interchangeable positive and negative electrode was fabricated. The device has robust flexibility and mechanical durability as well as fascinating electrochemical properties. Moreover, the positive and negative electrodes of this asymmetric device can be used interchangeably, and it can power the light-emitting diodes (LEDs) without distinguishing between positive and negative. The concept of asymmetric devices that do not need to distinguish between positive and negative electrodes will perhaps open a new trend in the design of high-energy-density flexible supercapacitors.

Reference

[1] M. Koo, K.-I. Park, S.H. Lee, M. Suh, D.Y. Jeon, J.W. Choi, K. Kang, K.J. Lee, Bendable inorganic thin-film battery for fully flexible electronic systems, Nano Lett. 12 (2012) 4810-4816.

[2] S.W. Chen, X. Cao, N. Wang, L. Ma, H.R. Zhu, M. Willander, Y. Jie, Z.L. Wang, An ultrathin flexible single-electrode triboelectric-nanogenerator for mechanical energy harvesting and instantaneous force sensing, Adv. Energy Mater. 7 (2017) 1601255.

[3] R.-Z. Li, R. Peng, K.D. Kihm, S. Bai, D. Bridges, U. Tumuluri, Z. Wu, T. Zhang, G. Compagnini, Z. Feng, High-rate in-plane micro-supercapacitors scribed onto photo paper using in situ femtolaser-reduced graphene oxide/Au nanoparticle microelectrodes, Energy Environ. Sci. 9 (2016) 1458-1467.

[4] Q. Shi, B. Dong, T. He, Z. Sun, J. Zhu, Z. Zhang, C. Lee, Progress in wearable electronics/photonics—Moving toward the era of artificial intelligence and internet of things, InfoMat 2 (2020) 1131-1162.

[5] Z. Lou, L. Wang, K. Jiang, Z. Wei, G. Shen, Reviews of wearable healthcare systems: Materials, devices and system integration, Mater. Sci. Eng. R Rep. 140 (2020) 100523.

[6] K. Dong, X. Peng, Z.L. Wang, Fiber/fabric-based piezoelectric and triboelectric nanogenerators for flexible/stretchable and wearable electronics and artificial intelligence, Adv. Mater. 32 (2020) 1902549.

[7] L. Li, Z. Wu, S. Yuan, X.-B. Zhang, Advances and challenges for flexible energy storage and conversion devices and systems, Energy Environ. Sci. 7 (2014) 2101-2122.

[8] L. Mao, Q. Meng, A. Ahmad, Z. Wei, Mechanical analyses and structural design requirements for flexible energy storage devices, Adv. Energy Mater. 7 (2017) 1700535.

[9] H. Li, Z. Tang, Z. Liu, C. Zhi, Evaluating flexibility and wearability of flexible energy storage devices, Joule 3 (2019) 613-619.

[10] W.-J. Song, S. Lee, G. Song, H.B. Son, D.-Y. Han, I. Jeong, Y. Bang, S. Park, Recent progress in aqueous based flexible energy storage devices, Energy Storage Mater. 30 (2020) 260-286.

[11] P. Yang, W. Mai, Flexible solid-state electrochemical supercapacitors, Nano Energy 8 (2014) 274-290.

[12] T. Tao, S. Lu, Y. Chen, A review of advanced flexible lithium-ion batteries, Adv. Mater. Technol. 3 (2018) 1700375.

[13] Y. Dai, Y. Huang, X. He, D. Hui, Y. Bai, Continuous performance assessment of thin-film flexible photovoltaic cells under mechanical loading for building integration, Solar Energy 183 (2019) 96-104.
[14] W. Liu, M.S. Song, B. Kong, Y. Cui, Flexible and stretchable energy storage: recent advances and future perspectives, Adv. Mater. 29 (2017) 1603436.
[15] Y. Zhao, J. Guo, Development of flexible Li-ion batteries for flexible electronics, InfoMat 2 (2020) 866-878.
[16] Z. Fang, J. Wang, H. Wu, Q. Li, S. Fan, J. Wang, Progress and challenges of flexible lithium ion batteries, J. Power Sources 454 (2020) 227932.
[17] Q. Liu, J. Qiu, C. Yang, L. Zang, G. Zhang, E. Sakai, H. Wu, S. Guo, Robust quasi-solid-state integrated asymmetric flexible supercapacitors with interchangeable positive and negative electrode based on all-conducting-polymer electrodes, J. Alloys Compd. 887 (2021) 161362.
[18] F. Meng, Q. Li, L. Zheng, Flexible fiber-shaped supercapacitors: design, fabrication, and multi-functionalities, Energy Storage Mater. 8 (2017) 85-109.
[19] L.L. Zhang, X. Zhao, Carbon-based materials as supercapacitor electrodes, Chem. Soc. Rev. 38 (2009) 2520-2531.
[20] X. Zhang, L. Hou, A. Ciesielski, P. Samorì, 2D materials beyond graphene for high-performance energy storage applications, Adv. Energy Mater. 6 (2016) 1600671.
[21] J.R. Miller, P. Simon, Electrochemical capacitors for energy management, Science Magazine 321 (2008) 651-652.
[22] T. Liu, F. Zhang, Y. Song, Y. Li, Revitalizing carbon supercapacitor electrodes with hierarchical porous structures, J. Mater. Chem. A 5 (2017) 17705-17733.
[23] L. Dong, C. Xu, Y. Li, Z.-H. Huang, F. Kang, Q.-H. Yang, X. Zhao, Flexible electrodes and supercapacitors for wearable energy storage: a review by category, J. Mater. Chem. A 4 (2016) 4659-4685.
[24] X. Lu, M. Yu, G. Wang, Y. Tong, Y. Li, Flexible solid-state supercapacitors: design, fabrication and applications, Energy Environ. Sci. 7 (2014) 2160-2181.
[25] Y. Qin, Z. Ou, C. Xu, Z. Zhang, J. Yi, Y. Jiang, J. Wu, C. Guo, Y. Si, T. Zhao, Progress of carbon-based electrocatalysts for flexible zinc-air batteries in the past 5 years: recent strategies for design, synthesis and performance optimization, Nanoscale Research Letters 16 (2021) 1-13.

[26] Y. Li, X. Han, T. Yi, Y. He, X. Li, Review and prospect of NiCo2O4-based composite materials for supercapacitor electrodes, Journal of energy chemistry 31 (2019) 54-78.
[27] J. Zhang, X. Wang, J. Ma, S. Liu, X. Yi, Preparation of cobalt hydroxide nanosheets on carbon nanotubes/carbon paper conductive substrate for supercapacitor application, Electrochim. Acta 104 (2013) 110-116.
[28] L. Yuan, N. Xin, Y. Liu, W. Shi, In situ construction of multi-dimensional Co3O4/NiCo2O4 hierarchical flakes on self-supporting carbon substrate with ultra-high capacitance for hybrid supercapacitors, J. Colloid Interface Sci. 599 (2021) 158-167.
[29] Z. Su, C. Yang, B. Xie, Z. Lin, Z. Zhang, J. Liu, B. Li, F. Kang, C.P. Wong, Scalable fabrication of MnO 2 nanostructure deposited on free-standing Ni nanocone arrays for ultrathin, flexible, high-performance micro-supercapacitor, Energy Environ. Sci. 7 (2014) 2652-2659.
[30] Y. Xu, Z. Lin, X. Huang, Y. Liu, Y. Huang, X. Duan, Flexible solid-state supercapacitors based on three-dimensional graphene hydrogel films, ACS nano 7 (2013) 4042-4049.
[31] T.Y. Ma, J. Ran, S. Dai, M. Jaroniec, S.Z. Qiao, Phosphorus-doped graphitic carbon nitrides grown in situ on carbon-fiber paper: flexible and reversible oxygen electrodes, Angew. Chem. 127 (2015) 4729-4733.
[32] S. Wang, Y. Liang, W. Zhuo, H. Lei, M.S. Javed, B. Liu, Z. Wang, W. Mai, Freestanding polypyrrole/carbon nanotube electrodes with high mass loading for robust flexible supercapacitors, Mater. Chem. Front. 5 (2021) 1324-1329.
[33] T. Wang, L.-C. Jing, Q. Zhu, A.S. Ethiraj, Y. Tian, H. Zhao, X.-T. Yuan, J.-G. Wen, L.-K. Li, H.-Z. Geng, Fabrication of architectural structured polydopamine-functionalized reduced graphene oxide/carbon nanotube/PEDOT: PSS nanocomposites as flexible transparent electrodes for OLEDs, Appl. Surf. Sci. 500 (2020) 143997.
[34] L. Wen, F. Li, H.M. Cheng, Carbon nanotubes and graphene for flexible electrochemical energy storage: from materials to devices, Adv. Mater. 28 (2016) 4306-4337.
[35] N. Yadav, N. Yadav, S. Hashmi, Ionic liquid incorporated, redox-active blend polymer electrolyte for high energy density quasi-solid-state carbon supercapacitor, J. Power Sources 451 (2020) 227771.

[36] K.-W. Nam, C.-W. Lee, X.-Q. Yang, B.W. Cho, W.-S. Yoon, K.-B. Kim, Electrodeposited manganese oxides on three-dimensional carbon nanotube substrate: Supercapacitive behaviour in aqueous and organic electrolytes, J. Power Sources 188 (2009) 323-331.

[37] Z. Chen, X. Wang, Z. Ding, Q. Wei, Z. Wang, X. Yang, J. Qiu, Biomass-based Hierarchical Porous Carbon for Supercapacitors: Effect of Aqueous and Organic Electrolytes on the Electrochemical Performance, ChemSusChem 12 (2019) 5099-5110.

[38] Q. Rong, W. Lei, J. Huang, M. Liu, Low temperature tolerant organohydrogel electrolytes for flexible solid-state supercapacitors, Adv. Energy Mater. 8 (2018) 1801967.

[39] K. Fic, G. Lota, M. Meller, E. Frackowiak, Novel insight into neutral medium as electrolyte for high-voltage supercapacitors, Energy Environ. Sci. 5 (2012) 5842-5850.

[40] C. Zhong, Y. Deng, W. Hu, J. Qiao, L. Zhang, J. Zhang, A review of electrolyte materials and compositions for electrochemical supercapacitors, Chem. Soc. Rev. 44 (2015) 7484-7539.

[41] S. Alipoori, S. Mazinani, S.H. Aboutalebi, F. Sharif, Review of PVA-based gel polymer electrolytes in flexible solid-state supercapacitors: Opportunities and challenges, journal of energy storage 27 (2020) 101072.

[42] W. Ye, H. Wang, J. Ning, Y. Zhong, Y. Hu, New types of hybrid electrolytes for supercapacitors, Journal of Energy Chemistry 57 (2021) 219-232.

[43] S.A. Hashmi, N. Yadav, M.K. Singh, Polymer electrolytes for supercapacitor and challenges, Polymer Electrolytes: Characterization Techniques and Energy Applications (2020) 231-297.

[44] C.W. Huang, C.A. Wu, S.S. Hou, P.L. Kuo, C.T. Hsieh, H. Teng, Gel electrolyte derived from poly (ethylene glycol) blending poly (acrylonitrile) applicable to roll-to-roll assembly of electric double layer capacitors, Adv. Funct. Mater. 22 (2012) 4677-4685.

[45] N. Choudhury, S. Sampath, A. Shukla, Hydrogel-polymer electrolytes for electrochemical capacitors: an overview, Energy Environ. Sci. 2 (2009) 55-67.

[46] H. Dai, G. Zhang, D. Rawach, C. Fu, C. Wang, X. Liu, M. Dubois, C. Lai, S. Sun, Polymer gel electrolytes for flexible supercapacitors: Recent progress, challenges, and perspectives, Energy Storage Mater. (2020).

[47] S. Jha, S. Mehta, Y. Chen, L. Ma, P. Renner, D.Y. Parkinson, H. Liang, Design and synthesis of lignin-based flexible supercapacitors, ACS Sustainable Chemistry & Engineering 8 (2019) 498-511.
[48] X. Li, R. Liu, C. Xu, Y. Bai, X. Zhou, Y. Wang, G. Yuan, High-performance polypyrrole/graphene/SnCl2 modified polyester textile electrodes and yarn electrodes for wearable energy storage, Adv. Funct. Mater. 28 (2018) 1800064.
[49] J. Chen, K. Fang, Q. Chen, J. Xu, C.-P. Wong, Integrated paper electrodes derived from cotton stalks for high-performance flexible supercapacitors, Nano Energy 53 (2018) 337-344.
[50] Y. Yang, H. Fei, G. Ruan, C. Xiang, J.M. Tour, Edge-oriented MoS2 nanoporous films as flexible electrodes for hydrogen evolution reactions and supercapacitor devices, Adv. Mater. 26 (2014) 8163-8168.
[51] K. Lu, B. Song, K. Li, J. Zhang, H. Ma, Cobalt hexacyanoferrate nanoparticles and MoO3 thin films grown on carbon fiber cloth for efficient flexible hybrid supercapacitor, J. Power Sources 370 (2017) 98-105.
[52] C. Wang, X. Wu, Y. Ma, G. Mu, Y. Li, C. Luo, H. Xu, Y. Zhang, J. Yang, X. Tang, Metallic few-layered VSe 2 nanosheets: high two-dimensional conductivity for flexible in-plane solid-state supercapacitors, J. Mater. Chem. A 6 (2018) 8299-8306.
[53] K. Sun, E. Feng, G. Zhao, H. Peng, G. Wei, Y. Lv, G. Ma, A single robust hydrogel film based integrated flexible supercapacitor, ACS Sustainable Chemistry & Engineering 7 (2018) 165-173.
[54] L. Liu, Y. Yu, C. Yan, K. Li, Z. Zheng, Wearable energy-dense and power-dense supercapacitor yarns enabled by scalable graphene–metallic textile composite electrodes, Nat. Commun. 6 (2015) 1-9.
[55] X. Lu, M. Yu, T. Zhai, G. Wang, S. Xie, T. Liu, C. Liang, Y. Tong, Y. Li, High energy density asymmetric quasi-solid-state supercapacitor based on porous vanadium nitride nanowire anode, Nano Lett. 13 (2013) 2628-2633.
[56] D.A. Kang, K. Kim, S.S. Karade, H. Kim, J.H. Kim, High-performance solid-state bendable supercapacitors based on PEGBEM-g-PAEMA graft copolymer electrolyte, Chem. Eng. J. 384 (2020) 123308.
[57] C. Choi, J.M. Lee, S.H. Kim, S.J. Kim, J. Di, R.H. Baughman, Twistable and stretchable sandwich structured fiber for wearable sensors and supercapacitors, Nano

Lett. 16 (2016) 7677-7684.
[58] T. An, W. Cheng, Recent progress in stretchable supercapacitors, J. Mater. Chem. A 6 (2018) 15478-15494.
[59] L. Sun, G. Song, Y. Sun, Q. Fu, C. Pan, MXene/N-Doped Carbon Foam with Three-Dimensional Hollow Neuron-like Architecture for Freestanding, Highly Compressible All Solid-State Supercapacitors, ACS Appl. Mater. Interfaces 12 (2020) 44777-44788.
[60] Z. Peng, J. Lin, R. Ye, E.L. Samuel, J.M. Tour, Flexible and stackable laser-induced graphene supercapacitors, ACS Appl. Mater. Interfaces 7 (2015) 3414-3419.
[61] L. Zang, X. Qiao, Q. Liu, C. Yang, L. Hu, J. Yang, Z. Ma, High-performance solid-state supercapacitors with designable patterns based on used newspaper, Cellulose 27 (2020) 1033-1042.
[62] C. Yang, Q. Liu, L. Zang, J. Qiu, X. Wang, C. Wei, X. Qiao, L. Hu, J. Yang, G. Song, High-performance yarn supercapacitor based on metal–inorganic–organic hybrid electrode for wearable electronics, Adv. Electron. Mater. 5 (2019) 1800435.
[63] I. Shown, A. Ganguly, L.C. Chen, K.H. Chen, Conducting polymer-based flexible supercapacitor, Energy Science & Engineering 3 (2015) 2-26.
[64] G. Wang, L. Zhang, J. Zhang, A review of electrode materials for electrochemical supercapacitors, Chem. Soc. Rev. 41 (2012) 797-828.
[65] Y. Wang, Z. Chang, M. Qian, Z. Zhang, J. Lin, F. Huang, Enhanced specific capacitance by a new dual redox-active electrolyte in activated carbon-based supercapacitors, Carbon 143 (2019) 300-308.
[66] B. Ding, D. Guo, Y. Wang, X. Wu, Z. Fan, Functionalized graphene nanosheets decorated on carbon nanotubes networks for high performance supercapacitors, J. Power Sources 398 (2018) 113-119.
[67] H. Zhang, D. Yang, A. Lau, T. Ma, H. Lin, B. Jia, Hybridized Graphene for Supercapacitors: Beyond the Limitation of Pure Graphene, Small 17 (2021) 2007311.
[68] Z. Li, S. Gadipelli, Y. Yang, G. He, J. Guo, J. Li, Y. Lu, C.A. Howard, D.J. Brett, I.P. Parkin, Exceptional supercapacitor performance from optimized oxidation of graphene-oxide, Energy Storage Mater. 17 (2019) 12-21.
[69] J. Lei, Q. Guo, W. Yao, T. Duan, P. Chen, W. Zhu, Bioconcentration of organic dyes via fungal hyphae and their derived carbon fibers for supercapacitors, J. Mater. Chem. A

6 (2018) 10710-10717.
[70] H. Zhou, H.-J. Zhai, X. Zhi, Enhanced electrochemical performances of polypyrrole/carboxyl graphene/carbon nanotubes ternary composite for supercapacitors, Electrochim. Acta 290 (2018) 1-11.
[71] L.x. Dai, W. Zhang, L. Sun, X.h. Wang, W. Jiang, Z.w. Zhu, H.b. Zhang, C.c. Yang, J. Tang, Highly Stretchable and Compressible Self-Healing P (AA-co-AAm)/CoCl2 Hydrogel Electrolyte for Flexible Supercapacitors, ChemElectroChem 6 (2019) 467-472.
[72] Y. Huang, M. Zhong, F. Shi, X. Liu, Z. Tang, Y. Wang, Y. Huang, H. Hou, X. Xie, C. Zhi, An intrinsically stretchable and compressible supercapacitor containing a polyacrylamide hydrogel electrolyte, Angew. Chem. Int. Ed. 56 (2017) 9141-9145.
[73] H. Zhang, W. Niu, S. Zhang, Extremely stretchable, sticky and conductive double-network ionic hydrogel for ultra-stretchable and compressible supercapacitors, Chem. Eng. J. 387 (2020) 124105.
[74] J. Zeng, L. Dong, W. Sha, L. Wei, X. Guo, Highly stretchable, compressible and arbitrarily deformable all-hydrogel soft supercapacitors, Chem. Eng. J. 383 (2020) 123098.
[75] Y. Hu, C. Guan, Q. Ke, Z.F. Yow, C. Cheng, J. Wang, Hybrid Fe2O3 nanoparticle clusters/rGO paper as an effective negative electrode for flexible supercapacitors, Chem. Mater. 28 (2016) 7296-7303.
[76] W. Ma, S. Chen, S. Yang, W. Chen, W. Weng, Y. Cheng, M. Zhu, Flexible all-solid-state asymmetric supercapacitor based on transition metal oxide nanorods/reduced graphene oxide hybrid fibers with high energy density, Carbon 113 (2017) 151-158.
[77] Y. Shao, H. Wang, Q. Zhang, Y. Li, High-performance flexible asymmetric supercapacitors based on 3D porous graphene/MnO 2 nanorod and graphene/Ag hybrid thin-film electrodes, Journal of Materials Chemistry C 1 (2013) 1245-1251.
[78] P. Xie, W. Yuan, X. Liu, Y. Peng, Z. Wu, Advanced carbon nanomaterials for state-of-the-art flexible supercapacitors, Energy Storage Mater. 36 (2020).
[79] Y.S.A. B, C.W. A, X.H. A, J.L. A, Q.P. A, E.S. B, R.W. A, S.D. A, A.C. B, Y.L. A, Self-stretchable, helical carbon nanotube yarn supercapacitors with stable performance under extreme deformation conditions, Nano Energy 12 (2015) 401-409.
[80] J. Smithyman, R. Liang, Flexible supercapacitor yarns with coaxial carbon nanotube network electrodes, Materials Science and Engineering: B 184 (2014) 34-43.

[81] J. Li, Z. Liu, Q. Zhang, Y. Cheng, B. Zhao, S. Dai, H.-H. Wu, K. Zhang, D. Ding, Y. Wu, Anion and cation substitution in transition-metal oxides nanosheets for high-performance hybrid supercapacitors, Nano Energy 57 (2019) 22-33.
[82] S.A. Delbari, L.S. Ghadimi, R. Hadi, S. Farhoudian, M. Nedaei, A. Babapoor, A.S. Namini, Q. Van Le, M. Shokouhimehr, M.S. Asl, Transition metal oxide-based electrode materials for flexible supercapacitors: A review, J. Alloys Compd. (2020) 158281.
[83] C. Jing, X. Song, K. Li, Y. Zhang, X. Liu, B. Dong, F. Dong, S. Zhao, H. Yao, Y. Zhang, Optimizing the rate capability of nickel cobalt phosphide nanowires on graphene oxide by the outer/inter-component synergistic effects, J. Mater. Chem. A 8 (2020) 1697-1708.
[84] C. Jing, X.D. Liu, K. Li, X. Liu, B. Dong, F. Dong, Y. Zhang, The pseudocapacitance mechanism of graphene/CoAl LDH and its derivatives: Are all the modifications beneficial?, Journal of Energy Chemistry 52 (2021) 218-227.
[85] C. Jing, B. Dong, Y. Zhang, Chemical modifications of layered double hydroxides in the supercapacitor, Energy & Environmental Materials 3 (2020) 346-379.
[86] X. Li, D. Du, Y. Zhang, W. Xing, Q. Xue, Z. Yan, Layered double hydroxides toward high-performance supercapacitors, J. Mater. Chem. A 5 (2017) 15460-15485.
[87] R. Zhong, M. Xu, N. Fu, R. Liu, X. Wang, Z. Yang, A flexible high-performance symmetric quasi-solid supercapacitor based on Ni-doped MnO2 nano-array@ carbon cloth, Electrochim. Acta 348 (2020) 136209.
[88] Y. Ma, H. Sheng, W. Dou, Q. Su, J. Zhou, E. Xie, W. Lan, Fe2O3 Nanoparticles Anchored on the Ti3C2T x MXene Paper for Flexible Supercapacitors with Ultrahigh Volumetric Capacitance, ACS Appl. Mater. Interfaces 12 (2020) 41410-41418.
[89] S. Zhai, K. Jin, M. Zhou, Z. Fan, H. Zhao, X. Li, Y. Zhao, F. Ge, Z. Cai, A novel high performance flexible supercapacitor based on porous carbonized cotton/ZnO nanoparticle/CuS micro-sphere, Colloids and Surfaces A: Physicochemical and Engineering Aspects 584 (2020) 124025.
[90] Y. Han, L. Dai, Conducting polymers for flexible supercapacitors, Macromol. Chem. Phys. 220 (2019) 1800355.
[91] Q. Meng, K. Cai, Y. Chen, L. Chen, Research progress on conducting polymer based supercapacitor electrode materials, Nano Energy 36 (2017) 268-285.
[92] M. Cheng, Y.N. Meng, Z.X. Wei, Conducting polymer nanostructures and their

derivatives for flexible supercapacitors, Isr. J. Chem. 58 (2018) 1299-1314.
[93] Z.-Q. Feng, J. Wu, W. Cho, M.K. Leach, E.W. Franz, Y.I. Naim, Z.-Z. Gu, J.M. Corey, D.C. Martin, Highly aligned poly (3, 4-ethylene dioxythiophene)(PEDOT) nano- and microscale fibers and tubes, Polymer 54 (2013) 702-708.
[94] Y. Han, X. Qing, S. Ye, Y. Lu, Conducting polypyrrole with nanoscale hierarchical structure, Synth. Met. 160 (2010) 1159-1166.
[95] X. Zhang, S.K. Manohar, Narrow pore-diameter polypyrrole nanotubes, J. Am. Chem. Soc. 127 (2005) 14156-14157.
[96] H. Mao, X. Liu, D. Chao, L. Cui, Y. Li, W. Zhang, C. Wang, Preparation of unique PEDOT nanorods with a couple of cuspate tips by reverse interfacial polymerization and their electrocatalytic application to detect nitrite, J. Mater. Chem. 20 (2010) 10277-10284.
[97] G. Li, Y. Li, Y. Li, H. Peng, K. Chen, Polyaniline nanorings and flat hollow capsules synthesized by in situ sacrificial oxidative templates, Macromolecules 44 (2011) 9319-9323.
[98] Q. Liu, L. Zang, C. Yang, C. Wei, J. Qiu, C. Liu, X. Xu, A Flexible and Knittable Fiber Supercapacitor for Wearable Energy Storage with High Energy Density and Mechanical Robustness, J. Electrochem. Soc. 165 (2018) A1515-A1522.
[99] Z. Yang, J. Ma, B. Bai, A. Qiu, D. Losic, D. Shi, M. Chen, Free-standing PEDOT/polyaniline conductive polymer hydrogel for flexible solid-state supercapacitors, Electrochim. Acta 322 (2019) 134769.
[100] W. Li, F. Gao, X. Wang, N. Zhang, M. Ma, Strong and robust polyaniline-based supramolecular hydrogels for flexible supercapacitors, Angew. Chem. Int. Ed. 55 (2016) 9196-9201.
[101] L. Zang, Q. Liu, J. Qiu, C. Yang, C. Wei, C. Liu, L. Lao, Design and fabrication of an all-solid-state polymer supercapacitor with highly mechanical flexibility based on polypyrrole hydrogel, ACS Appl. Mater. Interfaces 9 (2017) 33941-33947.

Chapter 2 Materials, experimental methods and characterizations

2.1 Materials

2.1.1 Chemical reagents

Pyrrole, ferric chloride hexahydrate ($FeCl_3 \cdot 6H_2O$), p-Toluenesulfonic acid sodium (TOSNa), polyvinyl alcohol (PVA, degree of polymerization 2000), ethylene glycol (EG), glutaraldehyde (GA, 25%), Sulfuric acid (H_2SO_4, 98%) were analytical grade and purchased from Nacalai Tesque, Inc. Poly(3,4-ethylenedioxythiophene):polystyrene sulfonate (PEDOT:PSS) aqueous suspension (CLEVIOS, PH1000, 1 wt%~1.3 wt%) was obtained from Sato Chemical Industry Co., Ltd. Commercialized fiberglass cloth (FC) was sourced from Chongqing international composite materials Co. Ltd. Commercial melamine foam (MF) was purchased from Enwode New Materials Co. Ltd.

2.2 General experimental methods

2.2.1 Synthesis of polypyrrole

1) Gas-phase polymerization of pyrrole

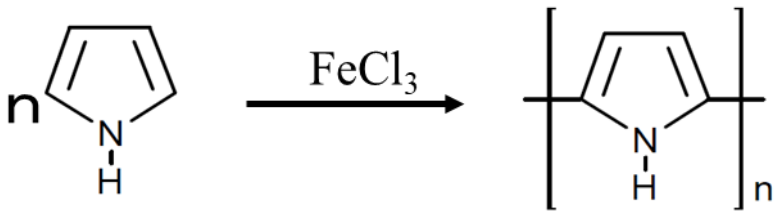

Fig. 2.1 Reaction equation for gas-phase polymerization of polypyrrole.

The gas-phase polymerization of pyrrole is carried out in pyrrole vapor with $FeCl_3$ as the oxidant, and the reaction equation is shown in **Fig. 2.1**. The specific experimental method is to soak the flexible substrate material in an ethanolic solution of $FeCl_3$ to

make it fully absorb the oxidant, and then place the flexible substrate material full of oxidant in pyrrole vapor and react for a certain time at low temperature (4°C).

2) Electrochemical polymerization of pyrrole

The electrochemical polymerization of PPy was carried out in a two-electrode system. A mixture of pyrrole (0.1 M) and sodium p-toluenesulfonate (TOSNa, 0.15 M) was used as the electrolyte, the substrate material on which the PPy was to be deposited was used as the working electrode, and a stainless steel mesh was used as the counter electrode. PPy was deposited on the substrate material by adopting the constant voltage of 2 V for the desired time at room temperature.

2.2.2 Preparation of cross-linked PVA hydrogel

The chemically cross-linked PVA hydrogel is obtained by the acid-catalyzed reaction of PVA and glutaraldehyde, the reaction equation of which is shown in **Fig. 2.2.** The PVA powder (2 g) was dissolved in dilute sulfuric acid (0.5 M, 40 mL) by heating in a water bath (90 °C) with mechanical stirring to obtain a homogeneous solution. After the PVA solution was cooled, added GA solution (1%, 4 mL) while stirring, and then pour it into the Teflon mold. After standing in a thermostat at 25 °C for 24 h, the chemically crosslinked PVA hydrogel film is obtained by peeling off the mold.

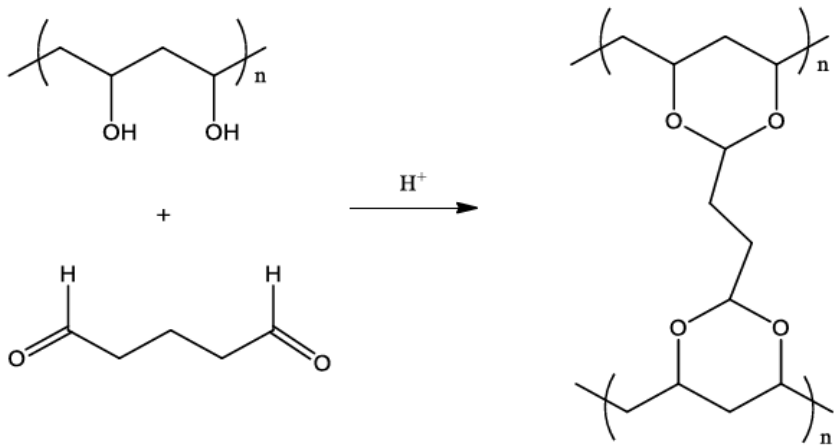

Fig. 2.2 Reaction equation of chemical cross-linking of PVA.

2.2.3 Preparation of cross-linked PVA/PEDOT:PSS hydrogel

PVA/PEDOT:PSS hydrogels are obtained by physical cross-linking with the following scheme. 10 g of PVA was added to 90 g of deionized water and mechanical stirring at 90 °C for 3 h until the PVA was completely dissolved (solution became transparent). Then the PEDOT:PSS dispersion and as-prepared PVA solution were mixed with a volume ratio of 1:1 and stirred for 2 h to mix thoroughly. After ultrasonication and evacuation to remove small bubbles, the mixture was poured into a Teflon mold, and then placed in a refrigerator at −25 °C for 24 h. Then it was taken out and thawed at 4 °C for 3 h. The freezing and thawing cycles were repeated three times. After that, the crosslinked PPPH was immersed in the EG solution for 3 h, and the excess EG on the surface was removed after cleaning to obtain EG-PPPH composite electrode.

2.3 Characterizations

2.3.1 Morphological, structure, component characterizations

1) Scanning electron microscopy (SEM)

Prior to sample testing, gold spraying is performed using an Ion sputterer (E-1030; Hitachi, Japan) to enhance the conductivity of the sample surface. Afterwards, morphological analysis is performed using an electron scanning microscope (SEM; Hitachi S-4300, Japan; SEM; Hitachi S-4800, Japan).

2) Energy-dispersive X-ray spectroscopy (EDS)

The EDS elemental mapping was obtained by an Energy Dispersive Spectrometer (Apollo XV, EDAX, USA).

3) Brunauer-Emmett-Teller (BET)

The specific surface area of the samples investigated by multi-point BET at 77 K using an Accelerated Surface Area and Porosimetry System (ASAP 2020; Micromeritics, USA).

4) Fourier transform infrared spectroscopy (FTIR)

The chemical structures of the samples were confirmed by Fourier transform infrared (FTIR, IN10MX, Thermo Fischer Scientific, USA) spectroscopy using KBr pellets.

5) Raman spectroscopy (Raman)

The chemical structure of the samples was characterized by a Raman spectrometer (Thermo Scientific DXR, USA).

6) X-ray diffraction (XRD)

The crystallographic structure of samples was tested by an X-ray diffraction system in the range of 2θ=5~90° by step scanning with a diffractometer (XRD-6000, Shimadzu Co., Ltd., Kyoto, Japan). Nickel-filter Cu Kα radiation (λ=0.15417 nm) was used with a generator voltage of 40 kV and a current of 30 mA.

2.3.2 Mechanical performance characterization

The tensile properties and compression properties were measured on a universal mechanical tester (Instron 3385, Instron Co., Ltd., Canton, USA). The tensile test was carried out on the rectangular specimens of 10 mm width × 30 mm length × 1 mm depth, with a gauge length, was 10 mm, with a stretching speed of 20 mm min^{-1} at room temperature. The compression test was performed on the cubic specimens of 10 mm with a constant speed of 10 mm min^{-1} at room temperature.

2.3.3 Electrochemical performance characterization

1) Electrochemical tests

The electrochemical tests were measured with an electrochemical workstation (CHI660E, Chen Hua, China; CS2350H, CORRTEST, China) in the three or two-electrode system. In a three-electrode test system, the platinum electrode is the counter electrode, the saturated calomel electrode is the reference electrode, and the 1 M H_2SO_4 solution is the electrolyte. The two-electrode system is assembled by two working electrodes, that is, an assembled supercapacitor. The electrochemical performance of

electrodes and devices is evaluated by 4 test items: Cyclic voltammetry (CV) and Galvanostatic Charge-Discharge (GCD), Electrochemical impedance spectroscopy (EIS), and cycle stability. CV and GCD tests were performed at different scan rates and current densities in specific potential windows, respectively. EIS test was performed at open circuit potentials in the frequency range of 10^6 to 10^{-2} Hz with an amplitude of 5 mV. Cyclic stability is a cyclic GCD test under a certain current density.

2) Calculation formula of electrochemical performance

Specific capacitance is an extremely important index for evaluating electrode materials and the entire device. The specific capacitance can be calculated from both CV curve data and GCD curve data. Because of the calculation result is more accurate using GCD curve data, the GCD curve data is usually used to calculate the specific capacitance. The calculation formula of the specific capacitance (C)is as follows:

$$C = \frac{I\Delta t}{2U} \qquad 2.1$$

where Δt is the discharged time (s); U is the discharged potential (V); I is the current density, the current density can be mass current density (A g^{-1}), area current density (A cm^{-2}), volume current density (A cm^{-3}).

Energy density and power density are also important parameters of supercapacitors. At this stage, the power of supercapacitors is already very high, and researchers are focusing on improving the energy density of the devices. Like the specific capacitance, energy density and power density are also divided into mass, area, and volume. In general, large devices are calculated using mass density, while small devices are more often calculated using area or volumetric density. The energy density (E) and power density (P) are calculated by the following equations.

$$E = \frac{1}{2 \times 3600} CU^2 \qquad 2.2$$

$$P = \frac{3600E}{\Delta t} \qquad 2.3$$

where C is the specific capacitance, U is the voltage window (V), and Δt is the discharge time (s).

Chapter 3 Textile-based flexible supercapacitors based on fiberglass cloth/polypyrrole composite electrodes

3.1 Introduction

Wearable electronic products have attracted widespread attention from both academia and industry.[1-6] Comfort is regarded as one of the most significant indicators of wearable electronics. The ideal wearable device electronics are supposed to feature lightweight, breathability, flexibility, and comfort, which requires the energy storage device to show the corresponding characteristics.[7] Supercapacitors have drawn increasing attention due to their high power density, long life cycle, high security, and ease of integration with wearable electronic device systems.[8-14] As for the manufacture of wearable supercapacitors, a major strategy is to coat electroactive materials on a variety of different flexible substrates. Flexible substrate materials, such as textiles,[1] carbon cloth,[13] plastic film,[14] metal fiber[15], and paper[16] are commonly used. Recently, plenty of studies have been conducted on flexible electrodes for various electroactive materials, which include carbon materials, metal oxides, and conductive polymers,[17-20] using such methods as immersion plating, steam coating, electrochemical deposition, in-situ solution polymerization.[21-23]

Textiles are one of the substrates suitable for the manufacture of energy-supplied devices used on wearable electronic products due to their lightweight, excellent air permeability, low cost, and ease to produce on a large scale.[24-26] Polypyrrole (PPy) is classed as a conductive polymer. It is an attractive electroactive material with high conductivity, easy preparation, environmental friendliness, excellent biocompatibility, and effective substrate adhesion, a combination of which makes it suited to energy storage, especially supercapacitor electrode materials. Recently, there have been reports on various textile PPy composite electrode materials. For instance, Yue et al. coated PPy onto commercial nylon lycra fabrics by chemical polymerization for the fabrication of

stretchable electrodes.[27] Liu and his working group fabricated a three-dimensional interconnected PPy nanowires/nanofibrous textile composite electrode through in-situ polymerization of PPy on a PVA-*co*-PE textile.[28] These works provided an effective guidance for the study of fabric-based supercapacitors, which is despite such drawbacks as insufficient capacitance. As these fabrics are electrically insulated, the electrodeposition method is impractical, which makes it necessary to choose chemical polymerization. However, the electrochemical performance of composite electrodes derived from chemical polymerization is usually less desirable than if electrochemical polymerization is chosen. To obtain high-performance electrode materials, the pretreatment of the fabric to obtain conductivity before electrochemical polymerization provides an effective way. A common method is to conduct fabrics by impregnating carbon materials. For example, the group led by Zhi designed a stretchable yarn electrode by impregnating CNTs and electrodeposited PPy on polyurethane fabric yarns, based on which excellent specific capacitance is achieved.[29] Nonetheless, it is not an ideal choice to achieve conductivity by impregnating carbon materials, as the bond between carbon materials and the fabric is of insufficient strength, which could have a negative impact on the cycle stability of the electrode. Besides, regarding the choice of textiles, the organic fabrics used in these works cannot withstand high temperatures and flame retardants, limiting their application environment. Therefore, it is a pressing need to find not only a suitable pretreatment method but also a base fabric.

In this study, a novel pretreatment method was applied, that is, gas-phase polymerization, and an inorganic fabric with flame retardancy and the general properties shown by organic fabrics, fiberglass cloth, was selected to prepare flexibility electrodes with high mechanical strength and high electrochemical for assembly into supercapacitors. Firstly, the conductive fiberglass cloth (CFC) was derived from gas-phase polymerization of pyrrole. Then, through electrochemical polymerization, a layer of PPy with a unique morphology was attached to the surface of the conductive fiberglass cloth for PPy/CFC composite electrode to be obtained. Finally, the supercapacitor was fabricated by sandwiching two PPy/CFC composite and a layer of PVA-H_2SO_4 gel electrolyte.

Compared with the fabric-based supercapacitors as reported previously, our device shows such advantages as simpler manufacturing processes and higher electrochemical performance. Moreover, it exhibits excellent flexibility and is capable of operating at

different bending angles. Otherwise, this device shows good flame retardancy. The assembled PPy/CFC supercapacitor could reach a maximum specific capacitance of 549.6 mF cm^{-2} and a high energy density of 48.85 μWh cm^{-2}. For demonstration, two PPy/CFC supercapacitors connected in series are used to drive an LCD electronic watch.

3.2 Experimental section

3.2.1 Materials

Pyrrole, ferric chloride hexahydrate ($FeCl_3 \cdot 6H_2O$), p-Toluenesulfonic acid sodium (TOSNa), polyvinyl alcohol (PVA), and Sulfuric acid (H_2SO_4, 98%) were purchased from Aladdin Co. Ltd. Commercialized fiberglass cloth (FC) was sourced from Chongqing international composite materials Co. Ltd.

3.2.2 Preparation of conductive fiberglass cloth

The conductive fiberglass cloth (CFC) was prepared by gas-phase polymerization of pyrrole. Firstly, FC sized 4 cm×4 cm was ultrasonically cleaned with ethanol, before drying. Then, the washed and dried FC was immersed in the ferric chloride ethanol solution (115 g L^{-1}) for 2 hours, followed by drying in an oven at 40 °C. Subsequently, the FC was placed in a vacuum dryer filled with pyrrole vapor and polymerized at 4 °C for 4 hours. After washing and drying, the CFC was obtained.

3.2.3 Fabrication of PPy/CFC composite

The PPy with a unique microstructure was electrochemically deposited on the surface of the CFC to fabricate PPy/CFC composites. Typically, a CFC sized 1 cm×2 cm was taken as a working electrode, and a ring-shaped 304 stainless steel wire mesh was taken as the counter electrode. Electrodeposition was performed in a mixed aqueous solution of 0.1 M pyrrole and 0.15 M TOSNa at room temperature with a constant voltage of 2.0 V for a certain time. The duration of polymerization was 30, 60, and 90 min, respectively. The as-prepared PPy/CFC composites were washed with deionized water, dried in a 45 °C drying oven, and then labeled as V-PPy/CFC-30, V-PPy/CFC-60, V-PPy/CFC-90, respectively. For comparison purposes, the other PPy/CFC composite was prepared to employ constant current electrochemical polymerization. The

polymerization electrolyte and the polymerization time were identical to the previous constant voltage polymerization. The polymerization current was set to 1 mA cm^{-2}, and the obtained sample was named C-PPy/CFC.

3.2.4 Fabrication of the PPy/CFC supercapacitor

The electrolyte used to assemble the device was PVA/H_2SO_4 gel, the percentage by mass of PVA was 10%, and the concentration of sulfuric acid was 1 M. Prior to assembly, the CFC electrodes were soaked in PVA/H_2SO_4 gel for 30 minutes. Subsequently, the CFC supercapacitor was assembled from two V-PPy/CFC electrodes sandwiching a gel electrolyte. Finally, to prevent the evaporation of moisture in the electrolyte, a layer of PP film was coated on the outside of the assembled supercapacitor.

3.2.5 Characterization

The FTIR spectrum was obtained by a Thermo Scientific Nicolet iN10 Infrared Microscope. The EDS elemental mapping was obtained by an Energy Dispersive Spectrometer (EDAX, USA). The specific surface area of the samples was investigated by Multi-point BET at 77 K using ASAP 2020 analyzer (Micromeritics, USA). The SEM image of the CFC electrode was measured by a field emission scanning electron microscope (S-4800, HITACHI, Japan). All of the data on electrochemical performance was tested by an electrochemical workstation (CHI660E, CHENHUA, China). The tests on CFC electrodes were performed using a platinum electrode as the counter electrode, Ag/AgCl electrode as reference electrode, and 1 M H_2SO_4 solution as the electrolyte. Moreover, the electrochemical performances of the device were evaluated in a two-electrode system. The calculation formulas of the electrochemical performance of CFC electrodes and their devices are expressed as follows:

$$C_{a,electrode} = \frac{I \times \Delta t}{S \times U} \quad (1)$$

$$C_a = \frac{I \times \Delta t}{2S \times U} \quad (2)$$

$$E_a = \frac{C_a \times U^2}{2 \times 3600} \quad (3)$$

$$P_a = \frac{3600 E_a}{\Delta t} \quad (4)$$

Where $C_{a,electrode}$ represents the area-specific capacitance of the electrode; C_a, E_a, and P_a

denote the specific capacitance, energy density, and power density of the device, respectively; I refers to current (A); Δt indicates discharged time (s); U stands for potential window (V); S denotes the area of one side electrode (cm^2).

3.3 Results and Discussion

3.3.1 Analysis of the preparation process

Fiberglass cloth (FC) was selected as the textile substrate due to its general properties of common fabrics, excellent mechanical properties, and effective resistance to heat, acid, and alkali. The general preparation process of the PPy/CFC supercapacitor is illustrated in **Fig. 3.1**. The PPy-based textiles, including V-PPy/CFC and C-PPy/CFC, were synthesized by going through a facile two-step polymerization process. The first step in polymerization is gas phase polymerization, the purpose of which is to make the insulated fiberglass cloth conductive.

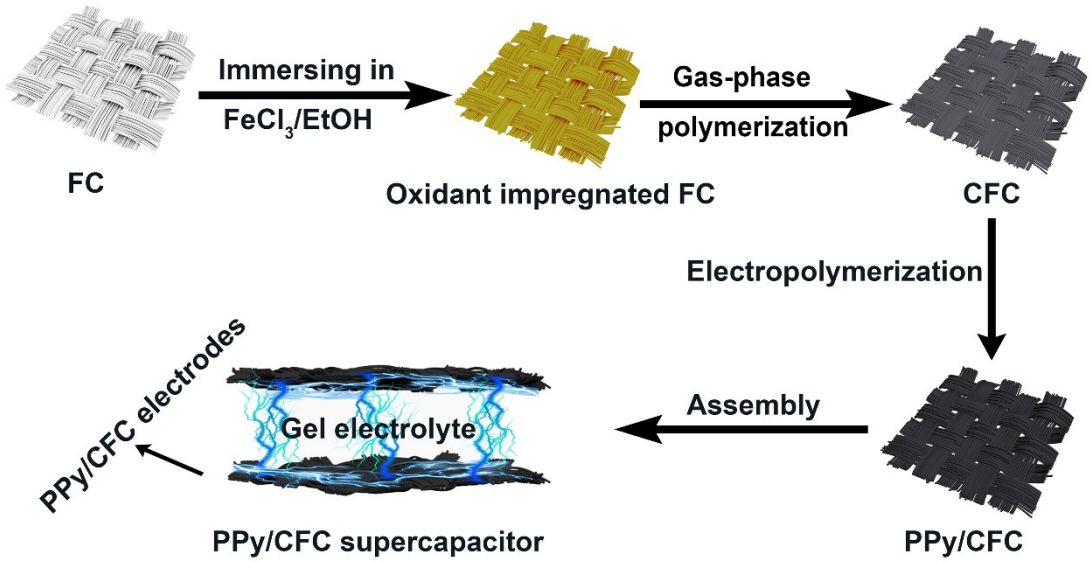

Fig. 3.1 Schematic illustration of preparation process of the PPy/CFC flexible supercapacitor.

Prior to the gas phase polymerization, the FC was immersed in the ferric chloride ethanol solution to fully adsorb $FeCl_3$, and the FC was changed from the original white to the golden yellow, as shown in **Fig. 3.2**. The oxidant impregnated FC plays multiple roles in the process of polymerization, with FC as a matrix, Fe^{3+}, and Cl^- as oxidants and dopants for gas-phase polymerization of PPy, respectively. When the pyrrole vapor

comes into contact with the oxidant impregnated FC, it will polymerize on the surface of the FC to form a black layer of PPy (**Fig. 3.2**). Then, an antennae-like PPy was constructed by electrochemical polymerization on the surface of the CFC. PPy is classed into a pseudocapacitance material, and the horn structure is capable to increase its specific surface area (The specific surface area of CFC and PPy/CFC was calculated to be 31.3 and 43.8 m^2 g^{-1}, respectively.), thereby improving the specific capacitance. Finally, a sandwich supercapacitor was assembled by PVA/H_2SO_4 gel and two PPy/CFC composites.

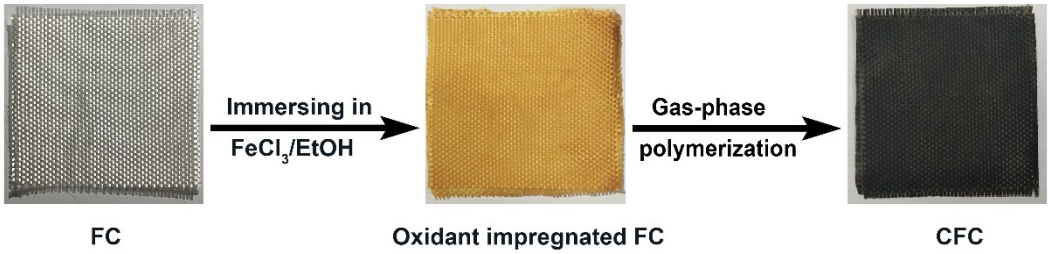

Fig. 3.2 The manufacturing process of the conductive glass fiber cloth (CFC).

3.3.2 Chemical composition and micromorphological characterization

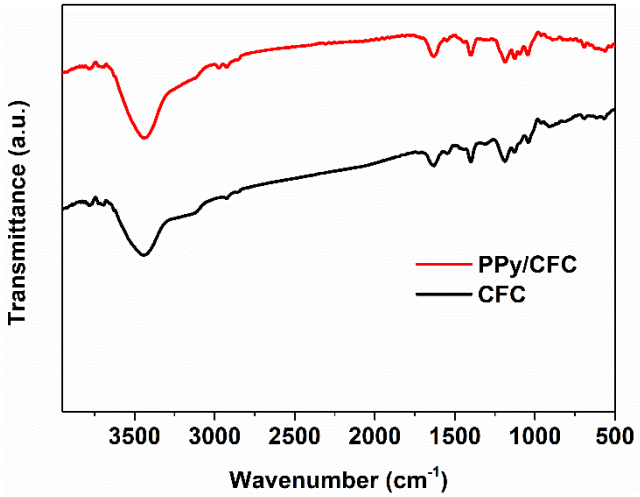

Fig. 3.3 FTIR spectra of the CFC and PPy/CFC.

Both of the FTIR spectra of the CFC and PPy/CFC electrode (**Fig. 3.3**) show the characteristic absorption peaks of PPy, including the peak of C−C stretching vibration absorption at 1548 cm^{-1}, the C−N stretching vibration absorption at 1400 cm^{-1},

breathing vibration of the pyrrole ring at 1187 cm^{-1}, and the in-plane deformation vibrations peaks for N−H and C−H at 1630 cm^{-1} and 1040 cm^{-1}, which indicate that the PPy was successfully synthesized.[30-32] In order to further prove the presence and distribution status of PPy, EDS elemental mapping of C, N, and Cl for CFC and C, N and S for PPy/CFC electrode are shown in **Fig. 3.4**. The existence of N elements proves the successful preparation of PPy. The Cl elements of the CFC and the S elements of the PPy/CFC come from the dopants in the synthesis process, respectively. In addition, the homogeneous brightness and distribution of elements can indicate that the uniformity of PPy distribution is good.

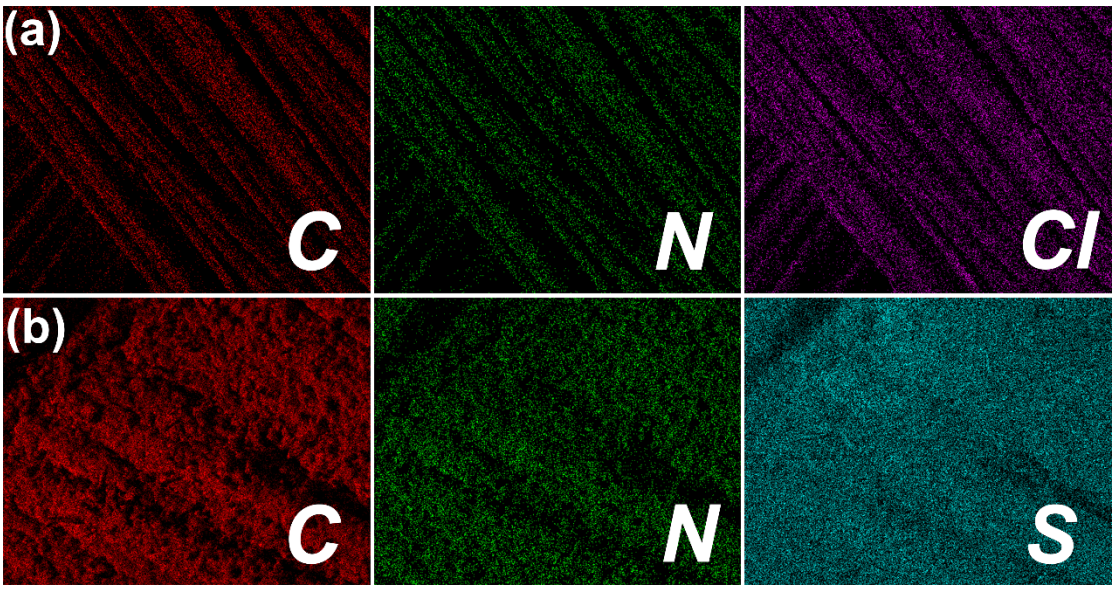

Fig. 3.4 Elemental mapping of (a) CFC and (b) PPy/CFC.

As shown in **Fig. 3.5**, Owing to the excellent mechanical strength of the fiberglass cloth, the ultimate PPy/CFC composite electrode material reaches a maximum tensile strength of 95.6 MPa. In addition, PPy/CFC composite electrode exhibits excellent flame retardancy, it is unlikely to be ignited even in the flame of an alcohol lamp, which is significant to the safety of energy storage devices.

The surface morphologies of the FC before and after gas phase polymerization are illustrated in **Fig. 3.6**. The FC comprised of crisscrossed glass monofilaments shows an average diameter of about 9 μm, as shown in **Fig. 3.6a**. As shown in **Fig. 3.6b**, the surface of each glass fiber monofilament is coated with a layer of irregular agglomerations of PPy particles after gas phase polymerization. The PPy layer coated

on the surface of the glass monofilament enables FC to obtain a conductive and rough surface, which creates favorable conditions for the next-step electrochemical polymerization of antenna-like PPy.

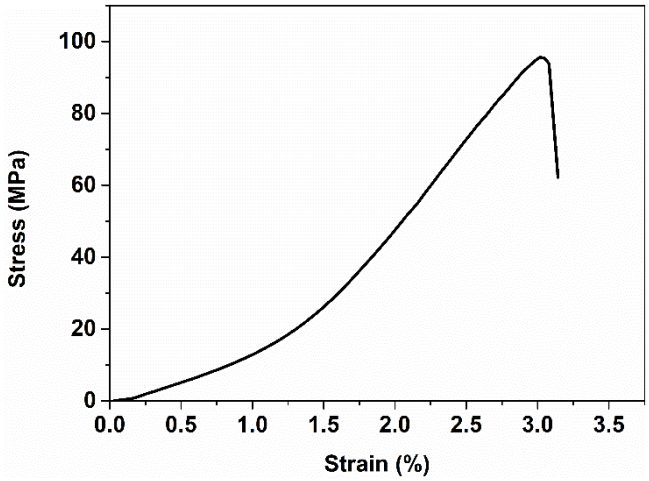

Fig. 3.5 The stress-strain curve of PPy/CFC composite.

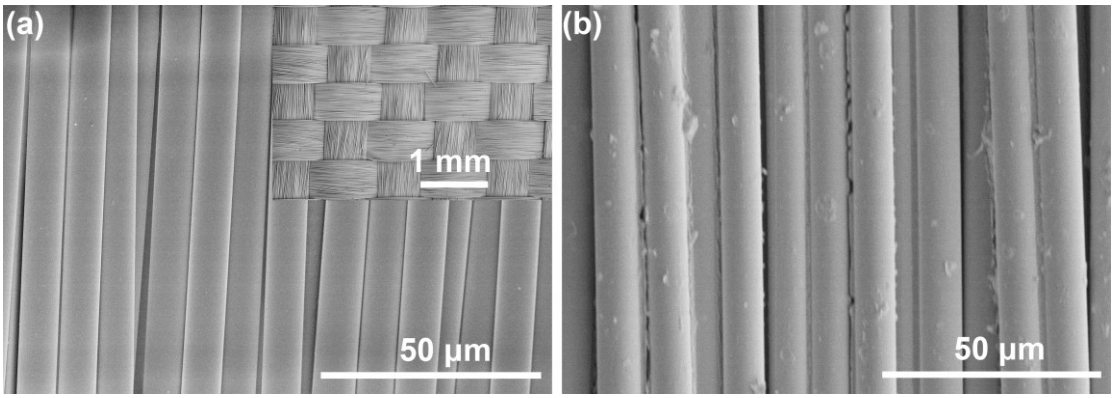

Fig. 3.6 SEM images of (a) FC and (b) conductive fiberglass cloth (CFC).

The growth mechanism of antennae-like PPy is primarily associated with the template effect of TOS^-, and is related to Polymerization conditions.[15, 33-37] To reveal the effect of polymerization conditions on the development of antennae-like PPy, potentiostatic and galvanostatic methods were applied for the preparation of PPy/CFC composite. **Fig. 3.7** shows the micromorphology of the V-PPy/CFC composites and C-PPy/CFC composites with different deposition times. The SEM images of V-PPy/CFC-30, V-PPy/CFC-60, V-PPy/CFC-90 are shown in **Fig. 3.7a, 3.7b, and 3.7c**, respectively. Compared with the surface of the CFC, the irregularly agglomerated PPy particles on the surface of the CFC show a significant increase in density after 30 minutes of

polymerization (**Fig 3.7a**). As the polymerization time is extended, an antennae-like PPy layer with a granular surface covers the entire surface of the CFC. Besides, the longer the polymerization time is, the denser PPy tentacles are. Different glass fiber monofilaments are capable to be connected by PPy tentacles, thus forming an interconnected network structure (**Fig. 3.7b,3.7c**). For C-PPy/CFC composites, the irregular PPy particles are deposited on the surface of CFC. Even though the polymerization time is extended, there are still no PPy tentacles, and only the irregularly agglomerated PPy particles become larger (**Fig 3.7d,3.7e,3.7f**), which indicates that the potentiostatic polymerization method is more likely to obtain PPy with extraordinary morphology. Not only do the PPy tentacles provide a larger specific surface area, but they also provide a better conductive path, which is advantageous to improve electrochemical performance.

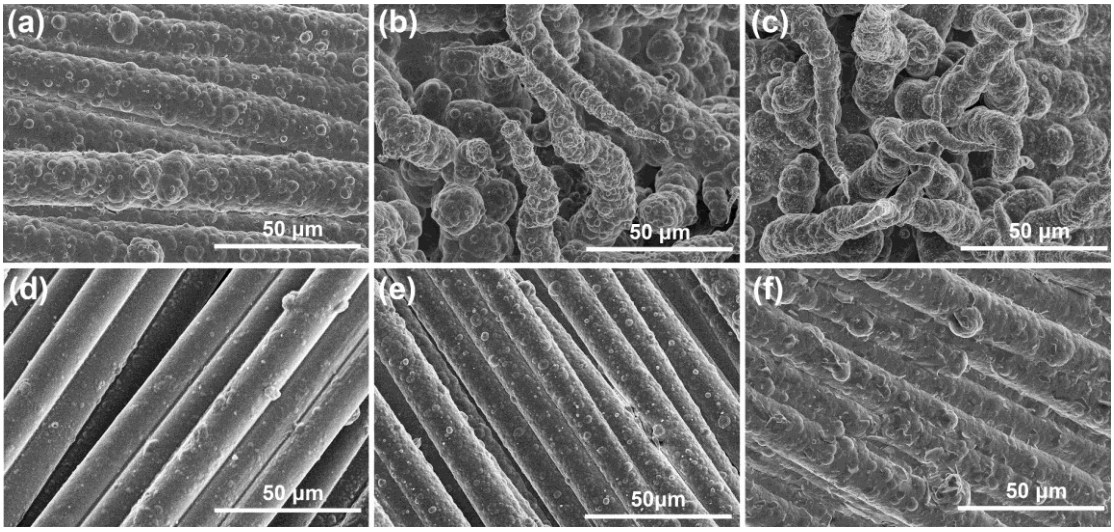

Fig. 3.7 SEM images of (a) V-PPy/CFC-30, (b) V-PPy/CFC-60, (c) V-PPy/CFC-90, (d) C-PPy/CFC-30, (e) C-PPy/CFC-60 and (f) C-PPy/CFC-90.

3.3.3 Electrochemical properties and mechanical stability

The electrochemical properties of V-PPy/CFC and C-PPy/CFC composites with different deposition times were evaluated by CV, GCD, and EIS in a three-electrode system, with the results presented in **Fig. 3.8** and **Fig. 3.9**. Through a comprehensive comparison of the CV curves, the GCD curves, and the Nyquist plots, it can be concluded that extending the polymerization time is effective in enhancing the

electrochemical performance of the composite electrode. Despite this, the polymerization time is excessively long, which will affect its electrochemical properties, which can be accounted for by the previous SEM images. As the polymerization time is extended, the amount of polymerized PPy increases, which improves electrochemical performance. However, excessive PPy will lead to the excessive accumulation of PPy, which is adverse to electrolyte penetration. The PPy present in the inner layer can neither make contact with the electrolyte nor perform its function, which causes the electrochemical performance to deteriorate. Therefore, both V-PPy/CFC-60 and C-PPy/CFC-60 show the most desirable performance in their respective comparison groups. In order to further compare the electrochemical properties of samples as prepared using the potentiostatic method and the galvanostatic method, V-PPy/CFC-60 and C-PPy/CFC-60 were compared thoroughly.

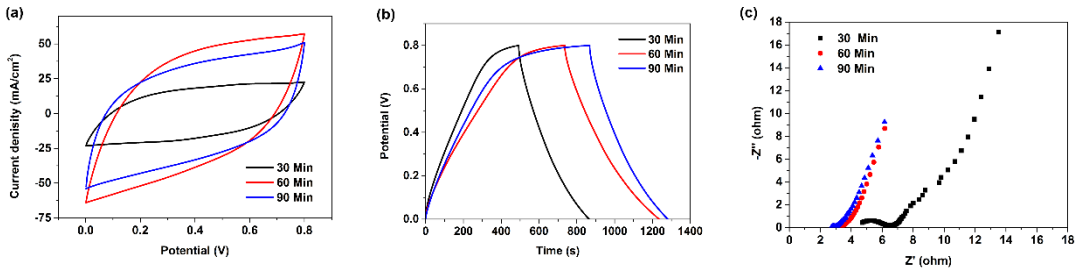

Fig. 3.8 CV curves (a), GCD curves (b), and Nyquist plot (c) of V-PPy/CFC electrode with different polymerization time.

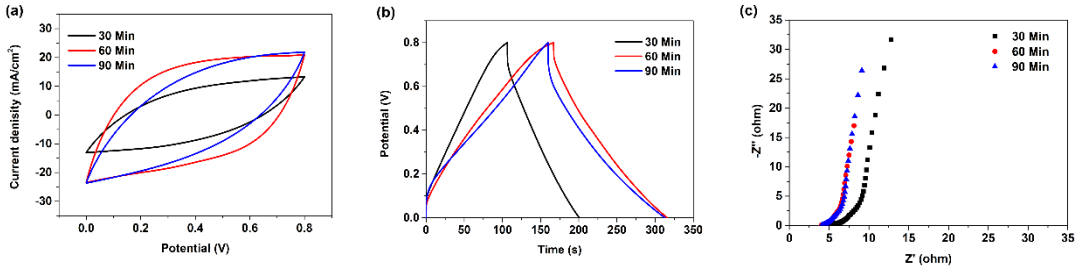

Fig. 3.9 CV curves (a), GCD curves (b), and Nyquist plot (c) of C-PPy/CFC electrode with different polymerization times.

Fig. 3.10a shows a comparison of CV curves between V-PPy/CFC-60 and C-PPy/CFC-60. It can be seen from the two figures that all CV curves exhibit a near-rectangular shape, while the CV curve of V-PPy/CFC-60 shows a closed area that is more than three times as large as C-PPy/CFC-60. The significantly larger closed area of

V-PPy/CFC-60 indicates that V-PPy/CFC-60 has a higher specific capacitance compared to C-PPy/CFC-60. Similarly, V-PPy/CFC-60 has a longer discharge time than C-PPy/CFC-60 as shown in **Fig. 3.10b**. **Fig. 3.10c** presents the comparison of specific capacitance at different current densities. The area-specific capacitances of V-PPy/CFC-60 and C-PPy/CFC-60 are 2747 mF cm^{-2} and 873 mF cm^{-2} at 2 mA cm^{-2}, while the specific capacitance are 1959 mF cm^{-2} and 429 mF cm^{-2} at 16 mA cm^{-2}, respectively. The mass loading of PPy on V-PPy/CFC-60 is 2.93 mg cm^{-2}, which exceeds twice the 1.43 mg cm^{-2} on C-PPy/CFC-60. The mass-specific capacitance of V-PPy/CFC-60 and C-PPy/CFC-60 is 937.5 F g^{-1} and 610.5 F g^{-1} at 2 mA cm^{-2}, while the mass-specific capacitance is 668.6 F g^{-1} and 300 F g^{-1} at 16 mA cm^{-2}, respectively. The capacitance retention from 2 mA cm^{-2} to 16 mA cm^{-2} are 71.3% (V-PPy/CFC-60) and 49.1% (C-PPy/CFC-60). Obviously, V-PPy/CFC-60 has a higher specific capacitance and a superior rate performance. The Nyquist plot of V-PPy/CFC-60 and C-PPy/CFC-60 is shown in **Fig. 3.10d**. The equivalent series resistance (Rs) is obtained by the value of the intercept on the horizontal axis, and charge-transfer resistance (Rct) is achieved by the diameter of the semicircle in the high-frequency region. The Rs of V-PPy/CFC-60 is 2.78 Ω, which is lower compared to C-PPy/CFC-60 (Rs = 3.98 Ω), and the Rct of V-PPy/CFC-60 is 0.43 Ω, which is similar to that of C-PPy/CFC-60 (Rct = 0.31 Ω). The lower Rs of V-PPy/CFC-60 is attributed to the extraordinary tentacle structure, while PPy tentacles provide a larger specific surface area and more sufficient contact with the electrolyte.

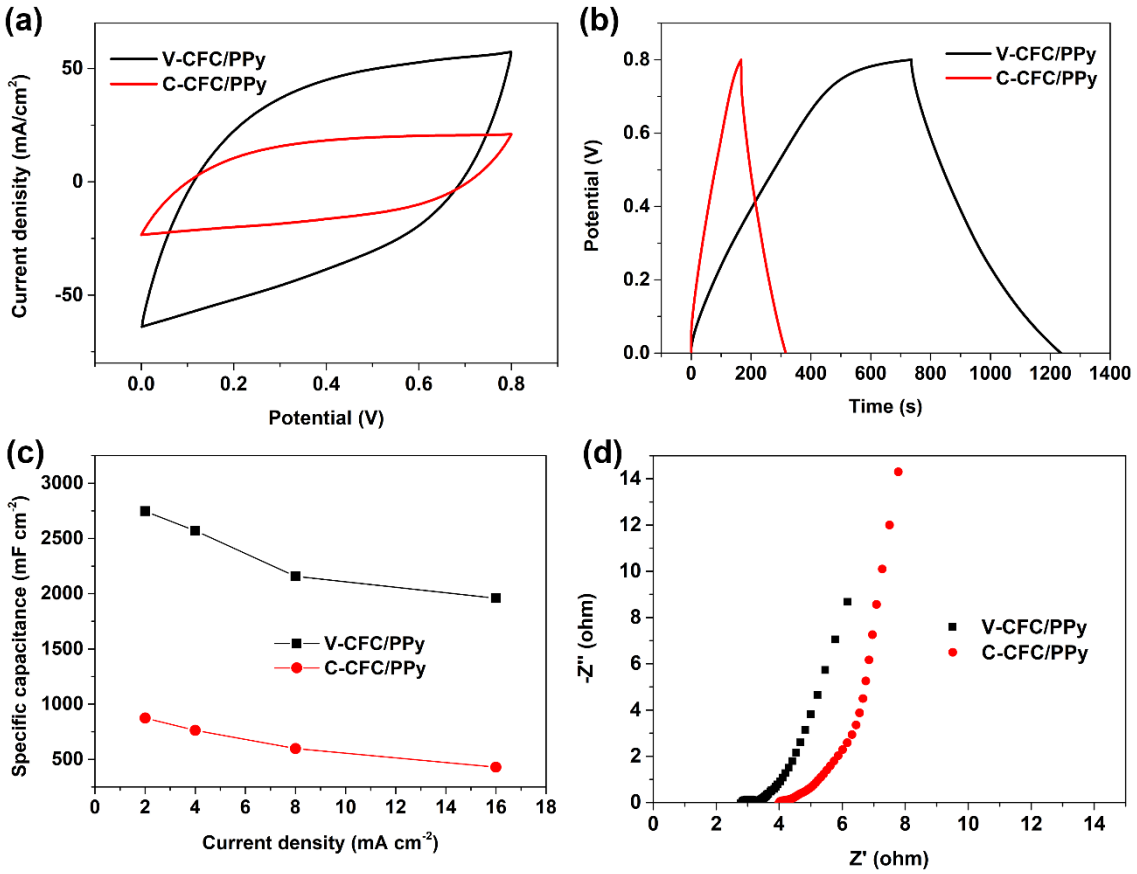

Fig. 3.10 Comparison of the electrochemical performance of V-PPy/CFC-60 and C-PPy/CFC-60. (a) CV curves of V-PPy/CFC-60 and C-PPy/CFC-60 at the scan rate of 40 mV s^{-1}; (b) GCD curves of V-PPy/CFC-60 and C-PPy/CFC-60 at the current density of 4 mA cm^{-2}; (c) Specific capacitance at different current density; (d) Nyquist plots in the frequency range from 0.01 Hz to 100 kHz.

All of the aforementioned data have demonstrated that V-PPy/CFC-60 has a better electrochemical performance, which is due to the following reasons: (1) The PPy tentacles are effective in expanding the actual contact area between PPy and electrolyte. In addition, PPy tentacles provide a larger specific surface area while improving the electric double-layer capacitance. (2) Different glass fiber monofilaments can be connected by PPy tentacles, thus forming an interconnected network structure that could provide a convenient channel for ion/electron transfer. (3) When polymerization is performed using the potentiostatic method, the conductivity of the CFC improves and the current is on the rise gradually due to the polymerization of pyrrole. Meanwhile, the amount of charge passing is higher than that in the constant current polymerization, which increases the loading of polypyrrole. Therefore, the mass loading of PPy on V-

PPy/CFC-60 is 2.93 mg cm^{-2}, which exceeds twice the 1.43 mg cm^{-2} on C-PPy/CFC-60. In addition, the V-PPy/CFC-60 has excellent flexibility and is prone to bending, even at 180° (**Fig. 3.11**). In view of the above-mentioned excellent electrochemical and mechanical properties, V-CFC/PPy-60 as prepared by potentiostatic polymerization is more suitable as an electrode for PPy/CFC supercapacitors.

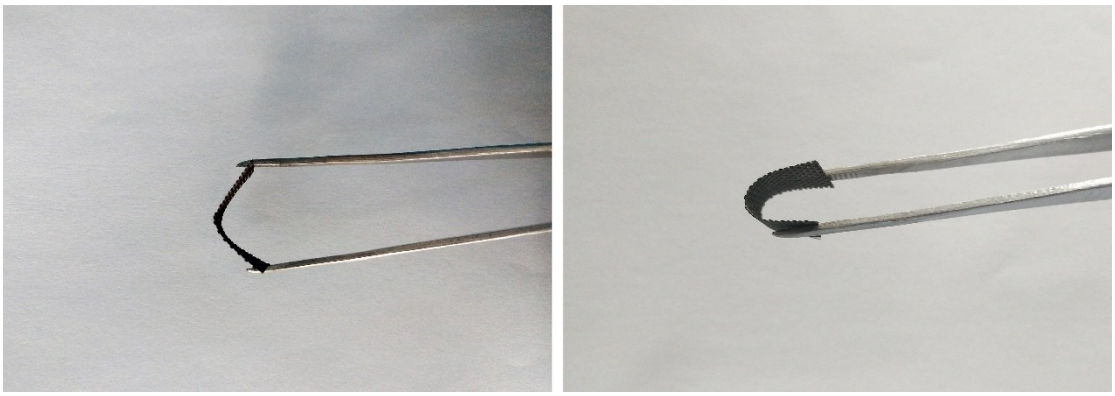

Fig. 3.11 The flexible performance of the V-PPy/CFC-60 composite.

The PPy/CFC supercapacitor was fabricated by sandwiching two V-CFC/PPy-60 composite electrodes and PVA/H_2SO_4 gel electrolyte. The Nyquist plot of the device is illustrated in **Fig. 3.12a**. The Rs and Rct of the device are 7.66 Ω and 2.68 Ω, which indicates that the device has lower internal resistance. In the intermediate frequency area, the angle between the Nyquist curve and the real axis approaches 45° which is a typical diffusion process. Besides, in the low-frequency region, the oblique line is nearly vertical to the horizontal axis, implying the desired capacitance characteristics. The CV curves of the device at different scan rates are illustrated in **Fig. 3.12b**. All of the CV curves invariably demonstrate a symmetric shape, which evidences the good capacitive behavior of the device.

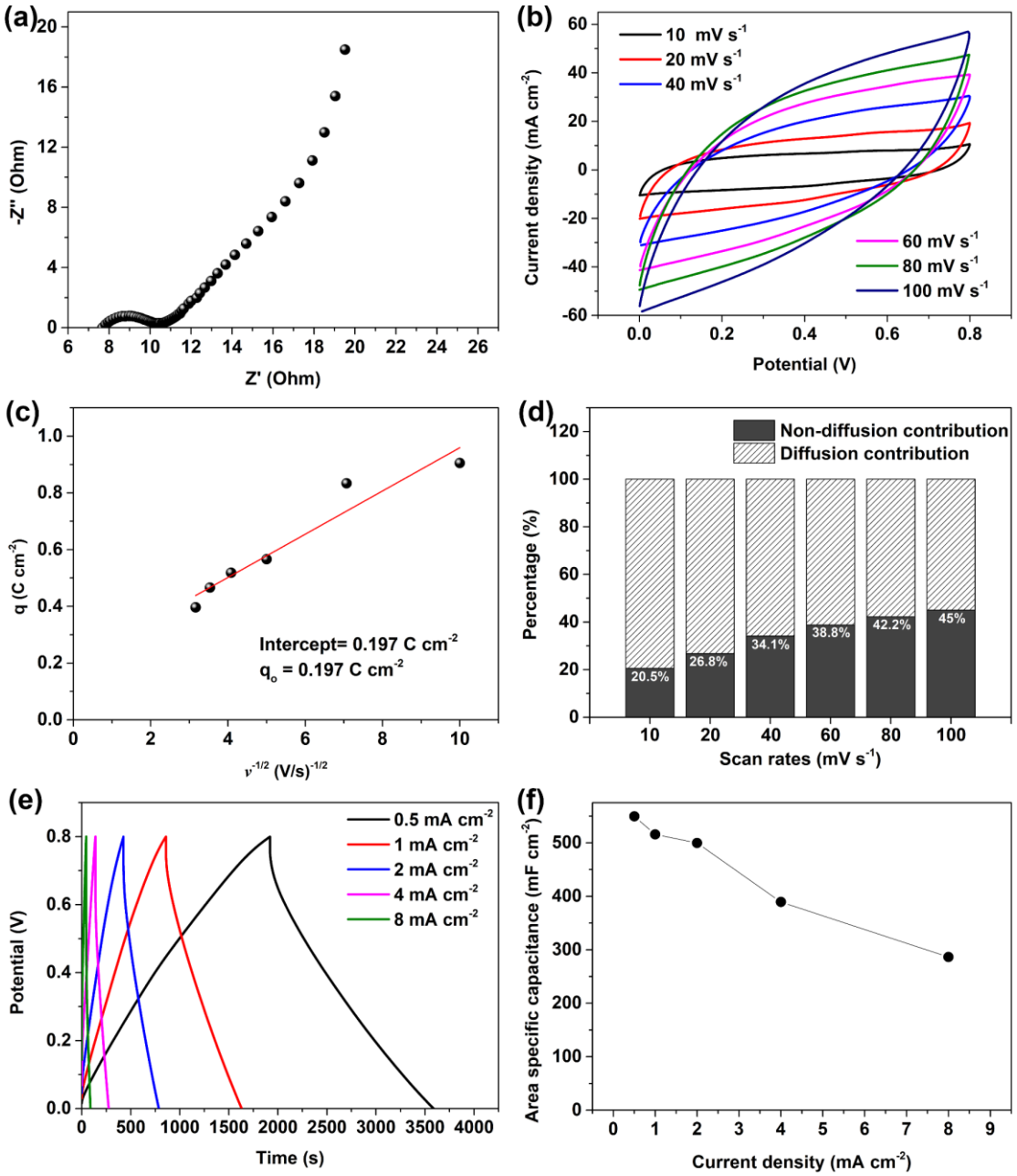

Fig. 3.12 Electrochemical properties of the device. (a) Nyquist plot; (b) CV curves at different scan rates; (c) The dependence of $q_{(v)}$ on $v^{-1/2}$; (d) The ratios of non-diffusion contribution to diffusion contribution; (e) GCD curves at different current density; (f) specific capacitance at different current density.

To study the mechanism of charge storage in this device, Trasatti analysis method was applied to assess the electrochemical kinetics, as it could quantify the charge storage on the inner surface (q_i) and outer surface (q_o) during the process of charge and discharge. The total stored charges (q_T) of the device consist of both inner and outer surface

charges as follows[38-40]:

$$q_T = q_i + q_o \quad (5)$$

The inner surface of the charge storage is a diffusion-controlled process, whereas the outer surface of the charge storage is regardless of the scan rate and diffusion. Therefore, the total charge measured by cyclic voltammetry $q_{(v)}$ can be calculated by the following formula[38-40]:

$$q_{(v)} = q_\infty + kv^{-1/2} \quad (6)$$

where $kv^{-1/2}$ is the charge storage related to semi-infinite diffusion and k is a constant.

The dependence of q on $v^{-1/2}$ is shown in **Fig. 3.12c**, which reveals that as the v is on the increase, the q declines slowly. Considering that the charge storage of q_i is determined by diffusion, the charge storage of q_o is not related to scan rate and diffusion. When the scan rate is infinite, the occurrence of charge storage is restricted to the outer surface where the ions are easily accessible. Therefore, the total charge from the cyclic voltammetry is equivalent to q_o. Based on the results of the linear fit, the q_o derived from the intercept of the fitted line on the vertical axis is 0.197 C cm^{-2}. In accordance with Formula (6), the actual charge storage from 10 to 100 mV s^{-1} were 0.959, 0.736, 0.578, 0.508, 0.466 and 0.438 C cm^{-2}, respectively.

As the storage of outer surface charge is irrelevant to scan rate and diffusion, it is considered a non-diffusion process. Therefore, the ratio of non-diffusion control contributions can be determined using the ratio of outer surface charge to the actual charge, and the ratio of non-diffusion control contributions at distinct scan rates are demonstrated in **Fig. 3.12d**, which shows that the non-diffusion contributions are 20.5% at 10 mV s^{-1} and 45% at 100 mV s^{-1}, respectively. At low scan rates, the ratio of non-diffusion contribution can still reach 20%, indicating that the non-diffusion control process is significant to the charge and discharge process. Conversely, at high scan rates, the ratio of diffusion contribution remains higher compared to non-diffusion control, which suggests that the diffusion control process has a considerable impact on charge storage. The GCD curves of the device at distinct current densities are demonstrated in **Fig. 3.12e**. All GCD curves resemble an equilateral triangle but no significant voltage drop can be observed, which indicates excellent capacitive behavior and low internal resistance. The area-specific capacitance at distinct current densities of the device is shown in **Fig. 3.12f**. The maximum area-specific capacitance of the device ($C_{a,device}$) is shown to be 549.6 mF cm^{-2}. As the current density is on the rise, the value of $C_{a,device}$

shows a gradual decline to 286.3 mF cm^{-2}. The current density is increased to 16 times, but the specific capacitance retention rate remains 52%, which implies that the device has excellent rate performance. The mass-specific capacitance ($C_{m,device}$) of the device on basis of mass per unit area (2.93 mg cm^{-2}) of active material is from 187.6 F g^{-1} to 97.7 F g^{-1}.

The area power density (P_a) and area energy density (E_a) of the device was calculated，and the result are presented in **Fig. 3.13a** as a Ragone plot. The highest E_a is 48.85 μWh cm^{-2} with the P_a of 105.4 μW cm^{-2} and maximum P_a is 2068 μW cm^{-2} at the E_a of 25.45 μWh cm^{-2}, which is higher compared to other reported fabric supercapacitors, including nonwoven fabric/RGO/MnO_2-SC (P_a was 200 μW cm^{-2} with E_a of 12.34 μWh cm^{-2}),[41] carbon fiber fabric/PANI/rGO-SC (P_a was 120 μW cm^{-2} with E_a of 28.2 μWh cm^{-2}),[42] PANI/CNT fabric -SC(P_a was 391 μW cm^{-2} with E_a of 29.4 μWh cm^{-2}),[43] dacron cloth/$Cu(OH)_2$-SC (P_a was 600 μW cm^{-2} with E_a of 36 μWh cm^{-2}),[44] rGO/CCF-SC (P_a was 124.99 μW cm^{-2} with E_a of 11.77 μWh cm^{-2}),[45] PET fabric/rGO/PPy-SC (P_a was 30 μW cm^{-2} with E_a of 11 μWh cm^{-2}),[46] graphene/PANI woven fabric-SC (P_a was 330 μW cm^{-2} with E_a of 1.5 μWh cm^{-2}).[47] The power density and energy density of the entire device based on gravimetric also be calculated. The highest mass power density (P_m) is 705.88 mW g^{-1}, the highest mass energy density (E_m) is 16.67 mWh g^{-1}.

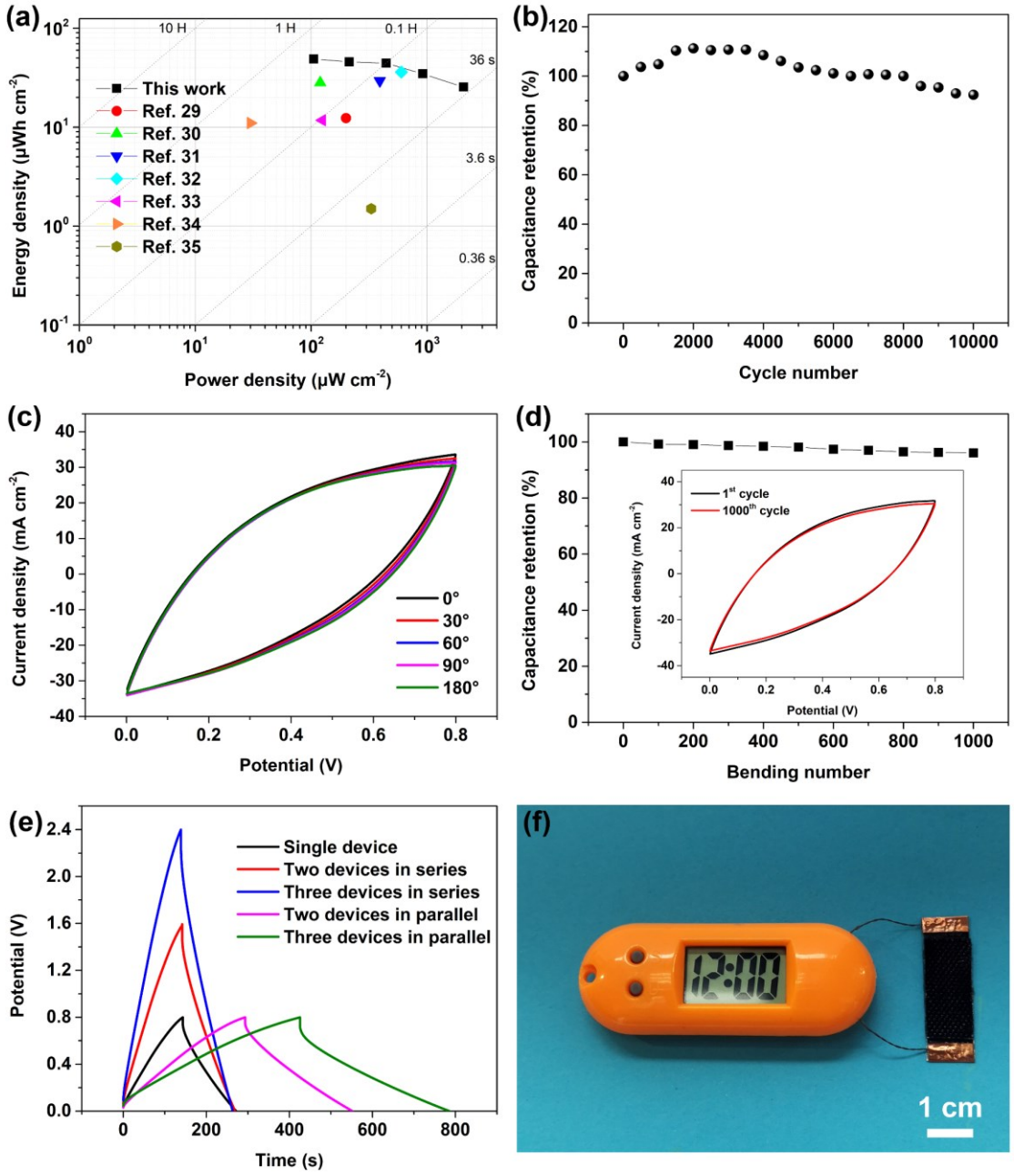

Fig. 3.13 Electrochemical properties of the device. (a) Ragone plots of the device compared to other SCs as reported recently; (b) Cycling stability and coulombic efficiency of 10,000 charge/discharge cycles; (c) CV curves of the device in different bending states at 40 mV s^{-1}; (d) Capacitance retention of the device after 1000 bends; (e) GCD curves of serial and parallel assembly of a single device and multiple devices; (f) Photographs of an LCD electronic watch powered by two CFC/PPy supercapacitors.

The cycle stability of the device was evaluated by 10,000 cycles of charge and discharge at 8 mA cm^{-2}. It can be seen from **Fig. 3.13b** that there is a significant

increase in the first 2000 cycles before a slow-paced decline. The improvement of capacitance retention at the early stage is an activated process. As the number of cycles increases, the repeated intercalation/deintercalation of ions can cause damage to the structure of PPy, thus resulting in a decrease in capacitance. The device proposed by us reaches capacitance retention of 92.4% after 10,000 cycles, which is superior to the previously reported supercapacitors of the same category.[26, 48-50]

The flexibility of the device was assessed by CV testing at different bending angles. **Fig. 3.13c** shows the CV curves of the device at different curvatures. When the bending degree varies, the CV curve shows a slight deformation, but the area enclosed by the CV curve remains unchanged, even if the curvature reaches 180°, which suggests that the device is capable to work under the different bending scenarios. In addition, the electrochemical stability of the device in 1000 bending cycles (at the bending angle of 90°) was investigated and the result is illustrated in **Fig 3.13d**. The device reaches capacitance retention of 96.08% after 1000 times of bending.

In some cases, a single supercapacitor is incapable to satisfy the voltage rating of the electronics. It is a common strategy for supercapacitors in series to increase the output voltage. The series and parallel GCD curves of different numbers of devices are illustrated in **Fig. 3.13e**. The voltage window of three devices connected in series could reach 2.4 V, which evidences that our device is capable of voltage expansion. In addition, as the number of parallel devices is on the increase, the discharge time is an increase in linear multiplied. In summary, our device is adaptive to the basic rules of series and parallel connection of power supply devices, which can satisfy any voltage and capacitance requirements by adjusting the number of connections of devices. As shown in **Fig. 3.13f**, two PPy/CFC supercapacitors are connected in series as a power supply, which is successful in powering an LCD electronic watch with a voltage rating of 1.5 V.

3.4 Conclusion

In this work, a flexible fabric supercapacitor is designed and fabricated, which demonstrates excellent electrochemical performance, outstanding flexibility, robust mechanical performance, and reliable flame retardancy. The gas-phase polymerization method is applied to obtain the conductivity fiberglass cloth. Then, a PPy fabric composite electrode with a unique micro-morphology was derived from electrochemical

polymerization and finally assembled into a supercapacitor. Due to the unique microstructure of PPy tentacles and the advantages of fiberglass cloth, the ultimate PPy/CFC supercapacitor possesses excellent electrochemical and mechanical properties, including excellent area-specific capacitance and energy density, outstanding cycle stability, and remarkable capacitance retention under repeated bending. As proved by the example of driving an LCD electronic watch, the device fabricated in this study has massive potential in the energy supply of electronics. Moreover, this study contributes an effective path for the application of insulating fabrics in the manufacture of wearable energy storage devices.

Reference

[1] Q. Huang, D. Wang, Z. Zheng, Textile-Based Electrochemical Energy Storage Devices, Adv. Energy Mater. 6 (2016) 1600783.

[2] W. Zeng, L. Shu, Q. Li, S. Chen, F. Wang, X.M. Tao, Fiber-based wearable electronics: a review of materials, fabrication, devices, and applications, Adv. Mater. 26 (2014) 5310-5336.

[3] Y. Meng, Y. Zhao, C. Hu, H. Cheng, Y. Hu, Z. Zhang, G. Shi, L. Qu, All-graphene core-sheath microfibers for all-solid-state, stretchable fibriform supercapacitors and wearable electronic textiles, Adv. Mater. 25 (2013) 2326-2331.

[4] K.L. Bae, K. Kim, Flexible sodium-ion supercapacitor based on polypyrrole/carbon electrode by use of harmless aqueous electrolyte for wearable devices, International Journal of Energy Research 41 (2017) 1335-1341.

[5] K. Yadav, M. Jassal, A.K. Agrawal, Highly conducting silver nanowire-polyacrylonitrile hollow fibres for flexible supercapacitors, International Journal of Energy Research (2019).

[6] K. Sharma, K. Pareek, R. Rohan, P. Kumar, Flexible supercapacitor based on three-dimensional cellulose/graphite/polyaniline composite, International Journal of Energy Research 43 (2019) 604-611.

[7] M. Ghahremani Honarvar, M. Latifi, Overview of wearable electronics and smart textiles, The Journal of The Textile Institute 108 (2017) 631-652.

[8] L. Dong, C. Xu, Y. Li, Z.-H. Huang, F. Kang, Q.-H. Yang, X. Zhao, Flexible electrodes and supercapacitors for wearable energy storage: a review by category, J. Mater. Chem. A 4 (2016) 4659-4685.

[9] Y. Huang, M. Zhu, Z. Pei, Y. Huang, H. Geng, C. Zhi, Extremely stable polypyrrole achieved via molecular ordering for highly flexible supercapacitors, ACS Appl. Mater. Interfaces 8 (2016) 2435-2440.

[10] T. Gao, Z. Zhou, J. Yu, D. Cao, G. Wang, B. Ding, Y. Li, All-in-one compact architecture toward wearable all-solid-state, high-volumetric-energy-density supercapacitors, ACS Appl. Mater. Interfaces 10 (2018) 23834-23841.

[11] Z. Wang, J. Cheng, Q. Guan, H. Huang, Y. Li, J. Zhou, W. Ni, B. Wang, S. He, H. Peng, All-in-one fiber for stretchable fiber-shaped tandem supercapacitors, Nano Energy

45 (2018) 210-219.
[12] C. Yang, Q. Liu, L. Zang, J. Qiu, X. Wang, C. Wei, X. Qiao, L. Hu, J. Yang, G. Song, High‐performance yarn supercapacitor based on metal–inorganic–organic hybrid electrode for wearable electronics, Adv. Electron. Mater. 5 (2019) 1800435.
[13] S. He, W. Chen, Application of biomass-derived flexible carbon cloth coated with MnO2 nanosheets in supercapacitors, J. Power Sources 294 (2015) 150-158.
[14] N. Wang, G. Han, Y. Xiao, Y. Li, H. Song, Y. Zhang, Polypyrrole/graphene oxide deposited on two metalized surfaces of porous polypropylene films as all-in-one flexible supercapacitors, Electrochim. Acta 270 (2018) 490-500.
[15] Q. Liu, L. Zang, C. Yang, C. Wei, J. Qiu, C. Liu, X. Xu, A Flexible and Knittable Fiber Supercapacitor for Wearable Energy Storage with High Energy Density and Mechanical Robustness, J. Electrochem. Soc. 165 (2018) A1515-A1522.
[16] Y. Seo, B. Hwang, Mulberry-paper-based composites for flexible electronics and energy storage devices, Cellulose 26 (2019) 8867-8875.
[17] Q. Xue, J. Sun, Y. Huang, M. Zhu, Z. Pei, H. Li, Y. Wang, N. Li, H. Zhang, C. Zhi, Recent progress on flexible and wearable supercapacitors, Small 13 (2017) 1701827.
[18] S. Liu, L. Yao, Y. Lu, X. Hua, J. Liu, Z. Yang, H. Wei, Y. Mai, All-organic covalent organic framework/polyaniline composites as stable electrode for high-performance supercapacitors, Mater. Lett. 236 (2019) 354-357.
[19] Y. Han, Q. Zhang, N. Hu, X. Zhang, Y. Mai, J. Liu, X. Hua, H. Wei, Core-shell nanostructure of single-wall carbon nanotubes and covalent organic frameworks for supercapacitors, Chin. Chem. Lett. 28 (2017) 2269-2273.
[20] Y. Han, N. Hu, S. Liu, Z. Hou, J. Liu, X. Hua, Z. Yang, L. Wei, L. Wang, H. Wei, Nanocoating covalent organic frameworks on nickel nanowires for greatly enhanced-performance supercapacitors, Nanotechnology 28 (2017) 33LT01.
[21] J. Lv, P. Zhou, L. Zhang, Y. Zhong, X. Sui, B. Wang, Z. Chen, H. Xu, Z. Mao, High-performance textile electrodes for wearable electronics obtained by an improved in situ polymerization method, Chem. Eng. J. 361 (2019) 897-907.
[22] J.D. Ryan, D.A. Mengistie, R. Gabrielsson, A. Lund, C. Müller, Machine-washable PEDOT: PSS dyed silk yarns for electronic textiles, ACS Appl. Mater. Interfaces 9 (2017) 9045-9050.
[23] J. Xu, D. Wang, Y. Yuan, W. Wei, S. Gu, R. Liu, X. Wang, L. Liu, W. Xu, Polypyrrole-coated cotton fabrics for flexible supercapacitor electrodes prepared using

CuO nanoparticles as template, Cellulose 22 (2015) 1355-1363.
[24] K. Jost, G. Dion, Y. Gogotsi, Textile energy storage in perspective, J. Mater. Chem. A 2 (2014) 10776-10787.
[25] L. Bao, X. Li, Towards textile energy storage from cotton T-shirts, Adv. Mater. 24 (2012) 3246-3252.
[26] L. Wang, C. Zhang, X. Jiao, Z. Yuan, Polypyrrole-based hybrid nanostructures grown on textile for wearable supercapacitors, Nano Res. 12 (2019) 1129-1137.
[27] B. Yue, C. Wang, X. Ding, G.G. Wallace, Polypyrrole coated nylon lycra fabric as stretchable electrode for supercapacitor applications, Electrochim. Acta 68 (2012) 18-24.
[28] Q. Liu, B. Wang, J. Chen, F. Li, K. Liu, Y. Wang, M. Li, Z. Lu, W. Wang, D. Wang, Facile synthesis of three-dimensional (3D) interconnecting polypyrrole (PPy) nanowires/nanofibrous textile composite electrode for high performance supercapacitors, Composites Part A: Applied Science and Manufacturing 101 (2017) 30-40.
[29] J. Sun, Y. Huang, C. Fu, Z. Wang, Y. Huang, M. Zhu, C. Zhi, H. Hu, High-performance stretchable yarn supercapacitor based on PPy@ CNTs@ urethane elastic fiber core spun yarn, Nano Energy 27 (2016) 230-237.
[30] C. Yang, L. Zhang, N. Hu, Z. Yang, H. Wei, Y. Zhang, Reduced graphene oxide/polypyrrole nanotube papers for flexible all-solid-state supercapacitors with excellent rate capability and high energy density, J. Power Sources 302 (2016) 39-45.
[31] J. Ren, R.-P. Ren, Y.-K. Lv, Stretchable all-solid-state supercapacitors based on highly conductive polypyrrole-coated graphene foam, Chem. Eng. J. 349 (2018) 111-118.
[32] L. Zang, X. Qiao, Q. Liu, C. Yang, L. Hu, J. Yang, Z. Ma, High-performance solid-state supercapacitors with designable patterns based on used newspaper, Cellulose 27 (2020) 1033-1042.
[33] Y. Yang, M. Wan, Microtubules of polypyrrole synthesized by an electrochemical template-free method, J. Mater. Chem. 11 (2001) 2022-2027.
[34] Z. Zhou, W. Zhu, J. Liao, S. Huang, J. Chen, T. He, G. Tan, C. Ning, Chondroitin sulphate-guided construction of polypyrrole nanoarchitectures, Materials Science and Engineering: C 48 (2015) 172-178.
[35] J. Liao, Y. Zhang, G. Tan, C. Ning, Nanostructured PPy coating on titanium fabricated via template-free electrochemical polymerization in PBS, Surf. Coat. Technol. 228 (2013) S41-S43.

[36] J. Wang, Y. Xu, F. Yan, J. Zhu, J. Wang, Template-free prepared micro/nanostructured polypyrrole with ultrafast charging/discharging rate and long cycle life, J. Power Sources 196 (2011) 2373-2379.
[37] Q. Liu, L. Zang, X. Qiao, J. Qiu, X. Wang, L. Hu, J. Yang, C. Yang, Compressible All - In - One Supercapacitor with Adjustable Output Voltage Based on Polypyrrole - Coated Melamine Foam, Adv. Electron. Mater. (2019) 1900724.
[38] S. Ardizzone, G. Fregonara, S. Trasatti, “Inner” and “outer” active surface of RuO 2 electrodes, Electrochim. Acta 35 (1990) 263-267.
[39] J. Yan, C.E. Ren, K. Maleski, C.B. Hatter, B. Anasori, P. Urbankowski, A. Sarycheva, Y. Gogotsi, Flexible MXene/Graphene Films for Ultrafast Supercapacitors with Outstanding Volumetric Capacitance, Adv. Funct. Mater. 27 (2017) 1701264.
[40] C. Yang, Y. Tang, Y. Tian, Y. Luo, Y. He, X. Yin, W. Que, Achieving of Flexible, Free-Standing, Ultracompact Delaminated Titanium Carbide Films for High Volumetric Performance and Heat-Resistant Symmetric Supercapacitors, Adv. Funct. Mater. 28 (2018) 1705487.
[41] Z. Li, M. Tian, X. Sun, H. Zhao, S. Zhu, X. Zhang, Flexible all-solid planar fibrous cellulose nonwoven fabric-based supercapacitor via capillarity-assisted graphene/MnO2 assembly, J. Alloys Compd. 782 (2019) 986-994.
[42] Y. Lin, H. Zhang, W. Deng, D. Zhang, N. Li, Q. Wu, C. He, In-situ growth of high-performance all-solid-state electrode for flexible supercapacitors based on carbon woven fabric/polyaniline/graphene composite, J. Power Sources 384 (2018) 278-286.
[43] L. Dong, G. Liang, C. Xu, D. Ren, J. Wang, Z.-Z. Pan, B. Li, F. Kang, Q.-H. Yang, Stacking up layers of polyaniline/carbon nanotube networks inside papers as highly flexible electrodes with large areal capacitance and superior rate capability, J. Mater. Chem. A 5 (2017) 19934-19942.
[44] S. Lei, Y. Liu, L. Fei, R. Song, W. Lu, L. Shu, C.L. Mak, Y. Wang, H. Huang, Commercial Dacron cloth supported Cu (OH) 2 nanobelt arrays for wearable supercapacitors, J. Mater. Chem. A 4 (2016) 14781-14788.
[45] Q. Zhou, X. Ye, Z. Wan, C. Jia, A three-dimensional flexible supercapacitor with enhanced performance based on lightweight, conductive graphene-cotton fabric electrode, J. Power Sources 296 (2015) 186-196.
[46] M. Barakzehi, M. Montazer, F. Sharif, T. Norby, A. Chatzitakis, A textile-based wearable supercapacitor using reduced graphene oxide/polypyrrole composite,

Electrochim. Acta 305 (2019) 187-196.
[47] X. Zang, X. Li, M. Zhu, X. Li, Z. Zhen, Y. He, K. Wang, J. Wei, F. Kang, H. Zhu, Graphene/polyaniline woven fabric composite films as flexible supercapacitor electrodes, Nanoscale 7 (2015) 7318-7322.
[48] Y. Bai, R. Liu, E. Li, X. Li, Y. Liu, G. Yuan, Graphene/Carbon Nanotube/Bacterial Cellulose assisted supporting for polypyrrole towards flexible supercapacitor applications, J. Alloys Compd. 777 (2019) 524-530.
[49] C.J. Raj, B.C. Kim, W.-J. Cho, W.-g. Lee, S.-D. Jung, Y.H. Kim, S.Y. Park, K.H. Yu, Highly flexible and planar supercapacitors using graphite flakes/polypyrrole in polymer lapping film, ACS Appl. Mater. Interfaces 7 (2015) 13405-13414.
[50] J. Cao, Y. Wang, J. Chen, X. Li, F.C. Walsh, J.-H. Ouyang, D. Jia, Y. Zhou, Three-dimensional graphene oxide/polypyrrole composite electrodes fabricated by one-step electrodeposition for high performance supercapacitors, J. Mater. Chem. A 3 (2015) 14445-14457.

Chapter 4 Compressible all-in-one flexible supercapacitors based on polypyrrole/melamine foam composite electrodes

4.1 Introduction

With the rapid development of portable and flexible electronics, energy storage devices with high mechanical flexibility, good electrochemical properties, and light weight have attracted widespread attention from academic and industrial fields.[1-8] Among numerous flexible energy storage devices, flexible supercapacitors are often regarded as the optimal candidate on account of their high power density, ultralong cycling stability, and fast charge and discharge capacity.[9-12] Recently, substantial effort has been devoted to endow flexible supercapacitors with more efficiency, more stability, and low cost to develop fully flexible electronics.[13-15]

High energy density and good mechanical durability are the major difficulties in the design and fabrication of flexible supercapacitors. Generally, the common flexible supercapacitors exhibit a multilayer laminated configuration, which is fabricated by placing a gel electrolyte layer between two flexible electrodes.[16-19] Compared with the common flexible supercapacitors with laminated structure, the major components of the all-in-one flexible supercapacitors including two electrodes, separator, electrolyte, and current collectors are integrated on the same substrate.[20, 21] This integrated design can not only reduce the contact resistance of the interface but also increase mechanical durability including compression stability and stretching and/or twisting reliability.

Up to now, a series of integrated flexible supercapacitors have been reported. Guo et al. reported healable supercapacitors with all-in-one configuration by in situ polymerization and deposition of SWCNT and PANI onto the two sides of the healable

hydrogel electrolyte separator.[17] Wang et al. integrated the electrode-electrolyte-electrode component in a free-standing PANI-PVA hydrogel film to fabricated an all-in-one supercapacitor.[22] Gao et al. designed an all-in-one asymmetric supercapacitor with high volumetric energy density by electrodeposition of metallic oxide onto each side of the CNT-modified porous polyamide nanofiber film.[23] Shao et al. fabricated a tunable integrated flexible supercapacitor using 3D rGO/GO/rGO foam via the laser direct writing technology.[24] These all-in-one supercapacitors can avoid unstable physical connections, which is of great importance for stable flexible supercapacitors in the future. Nonetheless, the integrated flexible supercapacitors still need further development when they are applied in practice. For example, the connection of the supercapacitors in series to extend the voltage window requires additional wires, which is unable to satisfy the portable and flexible electronics with compact structure. Thus, to further meet the particular demands for portable electronics, developing new candidates for multifunctional and stable energy storage devices is urgent.

In this work, we reported a facile approach to fabricate a lightweight and compressible all-in-one flexible supercapacitor. The commercial melamine foam (MF) was used as multiple roles to fabricate an all-in-one flexible supercapacitor (AFSC). First, the conductive layers were constructed on the two sides of the MF via gold-sputtering. Then, polypyrrole (PPy) was deposited on the gold-sputtered layers by electrochemical polymerization of pyrrole to obtain a sandwich structure in which two conductive sides were separated by the pure MF in the middle. The effect of the deposition time on the electrochemical properties of the PPy/MF composite was investigated. Finally, the AFSC was fabricated by making the PPy/MF composite fully absorb 1 M sulfuric acid (H_2SO_4) electrolyte. Compared with previously reported all-in-one supercapacitors, our device has the advantages of a simpler manufacturing process and higher specific capacitance. Furthermore, it has great compressibility and can work at different compressive strains. Besides, our device can extend the voltage window to suit the operating voltage of the electronic device by simply cutting method without connection of additional supercapacitors in series. For a demonstration, the AFSC with one cutting successfully powered an LCD digital watch. The results indicate our device is a promising energy storage device that can be applied in portable and wearable electronics.

4.2 Experimental section

4.2.1 Materials

Sodium p-toluenesulfonate (TOSNa), sulfuric acid (H_2SO_4) and pyrrole were analytical grade and obtained from Aladdin Co. Ltd. Commercial melamine foam (MF) was purchased from Enwode New Materials Co. Ltd.

4.2.2 Preparation of PPy/MF Composite

The MF (30×24×6 mm^3) was sonicated in ethanol and deionized water and dried prior to use. To make MF conductive, each side of the dried MF was treated by gold-sputtering using a Turbo sputter coater (Q150T, QUORUM, England) with a sputter duration of 30 s. PPy/MF composite was prepared by electrochemical polymerization of pyrrole. Briefly, a mixed solution including pyrrole (0.1 M) and sodium *p*-toluenesulfonate (TOSNa, 0.15 M) was used as an electrolyte solution, the gold-sputtered MF (20×10×6 mm^3) was used as a working electrode and the stainless steel mesh was used as the counter electrode. PPy was deposited on each side of the MF by adopting the constant voltage of 2 V for the desired time. The mass loading of PPy was controlled by adjusting the deposition time. Then, the PPy/MF composite was washed with deionized water to remove TOSNa on the surface of PPy and dried at 45 °C. For comparison, three deposition times (20, 40, and 60 min) were applied in this work, and the resultant composite was denoted as PPy/MF-20, PPy/MF-40, and PPy/MF-60 composite, respectively.

4.2.3 Assembly of All-in-One Flexible Supercapacitor (AFSC)

The AFSC was fabricated by immersing the as-prepared electrodes in 1 M H_2SO_4 solution to absorb sufficient electrolytes. As a connection pad, copper foils were

connected to external terminals of the AFSC by conductive silver adhesive. To protect the AFSC from electrolyte leakage, the device was packaged with polyethylene film.

4.2.4 Characterization

The micromorphology of the samples was observed by a field emission scanning electron microscope (SEM, S-4800, HITACHI, Japan). The compression property of the device was examined by an Instron 300 series Universal Testing Machine at a speed of 100 mm min^{-1}. CV, GCD, EIS, and charge/discharge cycling stability were measured using an electrochemical workstation (CHI660E, CHENHUA, China). The frequency recorded by EIS ranged from 0.01 Hz to100 kHz, and the potential amplitude was 5 mV. In order to facilitate the study of the electrochemical performance of a single electrode, the PPy/MF composite was divided in half from the middle of the separator layer. For the PPy/MF electrodes, the tests were executed in a three-electrode system using platinum foil as the counter electrode, Ag/AgCl electrode as the reference electrode, and 1 M H_2SO_4 solution as the electrolyte. The specific capacitance of the electrode ($C_{V,\ electrode}$) was calculated by Equation (9) from the data of GCD curves:

$$C_{V,electrode} = \frac{I \times \Delta t}{V \times U} \quad (1)$$

The electrochemical performance of the device was measured in a two-electrode system. The specific capacitance (C_V), energy density (E_V), and power density (P_V) of the AFSC were calculated by the following equations from the data of GCD curves:

$$C_V = \frac{I \times \Delta t}{2V \times U} \quad (2)$$

$$E_V = \frac{C_V \times U^2}{2 \times 3600} \quad (3)$$

$$P_V = \frac{3600 \times E_V}{\Delta t} \quad (4)$$

Where I represents current (A); Δt is discharged time (s); U is discharged potential (V); V is the effective volume of a single electrode (cm^3).

4.3 Results and Discussion

4.3.1 Analysis of the preparation process

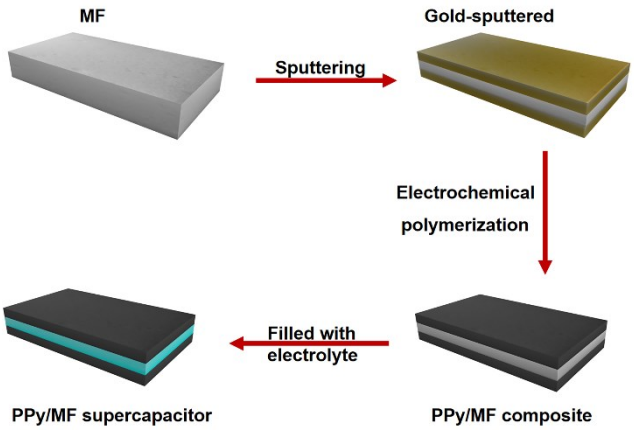

Fig. 4.1 Schematic illustration of preparation process of the all-in-one flexible supercapacitor.

The MF with lightweight, low price, high porosity, elasticity, and aqueous solution absorption is an ideal substrate for flexible supercapacitors. In this work, the MF is not only a flexible substrate but also a separator that prevents short circuits. Moreover, it is also a good carrier for absorbing and retaining electrolytes. **Fig. 4.1** is the schematic preparation process of the AFSC based on the PPy/MF composite. Firstly, each side of the MF was treated by gold-sputtering to achieve conductivity. From the digital photograph of MF before and after the sputtering process, we can see that each side of the MF changed from white (**Fig. 4.2a**) to gray (**Fig. 4.2b**). **Fig. 4.2c** shows the cross-section of gold-sputtered MF, where a typical sandwich structure with a relatively clear boundary is observed and the two gold layers are separated by the insulating pure MF. The thickness of the gold-sputtered layer and the separator layer is about 1.5 and 3 mm, respectively. Thereafter, the electroactive material (PPy) was deposited on each side of the MF via the electrochemical polymerization technique. The polymerization of pyrrole occurred only on the skeleton of the conductive gold-sputtered layer within a certain period due to the three-dimensional (3D) porous structure of MF. Hence after

electrochemical polymerization, the thickness of the PPy layer is consistent with that of the gold-sputtered layer. The PPy/MF composite still maintains a sandwich structure, and the boundaries become clearer (**Fig. 4.2d**). Finally, a symmetric AFSC was obtained by making the PPy/MF composite absorb sufficient electrolyte (1 M H_2SO_4). Since MF has an excellent capacity for absorbing and retaining aqueous solution, the electrolyte can be well stored in the MF. This simple preparation method offers a feasible strategy to realize the large-scale fabrication of the AFSCs.

4.3.2 Micromorphological characterization

Fig. 4.3 shows the micromorphology of the PPy/MF composites with different deposition times. The highly 3D porous network structure can be observed in all of them. Such structure is propitious to electron transmission as well as sufficient contact between the electrolyte and the electrode. The SEM image of gold-sputtered MF is presented in **Fig. 4.3a**. The continuous gold film on the skeleton endows it with excellent conductivity, providing a viable condition for subsequent electrochemical polymerization. The SEM images of PPy/MF composites with different deposition times are shown in **Fig. 4.3b-d**. A coating of holothurian-like PPy microcone arrays located on the surface of the skeleton is observed. For PPy/MF-20, a handful of PPy microcones with a length of ~2.5 μm and a diameter of ~1.5 μm (bottom) to ~200 nm (tip) are erected on the surface of the MF skeleton (**Fig. 4.3b**). Compared with PPy/MF-20, PPy/MF-40 (**Fig. 4.3c**) shows a large number of PPy microcones with a larger size, which reveals that the PPy microcones become large and thriving as the polymerization time increases. The PPy microcones provide a larger specific surface area than the irregular PPy particles, which is conducive to improving electrochemical performance. The formation mechanism of PPy microcones was supposed in our previous work.[16] In the initial stage of electrochemical polymerization, the pyrrole monomers interact with the micelles of *p*-toluenesulfonate ions adsorbed on the surface of the MF skeleton and then are polymerized to form a nanostructured PPy nucleus. With the progress of electrochemical polymerization, the nanostructured PPy nucleus grows vertically to form the PPy microcones due to the steric hindrance. When the deposition time increases to 60 min, the PPy microcones become much larger, and many of them stack on top of each other (**Fig. 4.3d**). The mass loading of PPy on a single gold-sputtered

side for PPy/MF-20, PPy/MF-40, and PPy/MF-60 composite is about 23.4, 39.1, and 46.8 mg cm^{-3}, respectively.

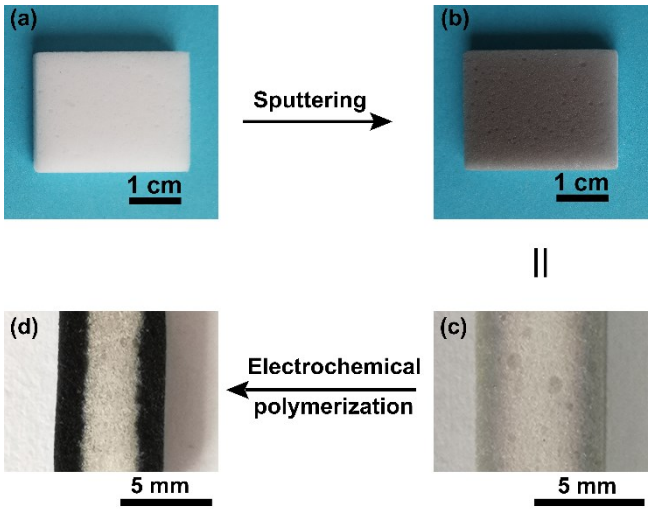

Fig. 4.2 Digital photograph of the production process for PPy/MF composite. The MF (a) before and (b) after sputtering; the cross-section of (c) gold-sputtered MF and (d) PPy/MF composite.

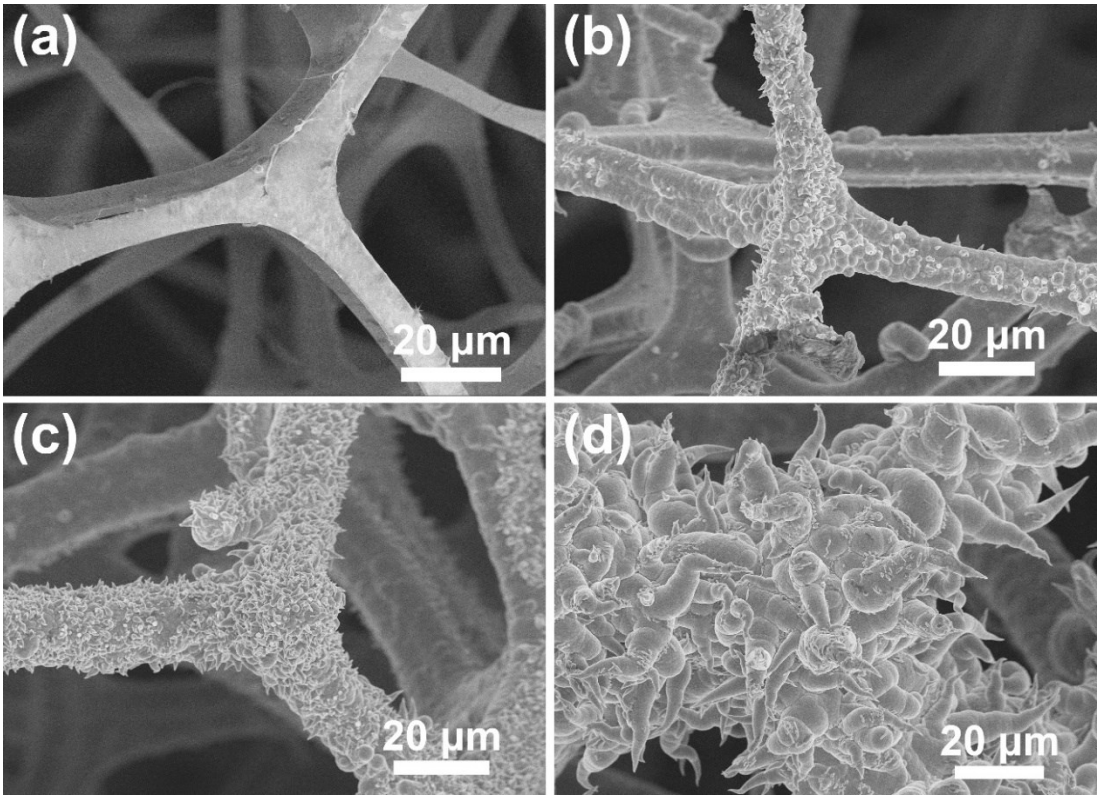

Fig. 4.3 SEM images of (a) gold-sputtered MF, (b) PPy/MF-20, (c) PPy/MF-40 and (d) PPy/MF-60 composite.

4.3.3 Electrochemical properties and mechanical stability

To further study the impact of deposition time on electrochemical performance, the PPy/MF composites were divided in half from the middle separator layer to obtain PPy/MF electrodes with a single-sided PPy layer. The electrochemical properties of PPy/MF-20, PPy/MF-40, PPy/MF-60 electrode are shown in **Fig. 4.4**. As shown in **Fig. 4.4a and Fig. 4.4b**, all the CV curves are approximately rectangle and all the GCD curves show an almost symmetric triangle, which demonstrates that all the samples have the ideal capacitive behavior with fast ion response.[25] In addition, PPy/MF-60 electrode exhibits the largest enclosed area in **Fig. 4.4a** and the longest discharge time in **Fig. 4.4b**, which means the specific capacitance of the PPy/MF-60 electrode is higher than that of other samples. For further comparison, the Nyquist plots of the three samples are presented in **Fig. 4.4c**. PPy/MF-60 electrode has smaller equivalent series resistance (ESR) of 1.63 Ω than that of PPy/MF-40 electrode (1.74 Ω) and PPy/MF-20 electrode (2.41 Ω). As shown in **Fig. 4.3**, the mass loading of PPy on the gold-sputtered MF is increased as the deposition time increases, and the increasing PPy coating can improve the conductivity of the electrode. The specific capacitances of the PPy/MF electrodes at varied current densities are given in **Fig. 4.4d**. Among the three samples, PPy/MF-60 electrode possesses the highest specific capacitance at the same current density since it has the highest mass loading of PPy. The specific capacitance ($C_{V,\ electrode}$) of PPy/MF-20, PPy/MF-40, PPy/MF-60 electrode at 50 mA cm^{-3} is 8.74, 13.96 and 19.80 F cm^{-3}, respectively. When the current density increases to 400 mA cm^{-3}, the capacitance retention of PPy/MF-20, PPy/MF-40, PPy/MF-60 electrode is 78.6%, 73.3% and 56.3%, respectively. The poor rate capability for PPy/MF-60 electrode can be explained as that: PPy/MF-60 electrode has the densest PPy coating, and there is not enough time for the ions to diffuse to the inner surface as the charge/discharge current density increases, which causes the inner part of the PPy has little capacitance contribution. Moreover, PPy/MF-60 composite exhibits poor flexibility because the mass loading of rigid PPy on the MF skeleton is too high. To enable a visual comparison, the digital photos of PPy/MF-20, PPy/MF-40, PPy/MF-60 electrode at bent state are given in **Fig. 4.5**. PPy/MF-60 electrode at bent state is fracted, indicating it is not a suitable candidate for flexible supercapacitors. PPy/MF-40 electrode exhibits relatively good specific capacitance and rate capability. Furthermore, PPy/MF-40

composite can withstand varying compressive strains and return to its original shape immediately when the pressure is released (**Fig. 4.6a**). As shown in **Fig. 4.6b** and **4.6c**, PPy/MF-40 composite can withstand 1000 compression cycles at a strain of 50% and remain 96.6% of its original volume and 95.8% of stress. This provides a powerful guarantee for the device to work properly under compression conditions. Considering the specific capacitance, rate capability, and compressibility, PPy/MF-40 composite with relatively outstanding comprehensive performance was chosen to fabricate the AFSC in this work.

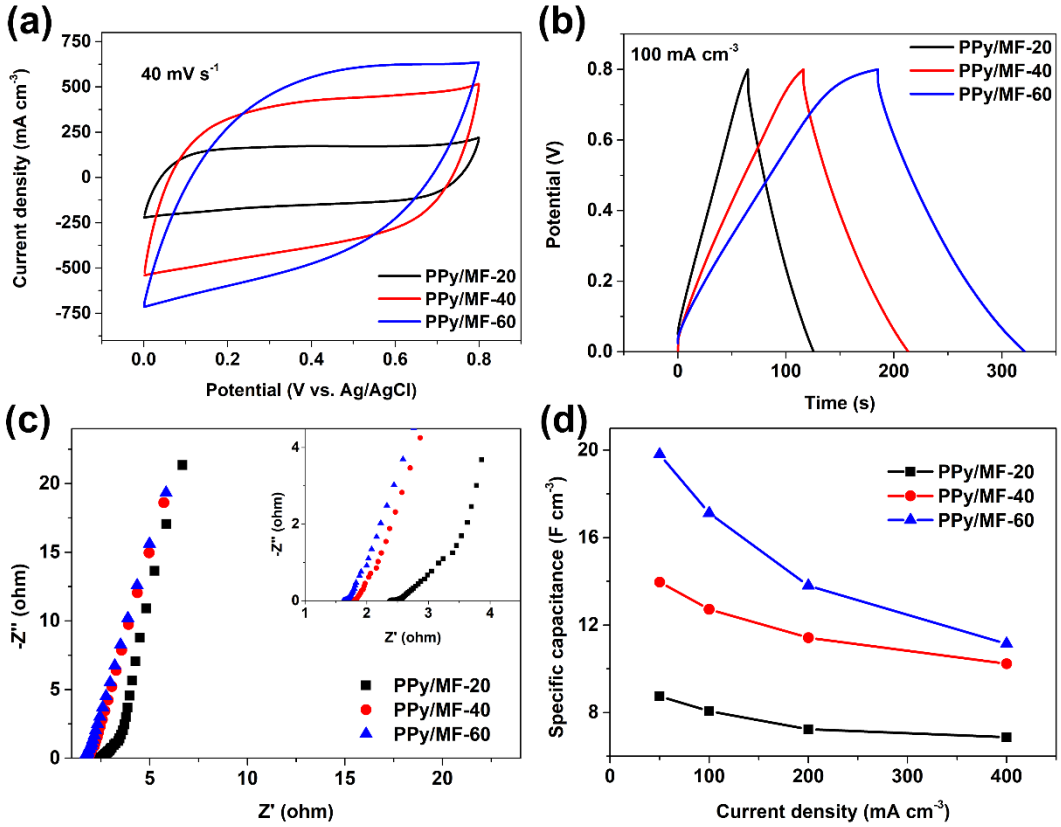

Fig. 4.4 Electrochemical properties of PPy/MF electrodes. (a) CV curves, (b) GCD curves, (c) Nyquist plots and (d) specific capacitance of PPy/MF-20, PPy/MF-40, PPy/MF-60 electrode.

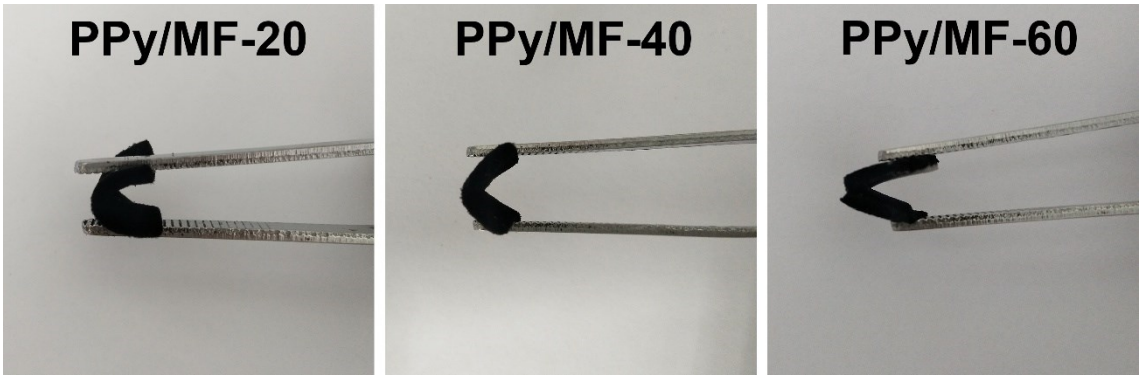

Fig. 4.5 the digital photos of PPy/MF-20, PPy/MF-40, PPy/MF-60 electrode at bent state.

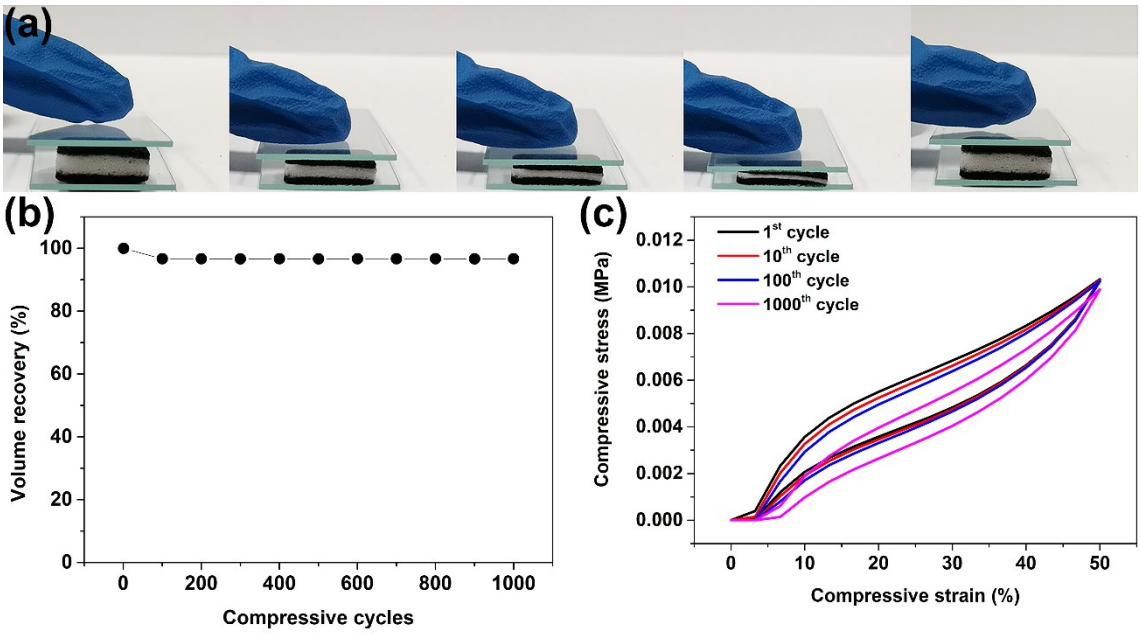

Fig. 4.6 The compressive properties of PPy/MF-40 composite. (a) The compression and recovery processes. (b) Volume retention for 1000 compression cycles at a strain of 50%. (c) Cyclic stress-strain curves at a strain of 50%.

The electrochemical performance of the AFSC fabricated by PPy/MF-40 composite was evaluated in a two-electrode system. The CV curves of the AFSC at all scan rates show symmetric shape, which suggests this device has a good capacitive behavior (**Fig. 4.7a**). It is well known that PPy has been widely used in pseudocapacitors as electrode material.[26, 27] Considering the PPy prepared in this work has a unique microcone structure that can increase the specific surface area, the capacitance of the AFSC may originate from two mechanisms based on charge transfer kinetics: (1) the capacitive

contribution associated with ion adsorption and desorption on the electrode surface; (2) the diffusion-controlled process contributed by ions intercalation and de-intercalation into the PPy matrix. It is can be analyzed with the following equations:

$$i = av^b \quad (5)$$

$$log\, i = log\, a + b log\, v \quad (6)$$

Where i is the corresponding response current at a particular potential; v is the scan rate; a and b are constants. The electrochemical kinetics can be evaluated by the b-value. When the b-value is 0.5, it is a diffusion-controlled process; whereas it is a non-diffusion-controlled behavior when the b-value is 1.[28, 29] The b-values can be obtained from the slope of particular potentials log(i)-log(v) plot, and the results are shown in **Fig. 4.7b**. All the b-values locate between 0.6 and 0.8, indicating that the AFSC based on PPy/MF-40 composite materials has both diffusion-controlled and non-diffusion-controlled contributions. In order to know more about the mechanism of the charge storage process, Trasatti analysis method was adopted to evaluate the electrochemical kinetics of the AFSC, which can quantify the charge stored at the inner surface (q_i) and the outer surface (q_o) during this process.[29-31] The total stored charges (q_T) of the device consist of inner and outer surface charges:[29-31]

$$q_T = q_i + q_o \quad (7)$$

The inner surface of the charge storage is a diffusion-controlled process, whereas the outer surface of the charge storage is regardless of the scan rate and diffusion. Therefore, the total charge measured by cyclic voltammetry ($q_{(v)}$) can be calculated by the equation below:[29-31]

$$q_{(v)} = q_\infty + kv^{-1/2} \quad (8)$$

where $kv^{-1/2}$ is the charge storage regarding to semi-infinite diffusion and k is a constant. When the scan rate is infinite, q_∞ can be regarded as equivalent to q_o. The relationship between $q_{(v)}$ and $v^{-1/2}$ is shown in **Fig. 4.7c**. According to the result of linear fitting, q_o deduced from the intercept of the fitted line is 1.026 C cm^{-3}. Based on Equation (4), the practical charge storage at 10, 20, 40, 60, 80 and 100 mV s^{-1} is 6.80, 5.10, 3.91, 3.38, 3.07 and 2.85 C cm^{-3}, respectively.

The non-diffusion contribution ratios at different scan rates were obtained from the ratio of outer charge to practical charge storage, and the results are shown in **Fig. 4.7d**. As the scan rate increases, the non-diffusion contribution increases from 15.1 % at 10 mV s^{-1} to 36 % at 100 mV s^{-1}. All the percentages of non-diffusion contribution are less

than diffusion contribution, indicating the diffusion-controlled process plays a dominant role in the process of charge storage.

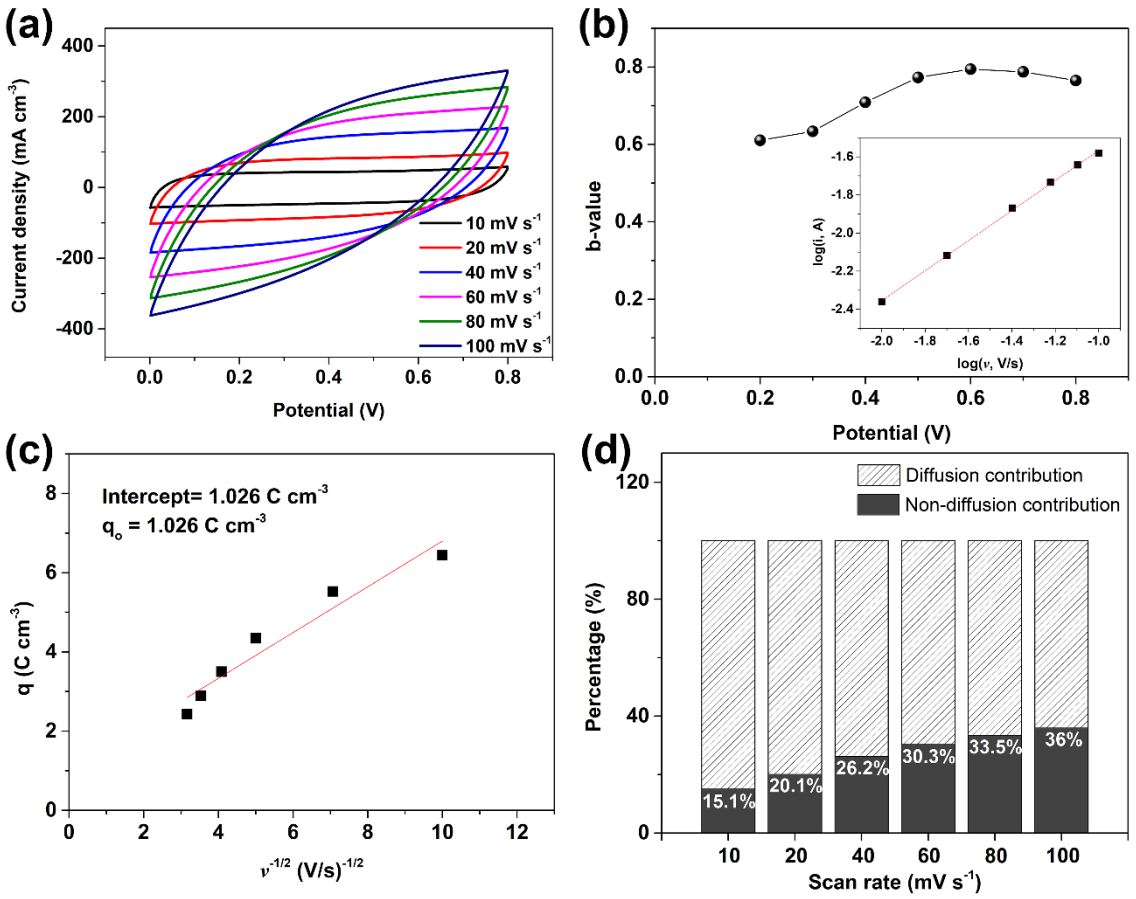

Fig. 4.7 Electrochemical properties of the AFSC. (a) CV curves. (b) b-values at different voltages. (c) The dependence of $q_{(v)}$ on $v^{-1/2}$. (d) The ratios of diffusion contribution to non-diffusion contribution.

The GCD curves of the AFSC at various current densities show symmetric shape (**Fig. 4.8a**), indicating the ideal capacitive behavior. All the voltage drops (iR_{drop}) at different current densities are less than 0.1 V (**Fig. 4.8b**), which reflects the AFSC has a small internal resistance. The ESR obtained from the Nyquist plot (**Fig. 4.8c**) is ~4.1 Ω, which is smaller than the values reported for PPy/stainless steel yarn fiber supercapacitor (~7.2 Ω),[16] PPy/MnO_2/stainless steel yarn supercapacitor (~5.33 Ω),[19] PEDOT/PSS-WMCNT flexible solid supercapacitor (~11.2 Ω)[32] and PPy/graphite/paper supercapacitor (280.8-536.6 Ω)[33]. Moreover, the curve at the high-frequency region shows an angle less than 90°, confirming its pseudocapacitive behavior.[34] In addition, there is a subvertical line at the low-frequency region, indicating great electrochemical

capacitive behavior of the AFSC.[31, 35] The maximum volumetric specific capacitance of the entire device (C_V) is 2.86 F cm^{-3}. With the current density increases, the value of C_V gradually decreases to 2.05 F cm^{-3} as shown in **Fig. 4.8d**. The specific mass capacitance normalized to the device based on the entire weight of active material ranges from 73.35 F g^{-1} at 10 mA cm^{-3} to 52.39 F g^{-1} at 100 mA cm^{-3}.

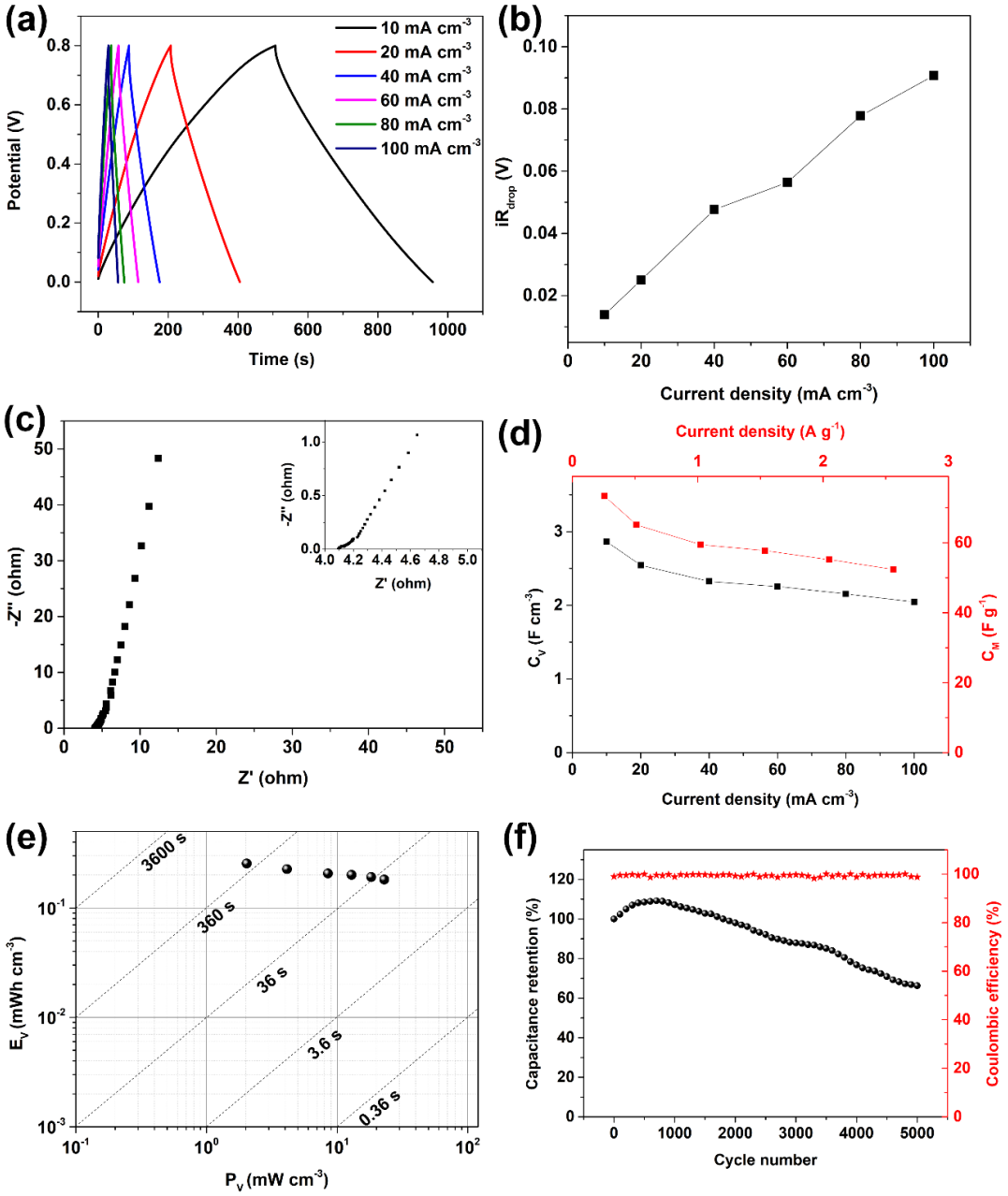

Fig. 4.8 Electrochemical properties of the AFSC. (a) GCD curves. (b) iR_{drop} at different current densities. (c) Nyquist plot. (d) Specific capacitance of the entire device at different current densities. (e) Ragone plots. (f) Cycling stability and coulombic efficiency.

The volumetric power density (P_V) and volumetric energy density (E_V) of the entire device were calculated, and the results are shown in **Fig. 4.8e**. The maximum P_V is 22.97 mW cm^{-3} with an E_V of 0.18 mWh cm^{-3} and the highest E_V is 0.26 mWh cm^{-3} with the P_V of 2.04 mW cm^{-3}. The comparison of the specific capacitance, power density, and energy density of this device with some previously reported all-in-one flexible supercapacitors are summarized in **Table 4.1**, suggesting our AFSC exhibits good electrochemical performance.

Table 4.1 Comparison of recently reported all-in-one flexible supercapacitors

Electrode materials	Specific capacitance	Max energy density	Max power density	Ref
SWCNT-PANI	15.8 mF cm^{-2}	-	-	[17]
RGO–GO–RGO	2.4 mF cm^{-2}	0.2 mWh cm^{-2}	36 mW cm^{-2}	[21]
MnO_2/CNT//FeOOH/CNT (Asymmetric)	3.1 F cm^{-3}	1.1 mWh cm^{-3}	-	[23]
HrGO/CNT//MnO_2 (Asymmetric)	200 mF cm^{-2}	106.2 μWh cm^{-2} 2.12 mWh cm^{-3}	400 μW cm^{-2} 320 mW cm^{-3}	[36]
PPy-GO/PPF/PPy-GO	108 mF cm^{-2}	2.6 μWh cm^{-2}	0.03 mW cm^{-2}	[37]
PVH–PANI	514 mF cm^{-2}	-	-	[38]
rGO-TiO_2/GO/rGO-TiO_2	237 F cm^{-3} 56 mF cm^{-2} 60 F g^{-1}	16 mWh cm^{-3}	-	[39]
rGO	17.9 F cm^{-3} 80.7 μF cm^{-2}	2.5 mWh cm^{-3}	495 W cm^{-3}	[40][a)]
rGO	2.35 F cm^{-3}	2.1 mWh cm^{-3}	141 W cm^{-3}	[41][a)]
rGO	2.5 mF cm^{-2} 257 F g^{-1}	-	-	[42][a)]
PPy microcones	2.86 F cm^{-3} 73.35 F g^{-1} 343.7 mF cm^{-2}	254.6 μWh cm^{-3} 6.52 mWh g^{-1} 30.6 μWh cm^{-2}	22.97 mW cm^{-3} 588.3 mW g^{-1} 2.76 mW cm^{-2}	This work

[a)] These supercapacitors are in-plane structures. Others are sandwich structures.

To evaluated the cycling stability of the AFSC, 5000 GCD cycles were performed at 100 mA cm^{-3} and the result is shown in **Fig. 4.8f**. It shows a significant increase at the early stage, and then gradually drops. At the early stage of GCD cycling test, the

electrolyte gradually diffuses into the PPy coating, leading to an activated process of the device and the increase in capacitance retention. However, when GCD cycling test continues to perform, the repeated intercalation and de-intercalation of the ions may lead to structural breakdown of PPy, resulting in decreased capacitance. Our device maintains 66.05 % capacitance retention after 5000 cycles at 100 mA cm^{-3}, which is comparable with the reported pure PPy-based supercapacitors.[43, 44] Moreover, the AFSC also reveals a high coulombic efficiency of above 98%.

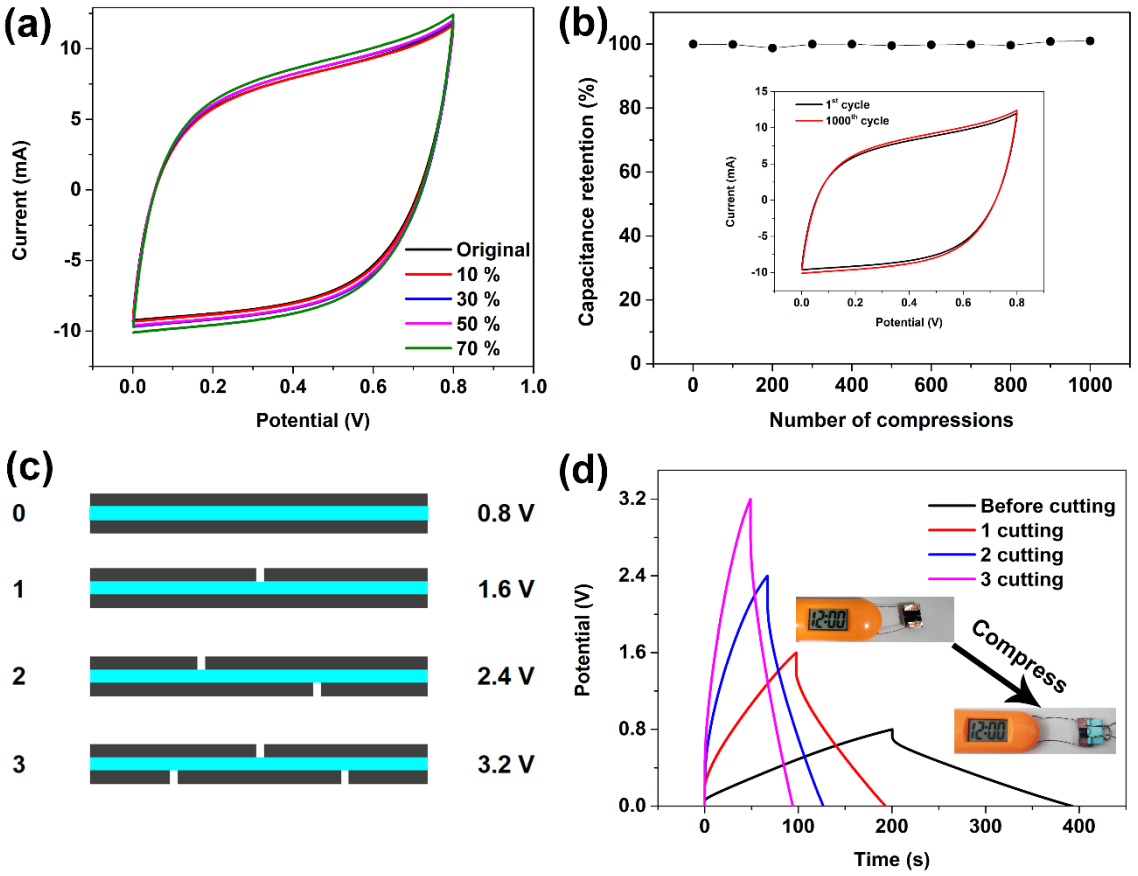

Fig. 4.9 (a) CV curves of the device under different compressive strains at 20 mV s^{-1}. (b) Capacitance retention of the device for 1000 compression cycles at a strain of 50%. Insets are the CV curves of the device after the first compression cycle and the 1000 compression cycles at a strain of 50%. (c)The schematic illustration of the cutting method to extend voltage window. (d) GCD curves of the device with different cutting times at 20 mA cm^{-3}. Insets are the digital photos of the LCD electronic watch powered by the AFSC with one cutting at original state and compressed state.

The CV curves of the device under different compressive strains are shown in **Fig. 4.9a.** All the CV curves are almost the same, indicating that the AFSC can work under different compressive strains with excellent electrochemical stability. The capacitance retention of the device for 1000 compression cycles has been investigated. As shown in **Fig. 4.9b**, the capacitance retention of the device can reach ~100% after 1000 compression cycles at a strain of 50%. In general, when the voltage window of a single supercapacitor cannot meet the operating voltage of an electronic device, it is often necessary to connect several individual supercapacitors in series to increase the voltage window. It is encouraging that our device can extend the voltage window by simply cutting method without connecting additional supercapacitors in series. **Fig. 4.9c** shows the schematic illustration of the cutting method to extend the voltage window. The volume of the device before and after cutting is nearly the same, and the operating voltage, capacitance, energy density, and power density of the device before and after cutting follow the formulas below:

$$U_{total} = (n+1)U_0 \quad (9)$$

$$C_{V,total} = (\frac{1}{n+1})^2 C_{V,0} \quad (10)$$

$$E_{V,total} = E_{V,0} \quad (11)$$

$$P_{V,total} = (n+1)P_{V,0} \quad (12)$$

Where n represents cutting times; U_{total} and U_0 is the total operating voltage before and after cutting, respectively; $C_{V,\,total}$ and $C_{V,\,0}$ is the total capacitance of the device before and after cutting, respectively; $E_{V,\,total}$ and $E_{V,\,0}$ is the total volumetric energy density of the device before and after cutting, respectively; $P_{V,\,total}$ and $P_{V,\,0}$ is the total volumetric power density of the device before and after cutting, respectively.

After cutting into several equal parts, in theory the as-obtained device is equivalent to connecting several "small" supercapacitors in series and obeys the basic rule of series connection of capacitors. The operating voltage and volumetric power density of the as-obtained device after cutting are n+1 times of those of the device before cutting. Like conventional connection of individual supercapacitors in series, the total volumetric energy density keeps the same and the total capacitance is reduced. However, for conventional connection method, individual supercapacitors are connected with each other by wires, and the contact between the terminal of the supercapacitor and the wire would directly affect the electrochemical performance. Our strategy can effectively

avoid poor contact between the terminal of the supercapacitor and the wire, which is beneficial to the practical applications. This simple strategy provides a novel way to satisfy the operating voltage of various electronic devices. As a demonstration, we give an example to verify the feasibility and practicability of this strategy in **Fig. 4.9d**. The voltage window of AFSC before cutting is 0.8 V, and it increases to 1.6, 2.4, and 3.2 V after cutting one, two, and three times, respectively. The AFSC with one cutting can successfully drive an LCD electronic watch, even at a compression state. As a prospect, this method may open a facile door of an all-in-one supercapacitor for practical applications.

4.4 Conclusion

In summary, a lightweight and compressible all-in-one flexible supercapacitor that can easily extend voltage windows was designed and fabricated in this work. The MF serves as the substrate for depositing PPy and the separator to avoid a short circuit. In addition, the MF can sufficiently absorb and lock in the electrolyte to make the electroactive material fully contact the electrolyte. The AFSC exhibits superior electrochemical performance, excellent electrochemical stability under different compressive strains, and outstanding capacitance retention for 1000 compression cycles. With the novel design, the AFSC can extend voltage windows without the connection of additional devices in series. In view of the above-mentioned advantages, this novel strategy may potentially guide the development of all-in-one supercapacitors for portable and wearable electronics.

Reference

[1] A.C. Forse, C. Merlet, J.M. Griffin, C.P. Grey, New perspectives on the charging mechanisms of supercapacitors, J. Am. Chem. Soc. 138 (2016) 5731-5744.

[2] K. Shi, X. Yang, E.D. Cranston, I. Zhitomirsky, Efficient lightweight supercapacitor with compression stability, Adv. Funct. Mater. 26 (2016) 6437-6445.

[3] J. Zhao, C. Li, Q. Zhang, J. Zhang, X. Wang, Z. Lin, J. Wang, W. Lv, C. Lu, C.-p. Wong, An all-solid-state, lightweight, and flexible asymmetric supercapacitor based on cabbage-like ZnCo 2 O 4 and porous VN nanowires electrode materials, J. Mater. Chem. A 5 (2017) 6928-6936.

[4] Y. Liu, G. Li, Z. Chen, X. Peng, CNT-threaded N-doped porous carbon film as binder-free electrode for high-capacity supercapacitor and Li–S battery, J. Mater. Chem. A 5 (2017) 9775-9784.

[5] Y. Zhang, Y. Jiao, L. Lu, L. Wang, T. Chen, H. Peng, An ultraflexible silicon–oxygen battery fiber with high energy density, Angew. Chem. Int. Ed. 56 (2017) 13741-13746.

[6] J. Cao, C. Chen, Q. Zhao, N. Zhang, Q. Lu, X. Wang, Z. Niu, J. Chen, A Flexible Nanostructured Paper of a Reduced Graphene Oxide–Sulfur Composite for High-Performance Lithium–Sulfur Batteries with Unconventional Configurations, Adv. Mater. 28 (2016) 9629-9636.

[7] F. Mo, G. Liang, Z. Huang, H. Li, D. Wang, C. Zhi, An overview of fiber-shaped batteries with a focus on multifunctionality, scalability, and technical difficulties, Adv. Mater. 32 (2020) 1902151.

[8] Q. Yang, F. Mo, Z. Liu, L. Ma, X. Li, D. Fang, S. Chen, S. Zhang, C. Zhi, Activating C-coordinated iron of iron hexacyanoferrate for Zn hybrid-ion batteries with 10 000-cycle lifespan and superior rate capability, Adv. Mater. 31 (2019) 1901521.

[9] L. Wen, F. Li, H.M. Cheng, Carbon nanotubes and graphene for flexible electrochemical energy storage: from materials to devices, Adv. Mater. 28 (2016) 4306-4337.

[10] L. Dong, C. Xu, Y. Li, Z.-H. Huang, F. Kang, Q.-H. Yang, X. Zhao, Flexible electrodes and supercapacitors for wearable energy storage: a review by category, J. Mater. Chem. A 4 (2016) 4659-4685.

[11] L. Liu, Z. Niu, J. Chen, Unconventional supercapacitors from nanocarbon-based electrode materials to device configurations, Chem. Soc. Rev. 45 (2016) 4340-4363.

[12] S. He, W. Chen, Application of biomass-derived flexible carbon cloth coated with MnO2 nanosheets in supercapacitors, J. Power Sources 294 (2015) 150-158.
[13] M. Li, Z. Tang, M. Leng, J. Xue, Flexible solid-state supercapacitor based on graphene-based hybrid films, Adv. Funct. Mater. 24 (2014) 7495-7502.
[14] Z. Liu, J. Xu, D. Chen, G. Shen, Flexible electronics based on inorganic nanowires, Chem. Soc. Rev. 44 (2015) 161-192.
[15] D. Yu, Q. Qian, L. Wei, W. Jiang, K. Goh, J. Wei, J. Zhang, Y. Chen, Emergence of fiber supercapacitors, Chem. Soc. Rev. 44 (2015) 647-662.
[16] Q. Liu, L. Zang, C. Yang, C. Wei, J. Qiu, C. Liu, X. Xu, A flexible and knittable fiber supercapacitor for wearable energy storage with high energy density and mechanical robustness, J. Electrochem. Soc. 165 (2018) A1515.
[17] Y. Guo, K. Zheng, P. Wan, A flexible stretchable hydrogel electrolyte for healable all-in-one configured supercapacitors, Small 14 (2018) 1704497.
[18] L. Manjakkal, C.G. Núñez, W. Dang, R. Dahiya, Flexible self-charging supercapacitor based on graphene-Ag-3D graphene foam electrodes, Nano Energy 51 (2018) 604-612.
[19] C. Yang, Q. Liu, L. Zang, J. Qiu, X. Wang, C. Wei, X. Qiao, L. Hu, J. Yang, G. Song, High-performance yarn supercapacitor based on metal–inorganic–organic hybrid electrode for wearable electronics, Adv. Electron. Mater. 5 (2019) 1800435.
[20] H. Guo, M.-H. Yeh, Y.-C. Lai, Y. Zi, C. Wu, Z. Wen, C. Hu, Z.L. Wang, All-in-one shape-adaptive self-charging power package for wearable electronics, ACS nano 10 (2016) 10580-10588.
[21] Y. Hu, H. Cheng, F. Zhao, N. Chen, L. Jiang, Z. Feng, L. Qu, All-in-one graphene fiber supercapacitor, Nanoscale 6 (2014) 6448-6451.
[22] K. Wang, X. Zhang, C. Li, X. Sun, Q. Meng, Y. Ma, Z. Wei, Chemically crosslinked hydrogel film leads to integrated flexible supercapacitors with superior performance, Adv. Mater. 27 (2015) 7451-7457.
[23] T. Gao, Z. Zhou, J. Yu, D. Cao, G. Wang, B. Ding, Y. Li, All-in-one compact architecture toward wearable all-solid-state, high-volumetric-energy-density supercapacitors, ACS Appl. Mater. Interfaces 10 (2018) 23834-23841.
[24] C. Shao, T. Xu, J. Gao, Y. Liang, Y. Zhao, L. Qu, Flexible and integrated supercapacitor with tunable energy storage, Nanoscale 9 (2017) 12324-12329.

[25] L.-Q. Fan, G.-J. Liu, J.-H. Wu, L. Liu, J.-M. Lin, Y.-L. Wei, Asymmetric supercapacitor based on graphene oxide/polypyrrole composite and activated carbon electrodes, Electrochim. Acta 137 (2014) 26-33.

[26] C. Yang, L. Zang, J. Qiu, E. Sakai, X. Wu, Y. Iwase, Nano-cladding of natural microcrystalline cellulose with conducting polymer: preparation, characterization, and application in energy storage, RSC advances 4 (2014) 40345-40351.

[27] Y. Huang, H. Li, Z. Wang, M. Zhu, Z. Pei, Q. Xue, Y. Huang, C. Zhi, Nanostructured polypyrrole as a flexible electrode material of supercapacitor, Nano Energy 22 (2016) 422-438.

[28] V. Augustyn, J. Come, M.A. Lowe, J.W. Kim, P.-L. Taberna, S.H. Tolbert, H.D. Abruña, P. Simon, B. Dunn, High-rate electrochemical energy storage through Li+ intercalation pseudocapacitance, Nature materials 12 (2013) 518-522.

[29] J. Yan, C.E. Ren, K. Maleski, C.B. Hatter, B. Anasori, P. Urbankowski, A. Sarycheva, Y. Gogotsi, Flexible MXene/graphene films for ultrafast supercapacitors with outstanding volumetric capacitance, Adv. Funct. Mater. 27 (2017) 1701264.

[30] S. Ardizzone, G. Fregonara, S. Trasatti, “Inner” and “outer” active surface of RuO2 electrodes, Electrochim. Acta 35 (1990) 263-267.

[31] C. Yang, Y. Tang, Y. Tian, Y. Luo, Y. He, X. Yin, W. Que, Achieving of Flexible, Free‐Standing, Ultracompact Delaminated Titanium Carbide Films for High Volumetric Performance and Heat‐Resistant Symmetric Supercapacitors, Adv. Funct. Mater. 28 (2018) 1705487.

[32] X. Li, J. Shao, S.-K. Kim, C. Yao, J. Wang, Y.-R. Miao, Q. Zheng, P. Sun, R. Zhang, P.V. Braun, High energy flexible supercapacitors formed via bottom-up infilling of gel electrolytes into thick porous electrodes, Nat. Commun. 9 (2018) 1-8.

[33] J. Tao, W. Ma, N. Liu, X. Ren, Y. Shi, J. Su, Y. Gao, High-performance solid-state supercapacitors fabricated by pencil drawing and polypyrrole depositing on paper substrate, Nano-micro letters 7 (2015) 276-281.

[34] K. Keum, G. Lee, H. Lee, J. Yun, H. Park, S.Y. Hong, C. Song, J.W. Kim, J.S. Ha, Wire-shaped supercapacitors with organic electrolytes fabricated via layer-by-layer assembly, ACS Appl. Mater. Interfaces 10 (2018) 26248-26257.

[35] J.-G. Wang, Y. Yang, Z.-H. Huang, F. Kang, Effect of temperature on the pseudo-capacitive behavior of freestanding MnO2@ carbon nanofibers composites electrodes in mild electrolyte, J. Power Sources 224 (2013) 86-92.

[36] Y. Wang, S. Su, L. Cai, B. Qiu, N. Wang, J. Xiong, C. Yang, X. Tao, Y. Chai, Monolithic integration of all-in-one supercapacitor for 3D electronics, Adv. Energy Mater. 9 (2019) 1900037.
[37] N. Wang, G. Han, Y. Xiao, Y. Li, H. Song, Y. Zhang, Polypyrrole/graphene oxide deposited on two metalized surfaces of porous polypropylene films as all-in-one flexible supercapacitors, Electrochim. Acta 270 (2018) 490-500.
[38] F. Liu, J. Wang, Q. Pan, An all-in-one self-healable capacitor with superior performance, J. Mater. Chem. A 6 (2018) 2500-2506.
[39] J. Du, C. Zheng, W. Lv, Y. Deng, Z. Pan, F. Kang, Q.H. Yang, A Three-Layer All-In-One Flexible Graphene Film Used as an Integrated Supercapacitor, Advanced Materials Interfaces 4 (2017) 1700004.
[40] Z.S. Wu, K. Parvez, X. Feng, K. Müllen, Graphene-based in-plane micro-supercapacitors with high power and energy densities, Nat. Commun. 4 (2013) 1-8.
[41] M.F. El-Kady, R.B. Kaner, Scalable fabrication of high-power graphene micro-supercapacitors for flexible and on-chip energy storage, Nat. Commun. 4 (2013) 1-9.
[42] A.M. Abdelkader, N. Karim, C. Vallés, S. Afroj, K.S. Novoselov, S.G. Yeates, Ultraflexible and robust graphene supercapacitors printed on textiles for wearable electronics applications, 2D Materials 4 (2017) 035016.
[43] X. Liu, T. Qian, N. Xu, J. Zhou, J. Guo, C. Yan, Preparation of on chip, flexible supercapacitor with high performance based on electrophoretic deposition of reduced graphene oxide/polypyrrole composites, Carbon 92 (2015) 348-353.
[44] M. Beidaghi, C. Wang, Micro-supercapacitors based on three dimensional interdigital polypyrrole/C-MEMS electrodes, Electrochim. Acta 56 (2011) 9508-9514.

Chapter 5 All-gel-state flexible supercapacitors based on PVA/PEDOT:PSS hydrogel electrodes

5.1 Introduction

To satisfy the portability and comfort of wearable electronics, tremendous efforts have been devoted to researching the flexible and wearable power supply devices with durable and robust mechanical flexibility.[1-4] A new generation of energy storage devices such as flexible ion batteries, flexible solar panels, and flexible supercapacitors has gradually replaced traditional batteries as an inevitable trend.[5-7] Among them, flexible supercapacitors are considered as the most potential candidates due to their high efficiency, long cycle life, and simple maintenance. Recently, researchers have devoted tremendous efforts to preparing flexible supercapacitors with bendable, foldable, and high softness characteristics.[8-12] Generally, a flexible supercapacitor is composed of flexible electrodes and a gel-state solid electrolyte. The flexible electrodes consist of electroactive materials that provide electrochemical performance and an elastic matrix that acts as the flexible skeleton. The electrochemical performance of the integrated composite electrode is mainly determined by the electroactive material, while the mechanical properties are determined by the flexible substrate material. At present, the commonly used flexible substrates are fabric, carbon cloth, elastoplastic film, and paper.[13-17] Although these flexible substrates can achieve a certain degree of bending deformation, they are far from the level of stretchable and compressible. Besides, the electroactive materials of the composite electrodes based on these traditional flexible substrates are usually covering on the surface of the flexible substrate. When large deformation occurs, the problem of electroactive materials falling off the substrate is likely to occur. Therefore, proper flexible substrates are the keys to the preparation of a high-quality flexible electrode.

Polyvinyl alcohol (PVA) hydrogel is a soft material with a three-dimensional (3D) network structure and high-water content.[18, 19] The cross-linked PVA hydrogel has superior mechanical properties, which is an ideal flexible substrate material for supercapacitors.[20, 21] A novel strategy is to embed electroactive materials in the PVA hydrogel matrix. This strategy can effectively solve the problem of electroactive materials falling off from the substrate during deformation. Furthermore, due to the high ion migration speed and strong water retention capacity, PVA hydrogel has been widely developed for the preparation of polymeric gel electrolytes.[22] Since the electrode material is based on PVA hydrogel, it can be closely combined with the PVA gel electrolyte through hydrogen bonds to assemble into an all-gel-state integrated supercapacitor, thereby avoiding delamination between the electrolyte and the electrode at long-term deformations. Recently, many integrated supercapacitors based on PVA hydrogel have been reported. For instance, Zang et al. used gas-phase polymerization to embed polypyrrole (PPy) in the cross-linked PVA film, and then assembled it into an all-solid-state integrated supercapacitor.[23] Wang et al. embedded polyaniline (PANI) in a chemically cross-linked PVA-H_2SO_4 hydrogel film by in situ polymerization to erect an integrated flexible supercapacitor with a PANI–hydrogel–PANI structure.[24] Li and co-workers prepared PANI-PVA hydrogel composite through the supramolecular assembly of PANI and PVA and assembled it into an all-solid-state flexible supercapacitor.[25] Pawar et al. used graphene oxide (GO) as an electroactive filler and synthesized a nanocomposite of GO and PVA in a solution phase in a PVA matrix.[26] These devices exhibit excellent mechanical durability and electrochemical cycling stability, which fully proves the advantages of this strategy. However, it is inevitable that the use of gas-phase polymerization or in situ polymerization to directly embed the electroactive material into the PVA hydrogel matrix may cause insufficient embedding, which will affect the electrochemical performance of the final device. Moreover, simply mixing the electroactive material and the PVA solution before molding will result in insufficient dispersibility, thereby greatly reducing the mechanical properties. Therefore, it is still a challenge to develop a universal and simple method to manufacture robust PVA hydrogel-based supercapacitors with high electrochemical properties.

Poly-(3,4-ethylenedioxythiophene):polystyrene sulfonate (PEDOT:PSS) is considered a promising electrode material for supercapacitors owing to its high electrical conductivity, good electrochemical properties, and excellent dispersion.[27,

28] However, PEDOT:PSS is limited by its low mechanical strength, and it is difficult to directly apply in flexible supercapacitors. A composite electrode formed by combining suitable materials with PEDOT:PSS can effectively improve mechanical flexibility while maintaining excellent electrochemical performance. For example, Liu et al. fabricated a flexible rGO-PEDOT/PSS composite membranes and assembled it into a flexible supercapacitor that can be rolled.[27] Zhao et al. synthesized a highly flexible supercapacitor based on cellulose-PEDOT:PSS/MWCNT composite films.[29] The electrode materials prepared by these works have excellent tensile strength but weak tensile deformation, which indicate that combining PVA and PEDOT:PSS to prepare a composite hydrogel electrode is a possible suitable strategy.

In this work, we report a 3D porous network structure free-standing conductive polymer hydrogel electrode with a special leaf-vein-like microstructure hole wall based on PVA and PEDOT:PSS. PEDOT:PSS is a mixed aqueous dispersion of two ionomers, which can fully be mixed with PVA solution in the state of a dispersion liquid before being cross-linked into a conducting-polymer hydrogel. This preparation method not only ensures that the electroactive substances can be uniformly dispersed in the flexible substrate but also facilitates large-scale preparation. In addition, the treatment of ethylene glycol (EG) greatly improves the conductivity of the composite electrode, which is conducive to electrochemical energy storage. Owing to the strong hydrogen bond formed between the hydroxyl group of PVA and the sulfonate group in PEDOT:PSS,[30-32] the as-prepared composite electrode has high porosity, stretchability, and compressibility, which is advantageous for enhancing the mechanical stability of the supercapacitor.

Thanks to this superior hydrogel electrode, the as-fabricated all-gel-state flexible supercapacitor has excellent mechanical durability and electrochemical performance, which can maintain stable power output after repeated deformation. As a practical application demonstration, it can successfully drive an LCD electronic watch, and continue to supply power even when it is bent, compressed, and even in a low-temperature environment. All in all, this device opens a door to a new generation of flexible energy storage devices for wearable electronics.

5.2 Experimental section

5.2.1 Materials

Polyvinyl alcohol (PVA, degree of polymerization 2000), ethylene glycol (EG), sulfuric acid (H_2SO_4, 98 wt%), poly(3,4-ethylenedioxythiophene):polystyrene sulfonate (PEDOT:PSS, 1.3 wt%) were analytical grade and purchased from Nacalai Tesque, Inc.

5.2.2 Preparation of PVA/PEDOT:PSS hydrogel composite electrodes

10 g of PVA was added to 90 g of deionized water and mechanical stirring at 90 °C for 3 hours until the PVA was completely dissolved (solution became transparent). Then the PEDOT:PSS dispersion and as-prepared PVA solution were mixed with a volume ratio of 1:1 and stirred for 2 hours to mix thoroughly. After ultrasonication and evacuation to remove small bubbles, the mixture was poured into a Teflon mold, and then placed in a refrigerator at -25 °C for 24 hours. Then it was taken out and thawed at 4 °C for 3 hours. The freezing and thawing cycles were repeated three times. After that, the crosslinked PVA/PEDOT:PSS hydrogel (PPPH) was immersed in the EG solution for 3 hours, and the excess EG on the surface was removed after cleaning to obtain EG-PPPH composite electrode.

5.2.3 Fabrication of the All-gel-state flexible supercapacitor:

The PVA/H_2SO_4 gel electrolyte was prepared by dissolving 6 g of PVA in 60 ml of 1 M H_2SO_4 solution. Before assembly, the EG-PPPH electrode was immersed in a 1M H_2SO_4 solution for 1 h, and then coated a layer of gel PVA/H_2SO_4 electrolyte to one side of the EG-PPPH electrode. Thereafter, two pieces of the EG-PPPH electrodes were clamped together and pressed under a certain pressure for 2 h to form an all-gel-state integrated flexible supercapacitor (AGSI-FSC). Finally, the AGSI-FSC was encapsulated with 3M VHB tape.

5.2.4 Characterization

The microscopic morphology of the sample was measured by the field emission scanning electron microscope (S-4300, HITACHI, Japan). The EDS elemental mapping

was obtained by an Energy Dispersive Spectrometer (Apollo XV; EDAX, USA). The chemical structure of the samples was characterized by a Raman spectrometer (Thermo Scientific^{TM} DXR, USA). XRD patterns of the samples were recorded with an X-ray diffractometer (XRD 6000, Shimadzu Co. Ltd., Japan) using Nickel-filter Cu Kα radiation. The specific surface area was measured Multi-point BET at 77 K using the ASAP 2020 analyzer (Micromeritics, USA). The tensile properties and compression properties were measured on a universal mechanical tester (Instron 3385, Instron Co., Ltd., Canton, USA). The tensile test was carried out on the rectangular specimens of 10 mm width × 30 mm length × 1 mm depth, with a gauge length, was 10 mm, with a stretching speed of 20 mm min^{-1} at room temperature. The compression test was performed on the cubic specimens of 10 mm with a constant speed of 10 mm min^{-1} at room temperature. All of the data on electrochemical performance was tested by an electrochemical workstation (CS2350H, CORRTEST, China). The electrochemical performance of the electrode was carried out in a three-electrode test system where a platinum electrode was used as a counter electrode, a saturated calomel electrode (SCE) was used as a reference electrode, and a 1 M H_2SO_4 solution was used as an electrolyte. The electrochemical performance of the electrode and the assembled device is obtained according to the following formulas:

$$C_{electrode} = \frac{i \times t}{S \times U} \quad (1)$$

$$C_{sc} = \frac{i \times t}{2S \times U} \quad (2)$$

$$E_{sc} = \frac{C_{SC} \times U^2}{2 \times 3600} \quad (3)$$

$$P_{sc} = \frac{3600 \times E_{SC}}{t} \quad (4)$$

Where $C_{electrode}$ represents the specific capacitance of the electrode in the three-electrode system; C_{sc}, E_{sc}, and P_{sc} denote the specific capacitance, energy density, and power density of the AGSI-FSC, respectively; *i, t, S,* and *U* stands for current (A), discharged time (s), the opposite area of one side electrode (cm^2), and voltage window (V), respectively.

5.3 Results and Discussion

5.3.1 Analysis of the preparation process

A novel all-gel-state integrated flexible supercapacitor (AGSI-FSC) was designed and fabricated, of which PEDOT:PSS was used as an electroactive substance, and PVA hydrogel was used as a flexible substrate. The preparation process of the AGSI-FSC is illustrated in **Fig. 5.1**. First of all, PEDOT:PSS and PVA aqueous solution are thoroughly mixed to obtain a precursor solution. Then the precursor solution is placed in a specific mold and repeatedly frozen and thawed, making it cross-linked to form a hydrogel. After that, the crosslinked PVA/PEDOT:PSS hydrogel (PPPH) is treated with EG to obtain an EG-PPPH electrode. Ultimately, two EG-PPPH electrodes and a layer of PVA/H_2SO_4 gel electrolyte are sandwiched together to form an AGSI-FSC.

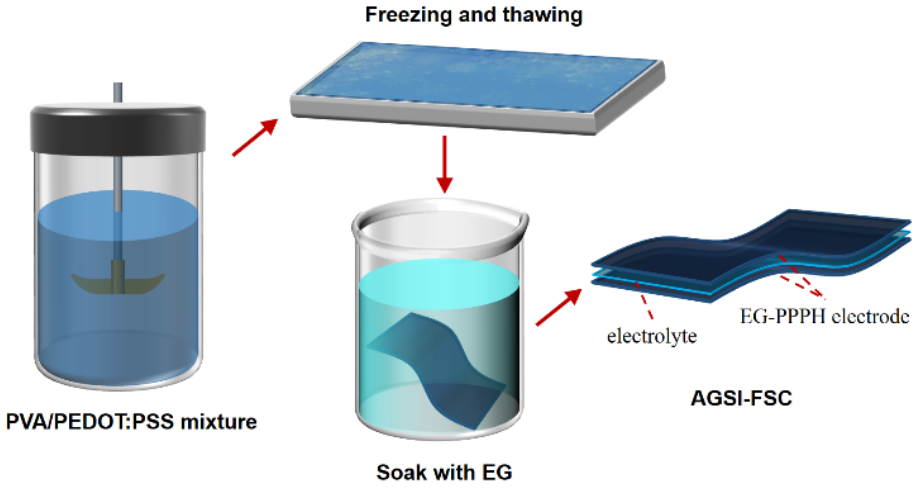

Fig. 5.1 Schematic illustration of preparation process of the all-gel-state integrated flexible supercapacitor.

5.3.2 Chemical composition and micromorphological characterization

To explore the changes in the crystalline state and aggregation structure of the EG-PPPH electrode, X-ray diffraction (XRD) patterns of PEDOT:PSS, PVA, PPPH, and EG-PPPH were obtained by XRD. As shown in the XRD pattern of the PEDOT:PSS in **Fig. 5.2**, a broad diffraction peak at 2θ of 25.7° assigned to (020) plane of the polymer backbone of PEDOT appears, which indicates that it is amorphous.[33] PVA shows three typical peaks at 2θ = 19.8°, 22.9°, and 40.9°, corresponding to the (101), (200),

and (102) planes of PVA semi-crystal.[34] By comparison, EG-PPPH and PPPH show the same diffraction peaks as pristine PVA, indicating that the mixing of PEDOT:PSS and the treatment of EG did not affect the aggregation structure and crystalline state of the composite electrode material, thereby not reducing the final mechanical performance.

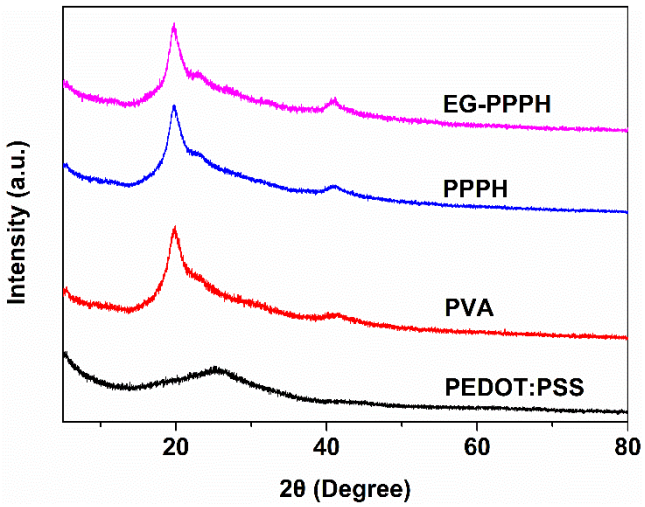

Fig. 5.2 XRD patterns of PEDOT:PSS, PVA, PPPH, and EG-PPPH.

The uniformity of the distribution of electroactive substances in the substrate tremendously affects the comprehensive performance of the composite electrode material, including mechanical properties and electrochemical properties. Fortunately, due to the good solubility of PEDOT:PSS, a precursor that is homogeneously mixed with the PVA aqueous solution can be easily obtained. The digital photos in **Fig. 5.3a** record this process. The colorless transparent PVA solution and black PEDOT:PSS dispersion is mixed to form a uniform navy blue precursor solution. By freezing and thawing, this precursor solution can be customized to any desired shape by using different molds (**Fig. 5.3b**), indicating that it has excellent moldability. After freeze-thaw cross-linking, the PPPH is endowed with excellent mechanical properties. As shown in **Fig. 5.4a**, the tensile strength of PPPH is 9.21 MPa, and elongation at break is about 180.9%. The excellent stretchability of the PPPH laid the foundation for the preparation of flexible EG-PPPH composite electrodes in the next step.

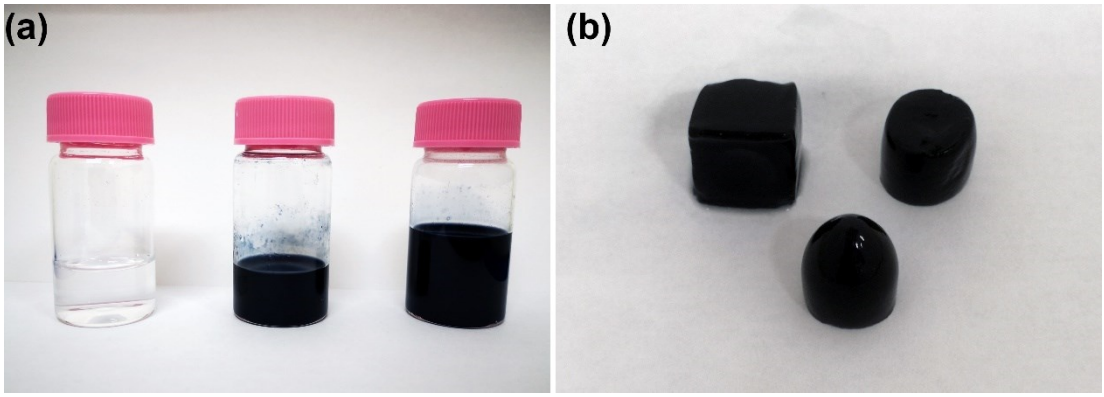

Fig. 5.3 (a) The photograph of the PVA aqueous solution, PEDOT:PSS, and PVA/PEDOT: PSS mixture; (b) Optical image of the crosslinked PPPH in different states.

To solve the problem that PEDOT is not easy to be dissolved and processed, PSS is introduced to improve solubility by co-dissolution, but the conductivity of PEDOT:PSS is greatly reduced. Previous studies have shown that treatment with organic solvents or polyols, such as N-methyl pyrrolidone (NMP), dimethylsulfoxide (DMSO), dimethylformamide (DMF), tetrahydrofuran (THF), glycerol, mannitol, and EG, can significantly increase the conductivity of PEDOT:PSS.[35-40] In this work, we chose EG to treat the PPPH. After EG treatment, the resistance of PPPH is reduced from 485.4 Ω to 70.9 Ω, which is mainly due to the effect of EG on the configuration of PEDOT chains. To investigate this effect, Raman spectroscopy was used to study the changes in the conformation of the PEDOT chain in PEDOT:PSS before and after EG treatment. The Raman spectrum in **Fig. 5.4b** shows that the symmetrical stretching vibration of the five-member ring of PEDOT located near 1440 cm^{-1} is shifted to the lower wavenumber side, which indicates that the PEDOT has changed from the benzoid to the quinoid structure (**Fig. 5.4c**). This result is consistent with previous reports.[36, 41] The EG plays a dual role in this work, in addition to improving the conductivity of PPPH, it also endows the PPPH with good frost resistance. Comparing PPPH with EG-PPPH after freezing at -25 ℃ for 4 hours, the EG-PPPH can remain intact, while the PPPH is frozen. Furthermore, after EG treatment, it still has excellent flexibility. The tensile strength of EG-PPPH is 8.97 MPa, and elongation at break is about 190.2% (**Fig. 5.4a**), which has no significant change compared with PPPH. In addition, we also tested the compression performance of the EG-PPPH. As shown in **Fig. 5.4d** and **Fig. 5.4e**, after 500 compression cycles with a 50% compression strain, the EG-PPPH can retain 84.5%

of the original stress with almost no residual deformation, showing excellent compressibility. The good flexibility and antifreeze characteristics provide possibilities for EG-PPPH application in low-temperature-resistant flexible energy storage devices.

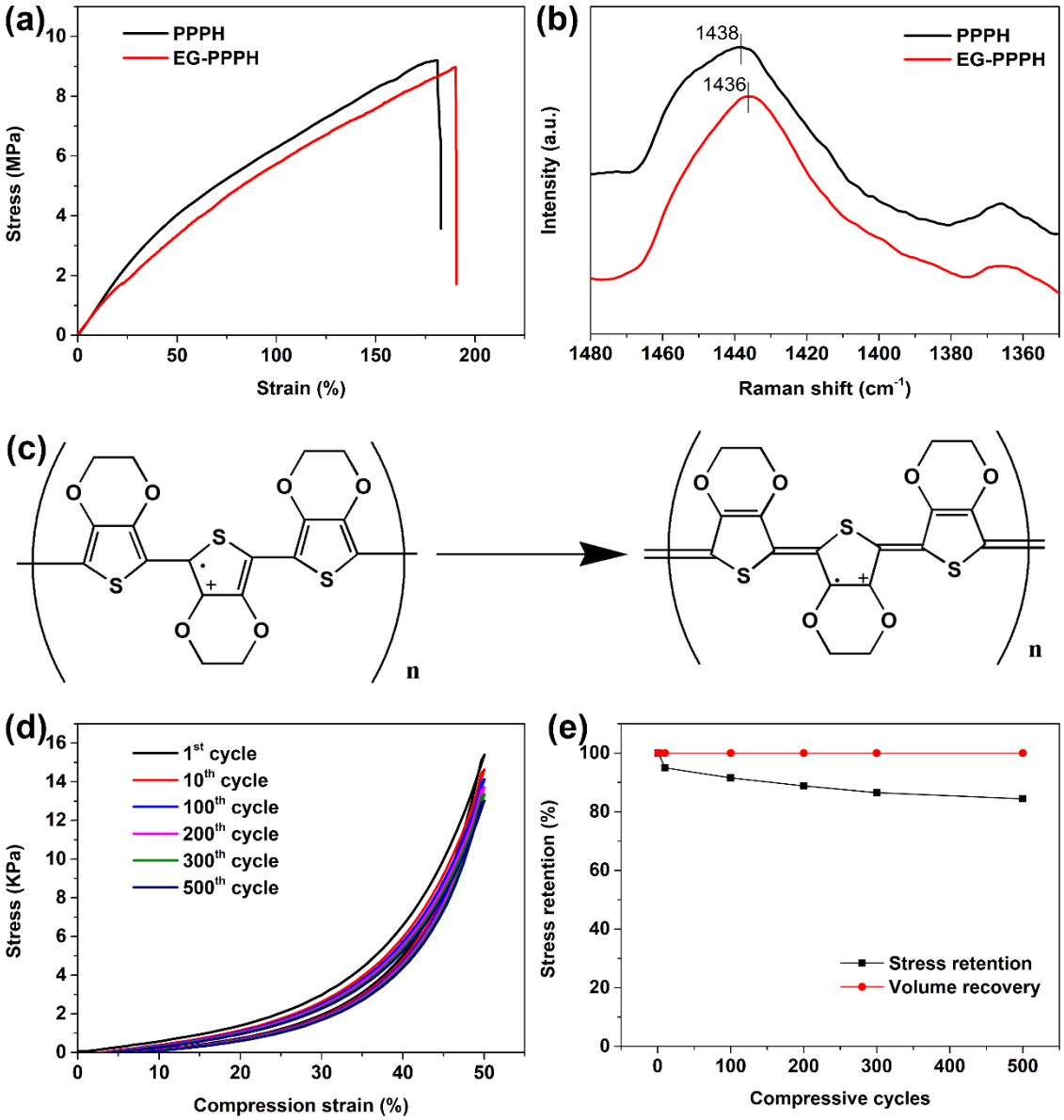

Fig. 5.4 (a) Tensile stress-strain curve of the PPPH and EG-PPPH. (b) Raman spectrum of the PPPH and EG-PPPH. (c) Scheme of transformation of the PEDOT chain from the benzoid to the quinoid structure. (d) The cyclic compression stress-strain curve of EG-PPPH at 50 % compression. (e) Volume retention and stress retention of EG-PPPH for 500 compression cycles at a strain of 50 %.

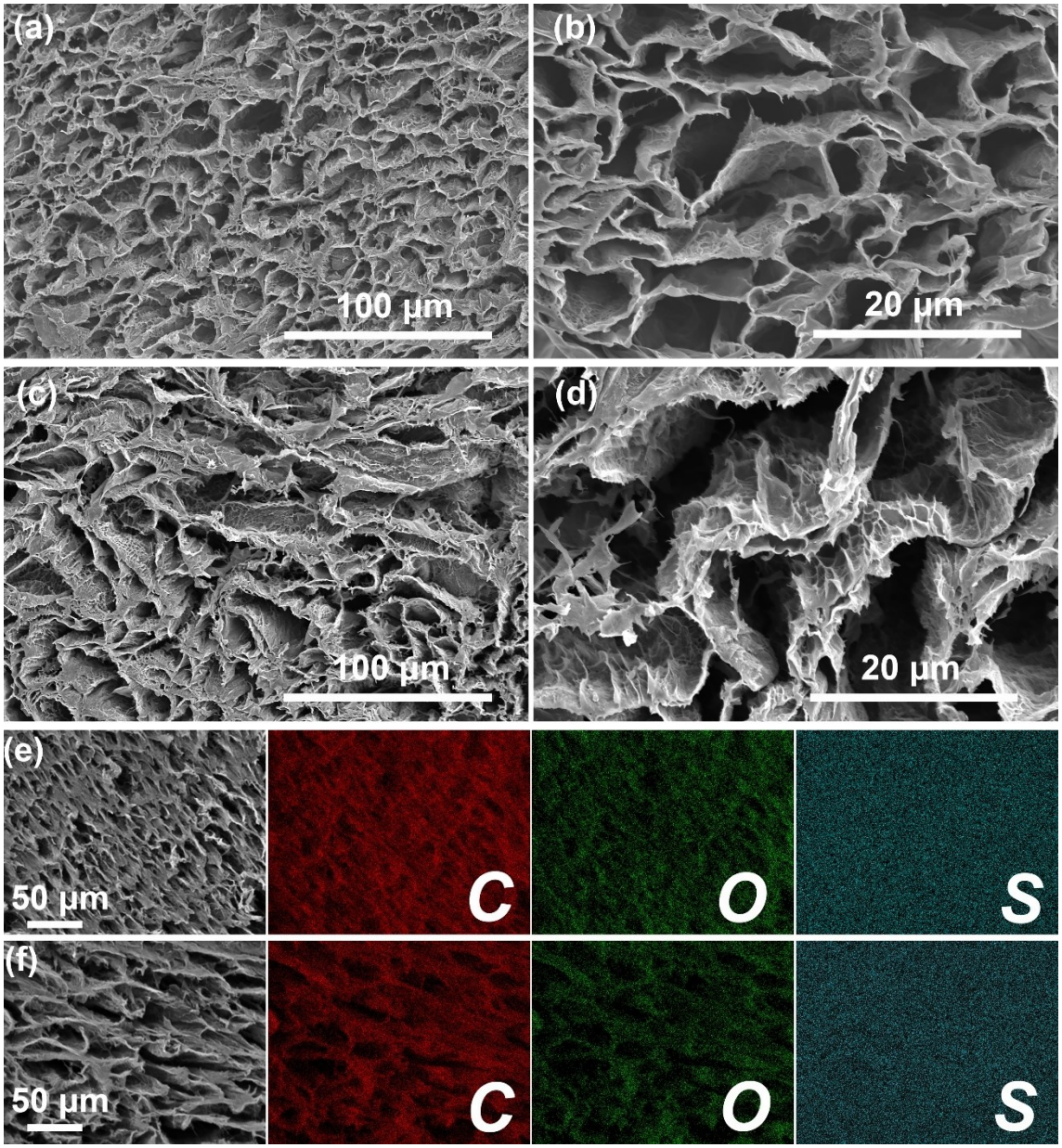

Fig. 5.5 SEM images of cross-section of the freeze-dried PPPH (a, b) and EG-PPPH (c, d). Energy-dispersive spectroscopy of the PPPH (e) and EG-PPPH (f).

Fig. 5.5 presents the micro-morphology of the cross-section of the freeze-dried PPPH and EG-PPPH. It is observed that both PPPH and EG-PHHH exhibit the same 3D porous network structure with a rough hole wall morphology. Compared with the microscopic morphology of PPPH, the hole wall of EG-PPPH presents a peculiar leaf vein-like structure and a higher surface roughness. This unique leaf vein network can promote the transmission of the electrons and improve electronic conductivity. Apart from this, it is capable to increase specific surface area. The specific surface area of EG-

PPPH calculated by Multi-point BET is 175.96 m^2 g^{-1} which is higher than that of the PPPH (97.19 m^2 g^{-1}).

The increase in surface area is beneficial to the improvement of specific capacitance. The elemental composition of the PPPH (**Fig. 5.5e**) and EG-PPPH (**Fig. 5.5f**) was analyzed by EDS elemental mapping. It can be seen that the main components of PPPH and EG-PPPH are C, O, and S elements, where C and O elements are mainly from PVA and PEDOT:PSS, and S elements are all from PEDOT:PSS. The homogeneous distribution of the S element indicates that PEDOT:PSS as an electroactive substance is evenly distributed in the PPPH and EG-PPPH. In addition, it is confirmed that EG treatment does not affect the dispersion uniformity of PEDOT:PSS.

5.3.3 Electrochemical properties and mechanical stability

Comparisons of mechanical properties between PPPH and EG-PPPH, as well as SEM images, have shown that EG treatment has no negative effects, but only improves the conductivity of composite electrode materials. The improvement of electrical conductivity will lead to the improvement of electrochemical performance. In order to confirm this, the electrochemical performance of PPPH and EG-PPPH was evaluated using a three-electrode system. The comparison of CV curves is shown in **Fig. 5.6a**, and it can be observed that the closed area of the EG-PPPH is much larger than that of the PPPH at the scan rate of 40 mV s^{-1}. The significantly larger closed area of the EG-PPPH at the same scan rate indicates that EG-PPPH has a higher specific capacitance than PPPH. Similarly, at the same current density, the discharge time of the EG-PPPH is more than ten times longer than that of the PPPH (**Fig. 5.6b**). According to the GCD data, the areal-specific capacitances of PPPH and EG-PPPH are calculated to be 23.8 mF cm^{-2} and 380.8 mF cm^{-2}, respectively. Unsurprisingly, the EG-PPPH has a superior specific capacitance.

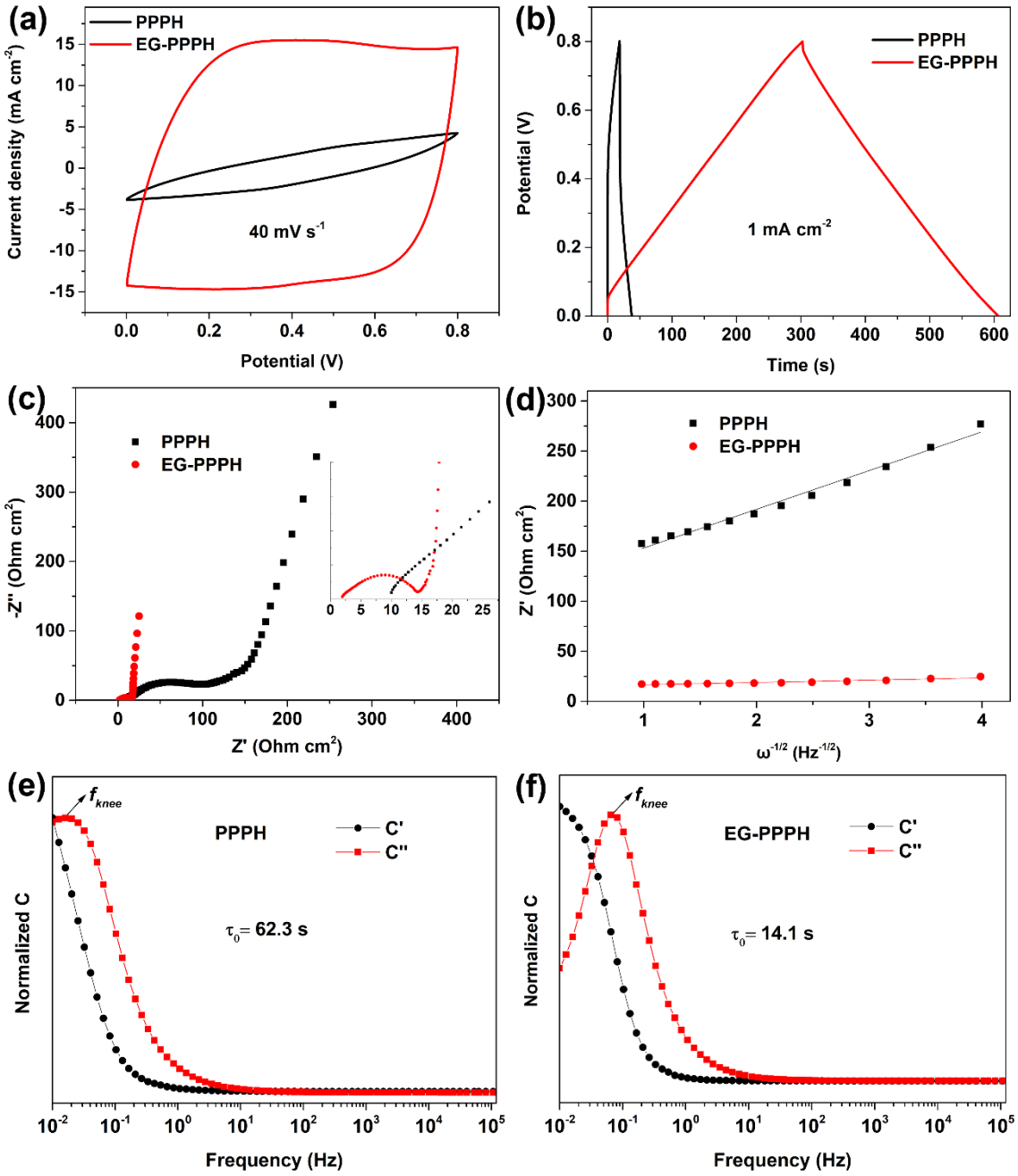

Fig. 5.6 Comparison of the electrochemical performance of PPPH and EG-PPPH electrodes. (a) CV curves ; (b) GCD curves; (c) Nyquist plots; (d) The correspondence between $\omega^{-1/2}$ and Z' in low-frequency region; Normalized real and imaginary capacitances of the (e) PPPH and (f) EG-PPPH vs. frequency.

The Nyquist plots of the PPPH and the EG-PPPH are shown in **Fig. 5.6c**. Obviously, the equivalent series resistance (R_s) and charge transfer resistance (R_{ct}) of EG-PPPH are smaller than PPPH. The R_s of the EG-PPPH is 1.63 Ω while the PPPH is 8.89 Ω, and the R_{ct} of the EG-PPPH is 14.22 Ω, which is much smaller than that of PPPH (R_{ct} =

227.8 Ω). The substantial reduction in R_{ct} is attributed to the improvement of electronic conductivity. The increase in electronic conductivity is due to the conversion of the PEDOT chain from benzoid structure to quinoid structure with higher conductivity after EG treatment. In the low-frequency region, the line of EG-PPPH is closer to vertical than the line of PPPH, which indicates that EG-PPPH has better capacitance performance.[42, 43] Additionally, the relationship between Z' and ($\omega = 2\pi f$) in the low-frequency region of **Fig. 5.6d** shows that the slope of EG-PPPH electrode is smaller than that of PPPH, which indicates lower charge transfer resistance and better ion migration kinetics.[44, 45]

To further compare the electrochemical impedance spectroscopy of PPPH with EG-PPPH, the impedance behaviors of the PPPH and EG-PPPH were studied by the complex model. **Fig. 5.6e** and **5.6f** show the normalized real capacitance (C′) and imaginary capacitance (C″) of the PPPH and EG-PPPH as a function of frequency. It can be seen that as the frequency increases, the C′ of EG-PPPH decreases more slowly than PPPH, which means that the diffusion and migration speed of ions in EG-PPPH is faster. This can be quantified by the relaxation time constant (τ_0) of the inflection point frequency (f_{knee}). According to the formula $\tau_0=1/f_{knee}$, it can be calculated that the τ_0 of EG-PPPH is 14.1 s, which is much smaller than 62.3 s of PPPH. The EG-PPPH has a shorter relaxation time constant, which means it has a higher power. All the above data have proved that the electrochemical performance of EG-PPPH obtained by EG treatment is far superior to PPPH. EG plays an important role in improving the electrochemical performance of composite electrode materials. The most significant impact is that the conductivity of the composite electrode material has been significantly improved after EG treatment. This is because EG makes the configuration of PEDOT chains in PEDOT:PSS has been transformed from a benzoid structure to a more conductive quinoid structure. The insulating PSS shell surrounding the PEDOT:PSS becomes thinner, which improves the contact between the conductive components, thereby enhancing the transport of carriers and enhancing the conductivity.[33, 46-48] On the other hand, EG changes the microstructure of the composite electrode, provides a better conductive path, and also increases the specific surface area, which is conducive to the improvement of electrochemical performance.

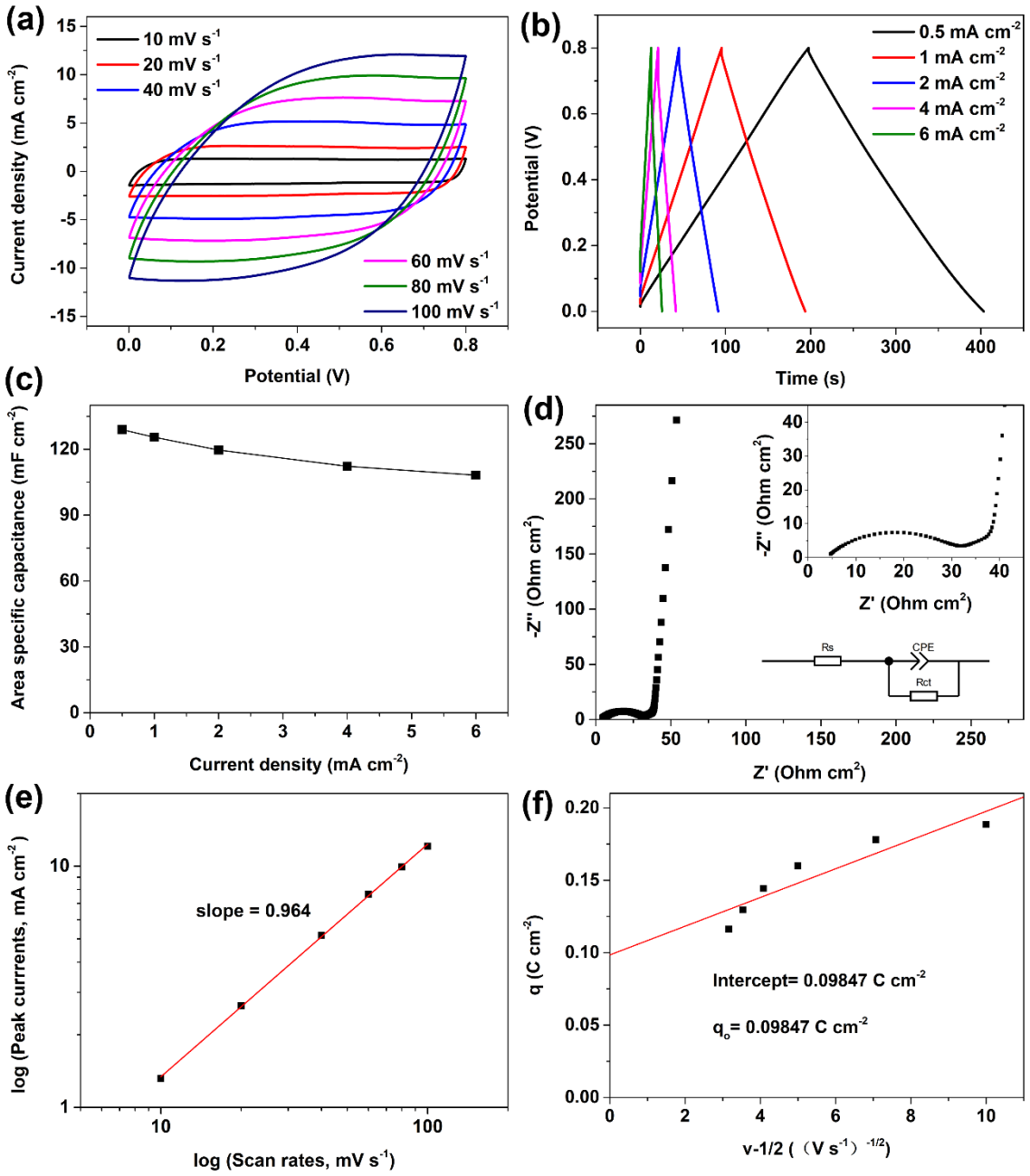

Fig. 5.7 The electrochemical performance of AGSI-FSC. (a) CV curves at different scan rates; (b) GCD curves at different current density ; (c) Area-specific capacitance under different current density; (d) Nyquist plot and equivalent circuit diagram; (e) The relationship between peak currents and scan rates from 10 to 100 mV s^{-1}, (f) the dependence of q(v) on $v^{-1/2}$.

Through a two-electrode system, the electrochemical performance of the assembled AGSI-FSC was comprehensively studied. **Fig. 5.7a** demonstrates the CV curves of the AGSI-FSC at different scan rates. At the scan rate of 10 ~100 mV s^{-1}, all CV curves

show a rectangular-like symmetrical shape, which indicates that the device has a good capacitive performance. The GCD curves of the AGSI-FSC at a current density from 0.5 to 6 mA cm^{-2} are demonstrated in **Fig. 5.7b**. It can be observed that all the GCD curves show almost linearity, which is a typical characteristic of pseudocapacitor materials.[49] The areal specific capacitances of the AGSI-FSC (C_{sc}) at a range from 0.5 to 6 mA cm^{-2} calculated by GCD data are shown in **Fig. 5.7c**. The value of C_{sc} is 128.9 mF cm^{-2} at 0.5 mA cm^{-2}. When the current is increased to 12 times, the value of C_{sc} still reaches 108.2 mF cm^{-2}, and the capacitance retention rate is as high as 83.9%, which implies that AGSI-FSC has an outstanding rate capability. In addition, the specific capacitance based on the mass loading of electroactive material was also calculated. The thickness of the AGSI-FSC is 1.5 mm and the density is approximately 1 g cm^{-3}. The mass loading of the PEDOT:PSS on AGSI-FSC is 0.975 mg cm^{-2}, and the corresponding mass-specific capacitances range from 132.2 F g^{-1} at 0.5 mA cm^{-2} to 110.97 F g^{-1} at 6 mA cm^{-2} (**Fig. S5**). The Nyquist plot of the AGSI-FSC is illustrated in **Fig. 5.7d**. The R_s is ~3.9 Ω, and the R_{ct} is ~29.5 Ω, which indicates that the AGSI-FSC has a lower internal resistance and excellent charge transferability. A straight line appears in the intermediate-frequency region, which is a typical diffusion impedance.[50] The angle of amplitude of the diffusion impedance is less than 45°, which indicates that the surface of the electrode is rough, and indirectly proves that the electrode has a high specific surface area.[51]

In the CV curve, there is an exponential relationship between the current (i) and the scan rate (v):[49]

$$i = av^b \quad (5)$$

A linear equation (Equation (6)) can be obtained by taking the logarithm on both sides of Equation (5):

$$\log i = \log a + b \log v \quad (6)$$

where a and b are constants. A value of b of 1 represents that the storage of charge is a non-diffusion control process, whereas a value of b of 0.5 is a diffusion control process. By calculating the value of b, it is possible to determine whether the electrochemical reaction process is controlled by diffusion. The plot of log(v) vs. log(i) is shown in **Fig. 5.7e**. The b value obtained from the slope of the function is 0.964, which is approximately equal to 1, indicating that the charge storage process is mainly limited by non-diffusion, thus providing excellent rate capability.[44, 49] To further study the

nature of charge storage for AGSI-FSC, the kinetic characteristics of the electrode reaction of AGSI-FSC were analyzed by the Trasatti analysis method which can quantify the external charges (q_o, charges stored on the outer surface where ions easily accessible) and internal charge (q_i, charges stored on the inner surface where ions less accessible). The functional relationship between the total charge stored (q(v)) in the CV test and the scan rate (v) is described as follows:[44, 52]

$$q_{(v)} = q_o + kv^{-\frac{1}{2}} \quad (7)$$

where k is a constant, $kv^{-1/2}$ is the charge storage of semi-infinite diffusion. When the scan rate is infinite, the charge storage associated with diffusion is 0, and the total charge storage amount at this moment is equal to q_o. The plots of q vs. $v^{-1/2}$ is shown in **Fig. 5.7f**. From the intercept of the fitted line, the q_o is calculated to be 0.09847 C cm^{-2}. The practical charge storage at the scan rates from 10 to 100 mV s^{-1} is calculated to be 0.18856, 0.17796, 0.15986, 0.14435, 0.12957 and 0.11623 C cm^{-2}, respectively. At a lower scan rate of 10 mV s^{-1}, q_o is accounted for 52.2% of the practical charge, which indicates that non-diffusion control dominates charge storage. This means that the storage of charge is primarily a surface process, most of which takes place on the outer surface. This is due to the leaf vein-like structure provides a good conductive path and a large specific surface area, making the ions in the electrolyte more accessible.

The Ragone plot of the AGSI-FSC and the other reported supercapacitors based on PEDOT are presented in **Fig. 5.8a**. The highest energy density (E_a) is 11.46 μWh cm^{-2} with a power density (P_a) of 200.5 μW cm^{-2}. When P_a reaches the highest 2720 μW cm^{-2}, the E_a can also reach 9.62 μWh cm^{-2}, which can retain 83.9% of the maximum energy density. The power density and energy density of the AGSI-FSC based on the mass loading of electroactive material were also calculated. The mass-energy density is 11.76 Wh Kg^{-1} at a mass power density of 205.64 Wh Kg^{-1}. The excellent energy storage capacity of this device is superior to many previously reported PEDOT:PSS-based supercapacitors.[53-57] The cycle stability and coulombic efficiency of AGSI-FSC were determined by 10,000 charge and discharge cycles at a current density of 4 mA cm^{-2}, and the final result is shown in **Fig. 5.8b**. Many previous reports have shown that the cycle stability curve will have a significant increasing trend at the beginning, and then decline slowly, which is explained as an activation process of the electrode. In this work, the capacitance retention decreases gently with the increase of the cycle

numbers, and there is no electrode activation process. This is due to the unique 3D porous network structure of the PPPH electrode and its excellent water-retaining ability, which makes the PEDOT equivalent to being immersed in the electrolyte. In addition, the leaf vein-like microstructure provides a larger specific surface area, which is conducive to the full contact of PEDOT and electrolyte and accelerates the transmission of ions between interfaces. After 10,000 charge and discharge cycles, the capacitance retention rate can still reach 89.8 %, which is comparable with the previously reported supercapacitors based on PEDOT:PSS, including PEDOT:PSS/AgNFs-SC (95%, 10,000 cycles),[54] PEDOT:PSS/MWNT fiber (98%, 1000 cycles),[57] ANFs/PEDOT:PSS-SC(84.5%, 10,000 cycles),[58] $Co(OH)_F$ on PEDOT:PSS/AgNW/PUS-SC (85.8%, 3000 cycles).[59]

The most important parameter for flexible energy storage devices is to maintain a stable energy supply in the event of deformation. The mechanical durability of AGSI-FSC was evaluated by measuring their electrochemical performance under different bending states and capacitance retention under repeated bending conditions. **Fig. 5.8c** shows the CV curves of AGSI-FSC under different bending degrees. It can be seen that when the bend angle is 90°, the CV curve is almost unchanged, and when the bend angle reaches 180°, there is only slight deformation. To study the durability of the device under repeated bending, the AGSI-FSC is repeatedly bent to 90° for CV testing, and the capacitance retention rate maintains 98.1% after 1000 cycles (**Fig. 5.8d**), indicating that the device is very attractive in flexible energy storage devices. The GCD curves of the AGSI-FSC series and parallel are shown in **Fig. 5.8e**. It can be observed that the output voltage can be easily expanded through series connection, and the discharge time can be increased in parallel, which indicates that AGSI-FSC is capable of the design requirements of modular energy storage devices with adjustable output voltage and capacitance by adjusting the number of device connections. **Fig. 5.8f** is a demonstration of a practical application case. Two AGSI-FSCs connected in series successfully drive an LCD electronic meter with an operating voltage of 1.5 V. What is even more surprising is that it can continue to power LCD electronic meter in bending, compression, and even in low-temperature environments.

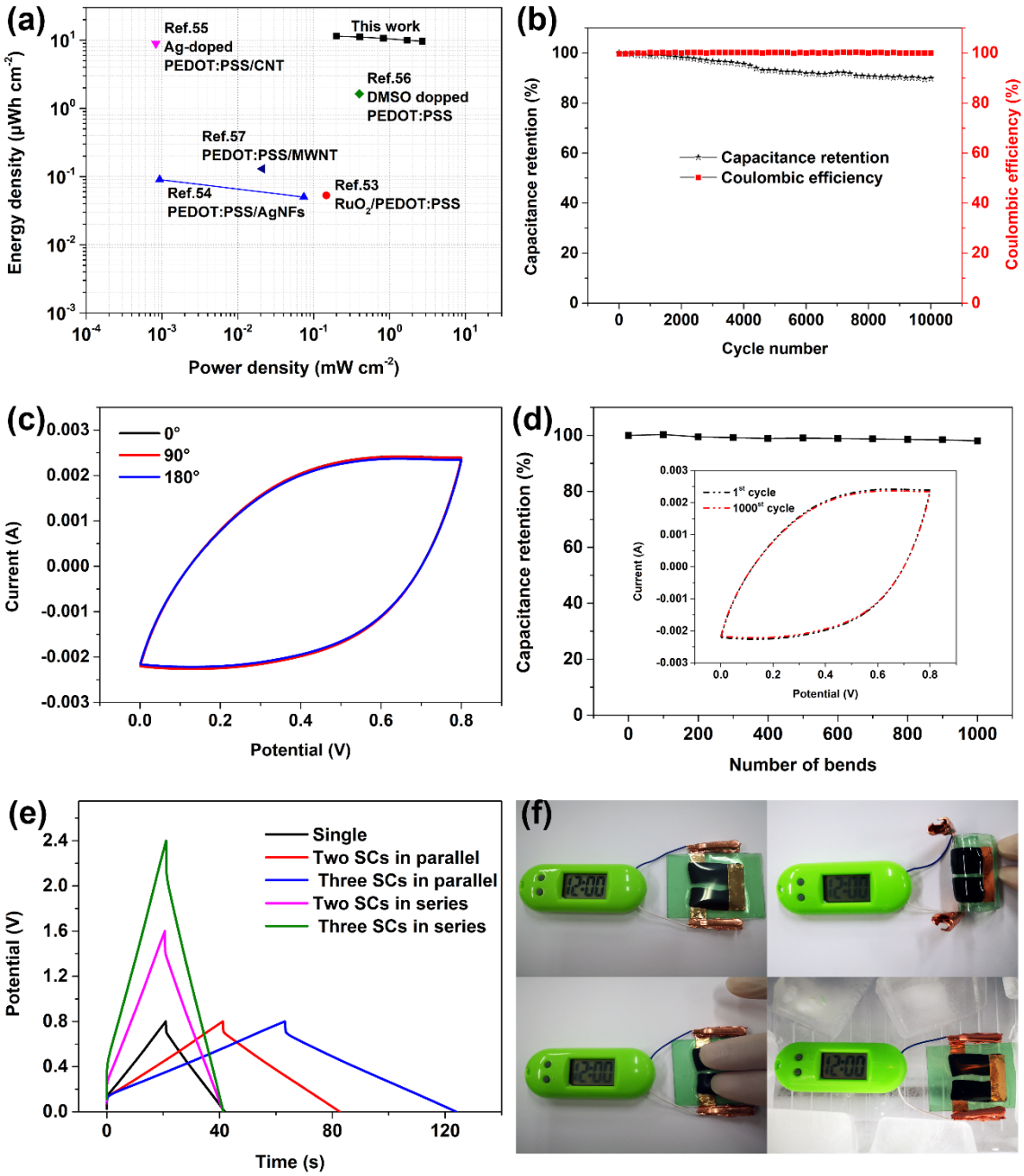

Fig. 5.8 The electrochemical performance of AGSI-FSC. (a) Ragone plot of the AGSI-FSC and the other reported supercapacitors. (b) Cycling stability and coulombic efficiency of 10,000 charge/discharge cycles; (c) CV curves of the AGSI-FSC under different bending states at 100 mV s^{-1}; (d) Capacitance retention of the device after 1000 bends at a bending angle of 90°; Insets are the CV curves of the first cycle and the 1000 bend cycles at a bending angle of 90°. (e) GCD curves of serial and parallel assembly of single AGSI-FSC and multiple AGSI-FSCs; (f). The digital photos of the LCD electronic watch powered by two AGSI-FSCs at original state, Bend state, compressed state and low-temperature environment.

5.4 Conclusion

In summary, a robust flexible electrode with special leaf-vein-like microstructure pore walls has been fabricated by freeze-thaw cross-linking the PVA/PEDOT:PSS hydrogel followed by a soaking process with EG solution. The immersion treatment of EG not only improves the conductivity of PPPH but also endows PPPH with good frost resistance. The EG-PPPH electrode has good mechanical properties and can be easily stretched, compressed, and customized into different shapes; it also has high conductivity, low internal resistance, and excellent specific capacitance. Owing to the fascinating characteristics of EG-PPPH electrode, the as-prepared AGSI-FSC has outstanding mechanical durability and excellent electrochemical performance, and can successfully drive an LCD watch under deformation and even in low-temperature environments. It is foreseeable that this strategy can provide a feasible scheme for the large-scale manufacturing of all-gel-state integrated flexible energy storage devices.

Reference

[1] F. Mo, G. Liang, Z. Huang, H. Li, D. Wang, C. Zhi, An overview of fiber-shaped batteries with a focus on multifunctionality, scalability, and technical difficulties, Adv. Mater. 32 (2020) 1902151.

[2] Y. Wang, S. Su, L. Cai, B. Qiu, N. Wang, J. Xiong, C. Yang, X. Tao, Y. Chai, Monolithic Integration of All-in-One Supercapacitor for 3D Electronics, Adv. Energy Mater. 9 (2019) 1900037.

[3] F. Liu, J. Wang, Q. Pan, An all-in-one self-healable capacitor with superior performance, J. Mater. Chem. A 6 (2018) 2500-2506.

[4] H. Li, Z. Tang, Z. Liu, C. Zhi, Evaluating flexibility and wearability of flexible energy storage devices, Joule 3 (2019) 613-619.

[5] X. Zhang, L. Yao, S. Liu, Q. Zhang, Y. Mai, N. Hu, H. Wei, High-performance lithium sulfur batteries based on nitrogen-doped graphitic carbon derived from covalent organic frameworks, Materials today energy 7 (2018) 141-148.

[6] Q. Yang, F. Mo, Z. Liu, L. Ma, X. Li, D. Fang, S. Chen, S. Zhang, C. Zhi, Activating C-Coordinated Iron of Iron Hexacyanoferrate for Zn Hybrid-Ion Batteries with 10 000-Cycle Lifespan and Superior Rate Capability, Adv. Mater. 31 (2019) 1901521.

[7] G. Chen, F. Zhang, Z. Zhou, J. Li, Y. Tang, A flexible dual-ion battery based on PVDF-HFP-modified gel polymer electrolyte with excellent cycling performance and superior rate capability, Adv. Energy Mater. 8 (2018) 1801219.

[8] J. Zeng, L. Dong, W. Sha, L. Wei, X. Guo, Highly stretchable, compressible and arbitrarily deformable all-hydrogel soft supercapacitors, Chem. Eng. J. 383 (2020) 123098.

[9] L. Dong, C. Xu, L. Yang, Z.H. Huang, F. Kang, Q.H. Yang, Z. Xin, Flexible electrodes and supercapacitors for wearable energy storage: A review by category, J. Mater. Chem. A 4 (2016) 4659-4685.

[10] Y. Wang, Q. Yang, Y. Zhao, S. Du, C. Zhi, Recent Advances in Electrode Fabrication for Flexible Energy - Storage Devices, Adv. Mater. Technol. 4 (2019) 1900083.

[11] M. Zhu, F. Zhang, X. Chen, Bioinspired Mechanically Interlocking Structures, Small Structures 2000045.

[12] J. Zhao, H. Lu, X. Zhao, O.I. Malyi, J. Peng, C. Lu, X. Li, Y. Zhang, Z. Zeng, G. Xing, Printable Ink Design towards Customizable Miniaturized Energy Storage Devices, ACS Materials Letters 2 (2020) 1041-1056.
[13] S. Liu, L. Yao, Y. Lu, X. Hua, J. Liu, Z. Yang, H. Wei, Y. Mai, All-organic covalent organic framework/polyaniline composites as stable electrode for high-performance supercapacitors, Mater. Lett. 236 (2019) 354-357.
[14] L. Zang, X. Qiao, Q. Liu, C. Yang, L. Hu, J. Yang, Z. Ma, High-performance solid-state supercapacitors with designable patterns based on used newspaper, Cellulose 27 (2020) 1033-1042.
[15] H. Qian, A.R. Kucernak, E.S. Greenhalgh, A. Bismarck, M.S. Shaffer, Multifunctional structural supercapacitor composites based on carbon aerogel modified high performance carbon fiber fabric, ACS Appl. Mater. Interfaces 5 (2013) 6113-6122.
[16] X. Wang, G. Li, M.H. Seo, G. Lui, F.M. Hassan, K. Feng, X. Xiao, Z. Chen, Carbon-coated silicon nanowires on carbon fabric as self-supported electrodes for flexible lithium-ion batteries, ACS Appl. Mater. Interfaces 9 (2017) 9551-9558.
[17] Z. Lv, Y. Tang, Z. Zhu, J. Wei, W. Li, H. Xia, Y. Jiang, Z. Liu, Y. Luo, X. Ge, Honeycomb‐Lantern‐Inspired 3D Stretchable Supercapacitors with Enhanced Specific Areal Capacitance, Adv. Mater. 30 (2018) 1805468.
[18] J. Han, H. Wang, Y. Yue, C. Mei, J. Chen, C. Huang, Q. Wu, X. Xu, A self-healable and highly flexible supercapacitor integrated by dynamically cross-linked electro-conductive hydrogels based on nanocellulose-templated carbon nanotubes embedded in a viscoelastic polymer network, Carbon 149 (2019) 1-18.
[19] H. Wang, S.K. Biswas, S. Zhu, Y. Lu, Y. Yue, J. Han, X. Xu, Q. Wu, H. Xiao, Self-healable electro-conductive hydrogels based on core-shell structured nanocellulose/carbon nanotubes hybrids for use as flexible supercapacitors, Nanomaterials 10 (2020) 112.
[20] H. Li, T. Lv, H. Sun, G. Qian, N. Li, Y. Yao, T. Chen, Ultrastretchable and superior healable supercapacitors based on a double cross-linked hydrogel electrolyte, Nat. Commun. 10 (2019) 1-8.
[21] R. Hu, J. Zhao, Y. Wang, Z. Li, J. Zheng, A highly stretchable, self-healing, recyclable and interfacial adhesion gel: preparation, characterization and applications, Chem. Eng. J. 360 (2019) 334-341.
[22] H.N. Fard, G.B. Pour, M.N. Sarvi, P. Esmaili, PVA-based supercapacitors, Ionics

(2019) 1-13.
[23] L. Zang, Q. Liu, J. Qiu, C. Yang, C. Wei, C. Liu, L. Lao, Design and Fabrication of an All-Solid-State Polymer Supercapacitor with Highly Mechanical Flexibility Based on Polypyrrole Hydrogel, ACS Appl. Mater. Interfaces 9 (2017) 33941-33947.
[24] K. Wang, X. Zhang, C. Li, X. Sun, Q. Meng, Y. Ma, Z. Wei, Chemically crosslinked hydrogel film leads to integrated flexible supercapacitors with superior performance, Adv. Mater. 27 (2015) 7451-7457.
[25] W. Li, F. Gao, X. Wang, N. Zhang, M. Ma, Strong and robust polyaniline-based supramolecular hydrogels for flexible supercapacitors, Angew. Chem. Int. Ed. 55 (2016) 9196-9201.
[26] P.B. Pawar, S. Shukla, S. Saxena, Graphene oxide–Polyvinyl alcohol nanocomposite based electrode material for supercapacitors, J. Power Sources 321 (2016) 102-105.
[27] Y. Liu, B. Weng, J.M. Razal, Q. Xu, C. Zhao, Y. Hou, S. Seyedin, R. Jalili, G.G. Wallace, J. Chen, High-performance flexible all-solid-state supercapacitor from large free-standing graphene-PEDOT/PSS films, Sci. Rep. 5 (2015) 17045.
[28] D. Kim, S.K. Ahn, J. Yoon, Highly Stretchable Strain Sensors Comprising Double Network Hydrogels Fabricated by Microfluidic Devices, Adv. Mater. Technol. 4 (2019) 1800739.
[29] D. Zhao, Q. Zhang, W. Chen, X. Yi, S. Liu, Q. Wang, Y. Liu, J. Li, X. Li, H. Yu, Highly flexible and conductive cellulose-mediated PEDOT: PSS/MWCNT composite films for supercapacitor electrodes, ACS Appl. Mater. Interfaces 9 (2017) 13213-13222.
[30] X.-y. Wang, G.-y. Feng, M.-j. Li, M.-q. Ge, Effect of PEDOT:PSS content on structure and properties of PEDOT:PSS/poly(vinyl alcohol) composite fiber, Polym. Bull. 76 (2019) 2097-2111.
[31] T. Zhang, K. Li, C. Li, S. Ma, H.H. Hng, L. Wei, Mechanically durable and flexible thermoelectric films from PEDOT: PSS/PVA/Bi0. 5Sb1. 5Te3 nanocomposites, Adv. Electron. Mater. 3 (2017) 1600554.
[32] C.h. Chen, J.C. LaRue, R.D. Nelson, L. Kulinsky, M.J. Madou, Electrical conductivity of polymer blends of poly (3, 4 - ethylenedioxythiophene): Poly (styrenesulfonate): N-methyl-2-pyrrolidinone and polyvinyl alcohol, J. Appl. Polym. Sci. 125 (2012) 3134-3141.

[33] T. Murakami, Y. Mori, H. Okuzaki, Effect of ethylene glycol on structure and carrier transport in highly conductive poly (3, 4-ethylenedioxythiophene)/poly (4-styrenesulfonate), Transactions of the Materials Research Society of Japan 36 (2011) 165-168.

[34] Y.-N. Chen, C. Jiao, Y. Zhao, J. Zhang, H. Wang, Self-assembled polyvinyl alcohol–tannic acid hydrogels with diverse microstructures and good mechanical properties, ACS omega 3 (2018) 11788-11795.

[35] J. Kim, J. Jung, D. Lee, J. Joo, Enhancement of electrical conductivity of poly (3, 4-ethylenedioxythiophene)/poly (4-styrenesulfonate) by a change of solvents, Synth. Met. 126 (2002) 311-316.

[36] J. Ouyang, C.W. Chu, F.C. Chen, Q. Xu, Y. Yang, High‐conductivity poly (3, 4-ethylenedioxythiophene): poly (styrene sulfonate) film and its application in polymer optoelectronic devices, Adv. Funct. Mater. 15 (2005) 203-208.

[37] J. Saghaei, A. Fallahzadeh, M.H. Yousefi, Improvement of electrical conductivity of PEDOT: PSS films by 2-Methylimidazole post treatment, Org. Electron. 19 (2015) 70-75.

[38] F. Zhang, M. Johansson, M.R. Andersson, J.C. Hummelen, O. Inganäs, Polymer photovoltaic cells with conducting polymer anodes, Adv. Mater. 14 (2002) 662-665.

[39] C.-J. Ko, Y.-K. Lin, F.-C. Chen, C.-W. Chu, Modified buffer layers for polymer photovoltaic devices, Appl. Phys. Lett. 90 (2007) 063509.

[40] J. Cárdenas-Martínez, B.L. España-Sánchez, R. Esparza, J.A. Ávila-Niño, Flexibleand transparent supercapacitors using electrospun PEDOT: PSS electrodes, Synth. Met. 267 (2020) 116436.

[41] J. Ouyang, C. Qianfei, On the mechanism of conductivity enhancement in poly(3,4-ethylenedioxythiophene):poly(styrene sulfonate) film through solvent treatment, Polymer 45 (2004) 8443-8450.

[42] S. Wang, N. Liu, J. Rao, Y. Yue, K. Gao, J. Su, L. Li, X. Jiang, Z. Liu, Y. Gao, Vertical finger-like asymmetric supercapacitors for enhanced performance at high mass loading and inner integrated photodetecting systems, J. Mater. Chem. A 5 (2017) 22199-22207.

[43] C. Yang, Q. Liu, L. Zang, J. Qiu, X. Wang, C. Wei, X. Qiao, L. Hu, J. Yang, G. Song, C. Liu, High-Performance Yarn Supercapacitor Based on Metal–Inorganic–Organic Hybrid Electrode for Wearable Electronics, Adv. Electron. Mater. 5 (2019)

1800435.
[44] J. Yan, C.E. Ren, K. Maleski, C.B. Hatter, B. Anasori, P. Urbankowski, A. Sarycheva, Y. Gogotsi, Flexible MXene/graphene films for ultrafast supercapacitors with outstanding volumetric capacitance, Adv. Funct. Mater. 27 (2017) 1701264.
[45] M. Fan, Y. Chen, Y. Xie, T. Yang, X. Shen, N. Xu, H. Yu, C. Yan, Half-cell and full-cell applications of highly stable and binder-free sodium ion batteries based on Cu3P nanowire anodes, Adv. Funct. Mater. 26 (2016) 5019-5027.
[46] G. Greczynski, T. Kugler, M. Keil, W. Osikowicz, M. Fahlman, W.R. Salaneck, Photoelectron spectroscopy of thin films of PEDOT–PSS conjugated polymer blend: a mini-review and some new results, J. Electron. Spectrosc. Relat. Phenom. 121 (2001) 1-17.
[47] S. Ashizawa, R. Horikawa, H. Okuzaki, Effects of solvent on carrier transport in poly (3, 4-ethylenedioxythiophene)/poly (4-styrenesulfonate), Synth. Met. 153 (2005) 5-8.
[48] H. Okuzaki, Y. Harashina, H. Yan, Highly conductive PEDOT/PSS microfibers fabricated by wet-spinning and dip-treatment in ethylene glycol, Eur. Polym. J. 45 (2009) 256-261.
[49] Y. Jiang, J. Liu, Definitions of pseudocapacitive materials: a brief review, Energy & Environmental Materials 2 (2019) 30-37.
[50] P. Xu, J. Liu, P. Yan, C. Miao, K. Ye, K. Cheng, J. Yin, D. Cao, K. Li, G. Wang, Preparation of porous cadmium sulphide on nickel foam: a novel electrode material with excellent supercapacitor performance, J. Mater. Chem. A 4 (2016) 4920-4928.
[51] A. Sharifi-Viand, M. Mahjani, M. Jafarian, Investigation of anomalous diffusion and multifractal dimensions in polypyrrole film, J. Electroanal. Chem. 671 (2012) 51-57.
[52] Q. Liu, L. Zang, X. Qiao, J. Qiu, X. Wang, L. Hu, J. Yang, C. Yang, Compressible All-In-One Supercapacitor with Adjustable Output Voltage Based on Polypyrrole-Coated Melamine Foam, Adv. Electron. Mater. 5 (2019) 1900724.
[53] C.J. Zhang, T.M. Higgins, S.-H. Park, S.E. O'Brien, D. Long, J.N. Coleman, V. Nicolosi, Highly flexible and transparent solid-state supercapacitors based on RuO2/PEDOT: PSS conductive ultrathin films, Nano Energy 28 (2016) 495-505.
[54] S.B. Singh, T. Kshetri, T.I. Singh, N.H. Kim, J.H. Lee, Embedded PEDOT: PSS/AgNFs network flexible transparent electrode for solid-state supercapacitor, Chem.

Eng. J. 359 (2019) 197-207.
[55] Y. Zhu, N. Li, T. Lv, Y. Yao, H. Peng, J. Shi, S. Cao, T. Chen, Ag-Doped PEDOT: PSS/CNT composites for thin-film all-solid-state supercapacitors with a stretchability of 480%, J. Mater. Chem. A 6 (2018) 941-947.
[56] L. Manjakkal, A. Pullanchiyodan, N. Yogeswaran, E.S. Hosseini, R. Dahiya, A Wearable Supercapacitor Based on Conductive PEDOT: PSS‐Coated Cloth and a Sweat Electrolyte, Adv. Mater. (2020) 1907254.
[57] H.J. Sim, C. Choi, D.Y. Lee, H. Kim, J.-H. Yun, J.M. Kim, T.M. Kang, R. Ovalle, R.H. Baughman, C.W. Kee, Biomolecule based fiber supercapacitor for implantable device, Nano Energy 47 (2018) 385-392.
[58] Y. Li, G. Ren, Z. Zhang, C. Teng, Y. Wu, X. Lu, Y. Zhu, L. Jiang, A strong and highly flexible aramid nanofibers/PEDOT: PSS film for all-solid-state supercapacitors with superior cycling stability, J. Mater. Chem. A 4 (2016) 17324-17332.
[59] I.K. Moon, S. Yoon, J. Oh, 3D Highly Conductive Silver Nanowire@ PEDOT: PSS Composite Sponges for Flexible Conductors and Their All‐Solid‐State Supercapacitor Applications, Advanced Materials Interfaces 4 (2017) 1700860.

Chapter 6 Flexible asymmetric supercapacitors based on all-conducting-polymer electrodes

6.1 Introduction

The rapid development of smart electronic communication technology and the Internet of Things, which can work under deformation conditions such as bending, folding, twisting, compressing, or stretching have become the main development direction of the next generation of intelligent electronics.[1-3] The new generation of flexible wearable devices requires novel structural designs and good deformation to ensure a comfortable wearing experience, which places higher demands on their energy supply systems.[4, 5] At present, even for ordinary electronics, batteries are still the main bottleneck in their development due to the difficulty in meeting the durability requirements. For flexible wearable electronic devices, the power supply not only needs to have a considerable capacity to ensure sufficient usage time but also needs to match the corresponding flexibility, even with stretchable, compressible, and twistable functions, which puts a higher level of requirements on its energy supply system. [6, 7] Consequently, there is an urgent need for flexible energy storage devices that are bendable, foldable, and stretchable. Currently, among the many flexible energy storage devices, flexible lithium-ion batteries (FLIBs) and flexible supercapacitors (FSCs) have the greatest potential for commercial application.[2, 8, 9] Compared with FLIBs, FSCs have the advantages of high power density, rapid charge, and discharge, long service life, low maintenance cost, wide operating temperature range, which is an extremely promising flexible energy storage device.[10, 11]

However, the main shortcoming of FSCs is their low energy density. It is a challenging task to increase the energy density without sacrificing its power density and stable cycling performance. Improve the energy density of supercapacitors, it can be achieved by increasing the specific capacitance and widening the voltage window. From

the energy density formula $E=1/2CU^2$ (E, C, and U represent energy density, specific capacitance, and voltage window respectively), it can be concluded that the improvement of the voltage window is more efficient in improving the energy density.[12, 13] Currently, a common strategy is to use organic electrolytes or ionic liquids instead of aqueous electrolytes to enhance the voltage window.[14, 15] However, organic electrolytes are flammable and toxic, posing safety risks; ionic liquids are expensive, limiting practical applications, and the trace water they adsorb still limits the further expansion of the voltage window. Another effective strategy is to develop aqueous asymmetric supercapacitors (ASCs), where the preparation of asymmetric devices with the different cathode and anode materials can take full advantage of the different potential windows of the two electrodes to maximize the operating voltage of the entire device.[16-18] Compared with organic electrolytes and ionic liquids, aqueous electrolytes have better ionic conductivity, higher safety, and low prices. The disadvantage is limited by the water decomposition voltage, the voltage window is not high enough. Fortunately, the asymmetric design concept can perfectly solve this defect, which allows the aqueous electrolyte system to easily break through the operating voltage of 1.23 V or even exceed 2 V.[19-21] For this reason, researchers have devoted extensive effort to the fabrication of the ASCs. A common strategy is to couple the positive electrode of the pseudocapacitor material with the negative electrode of the double-layer capacitor material. For example, metal oxide or metal hydroxide as the positive electrode coupled with other negative electrodes such as activated carbon (AC)[22, 23], carbon nanotube (CNT)[24], graphene[25]. All of this work has led to an expansion of the voltage window and a significant increase in energy density, but it has not led to the flexibility of the device. Although carbon materials are easy to achieve flexibility, it is hard to achieve high mechanical strength, while metal oxides and metal hydroxides are not easily processed for flexibility, which makes it difficult to meet the design requirements of flexible supercapacitors with high mechanical strength. Besides, these ASCs are required to strictly distinguish between positive and negative electrodes, since these electroactive materials can only operate properly at the corresponding voltage windows. For example, MnO_2 is only suitable as a positive material, and using asymmetric devices based on MnO_2 and carbon materials in reverse will lead to a significant decrease in capacitance or even damage the device. If the ASCs can be used like symmetric supercapacitors without differentiating between positive and negative

electrodes, it would be a great improvement in efficiency and safety for modular applications of the ASCs. To develop a highly flexible supercapacitor with interchangeable positive and negative electrodes, it is essential to find a suitable electroactive material.

Conductive polymers (CPs) are easy preparation, low cost, high conductivity, and good flexibility which is an ideal supercapacitor electrode material.[26, 27] Moreover, CPs exhibit good electrochemical properties in aqueous electrolytes with a large working potential range from -1.0 to 1.0 V, which allows them to have great potential both as positive and negative electrodes.[28] CPs have inherently flexible properties and can also be easily deposited chemically or electrochemically on flexible substrates without adhesives, offering great potential in the field of flexible energy storage devices. Recently, asymmetric supercapacitors were designed based on the combination of CPs each other such as polypyrrole (PPy), polyaniline (PANI), and poly(3,4-ethylenedioxythiophene) (PEDOT) has shown impressive electrochemical performance, but lack the exploration of mechanical flexibility function.[28-30] Fortunately, there is a range of conductive polymer hydrogels (CPHs) that have been reported to have good conductive properties while balancing electrochemical and mechanical properties.[31-33] It is hypothesized that aqueous asymmetric flexible supercapacitors (AFSCs) composed of two CPHs with excellent electrochemical properties and robust mechanical flexibility would deliver excellent comprehensive performance. To verify this hypothesis, a comprehensive study of the electrochemical and mechanical properties of all-gel-state AFSCs composed of two different CPHs has been carried out.

In this study, we employ a simple way to fabricate an all-gel-state integrated AFSC based on free-standing conductive polymer hydrogel electrodes with robust flexibility and fascinating electrochemical properties. Specifically, we used a physically cross-linked Polyvinyl alcohol (PVA)-poly-(3,4-ethylenedioxythiophene):polystyrene sulfonate (PEDOT:PSS) hydrogel electrode (PVA-PEDOT:PSS) as the negative electrode and a chemically cross-linked PVA-polypyrrole (PPy) hydrogel electrode (PVA-PPy) as the positive electrode, while applying PVA/H_2SO_4 hydrogel as the electrolyte. The cross-linked hydrogel composite electrodes have high conductivity and strong mechanical flexibility, which is advantageous for enhancing the capacitance and the mechanical stability of the device. The PVA-based all-gel design allows the sandwich-shaped supercapacitors to be tightly connected by hydrogen bonding to form

an integrated structure, eliminating slippage and delamination between the electrodes and electrolyte under large deformation, and reducing the internal resistance of the device. The combination of the aqueous asymmetric structure broadens the voltage window and allows for a significant increase in the energy density of the device. Owing to the above-mentioned points, the resulting AFSCs have reliable mechanical flexibility (22.3 MPa with the break elongation of 286%) and extremely attractive energy density (397.99 μWh cm^{-3}). It also exhibits outstanding cycling stability, with nearly 90% capacitance retention after 10,000 charge/discharge cycles. More surprisingly, the AFSCs we prepared can interchange the positive and negative electrodes, and the electrochemical performance can remain almost unchanged, and the cycle stability does not significantly decrease. Furthermore, our devices can be configured in series as symmetrical devices without differentiating between positive and negative to glow a light-emitting diode (LED). All in all, this device provides a design idea for a new generation of flexible energy storage devices for wearable electronics. Meanwhile, it provides a guide for the design of asymmetric supercapacitors that do not distinguish between positive and negative electrodes.

6.2 Experimental section

6.2.1 Materials

Polyvinyl alcohol (PVA, degree of polymerization 2000), Pyrrole, iron(III) chloride hexahydrate ($FeCl_3 \cdot 6H_2O$), glutaraldehyde (GA, 25%,), sulfuric acid (H_2SO_4, 98%), ethylene glycol (EG) were analytical grade and purchased from Nacalai Tesque, Inc. Poly(3,4-ethylenedioxythiophene):polystyrene sulfonate (PEDOT:PSS) aqueous suspension (CLEVIOS, PH1000, 1 wt%~1.3 wt%) was obtained from Sato Chemical Industry Co., Ltd.

6.2.2 Preparation of EG-PCPPH electrodes

10 mL of PEDOT:PSS dispersion and 10 mL of 10% PVA solution were mixed and stirred for 2 hours, then micro-bubbles in the solution were removed by sonication and vacuum. Then pour the homogeneous mixture into the Teflon mold and put it in the refrigerator at -25 ℃ for 24 hours, after freezing, thaw it at 4 ℃, and repeat the freezing and thawing three times to obtain a physically cross-linked PEDOT:PSS-PVA hydrogel

film (PCPPH). Afterward, the PCPPH was soaked in EG solution for 3 hours and rinsed with distilled water to remove excess EG to obtain the PEDOT:PSS-PVA hydrogel (EG-PCPPH) electrode.

6.2.3 Preparation of CCPH-PPy electrodes

The PVA powder (2 g) was dissolved in dilute sulfuric acid (0.5 M, 40 mL) by heating in a water bath (90 °C) with mechanical stirring to obtain a homogeneous solution. After the PVA solution was cooled, added GA solution (1%, 4 mL) while stirring, and then pour it into the Teflon mold. After standing in a thermostat at 25 °C for 24 hours, the chemically crosslinked PVA hydrogel film (CCPH) is obtained by peeling off the mold. PPy was then embedded in the CCPH film using a gas-phase polymerization method. Typically, the as-prepared CCPH film was immersed in an ethanol solution of $FeCl_3$ for 30 minutes and then dried in the vacuum drying oven at room temperature. Immediately afterward, the oxidant-saturated CCPH films were placed in a vacuum drier saturated with pyrrole vapor and vapor phase polymerized at 4 °C for 8 hours. Then wash with deionized water and dried to obtain a CCPH-PPy composite electrode.

6.2.4 Assembly of all-gel-state integrated asymmetric flexible supercapacitor

First, 10 g of PVA was dissolved in 100 ml of 1 M H_2SO_4 solution at 90 °C under stirring to prepare the PVA-H_2SO_4 gel electrolyte. Then, the gel electrolyte films were prepared according to the previous method of preparing CCPH. Before use, the gel electrolyte film was cut into the desired shape and placed in a 1M H_2SO_4 solution soaked thoroughly. Finally, two electrodes (EG-PCPPH and CCPH-PPy) sandwiched the gel electrolyte film and pressed together under a certain pressure for 4 hours to form an all- gel-state integrated asymmetric flexible supercapacitor (AFSC).

6.2.5 Electrochemical measurements and materials characterization

All electrochemical properties were tested using an electrochemical workstation (CS2350H, CORRTEST, China). The chemical structure of the samples was characterized by the Thermo Scientific DXR Raman spectrometer and Thermo Scientific Nicolet iN 10 Infrared spectrometers. The mechanical performance evaluation

was measured on a universal mechanical tester (Instron 3385, Instron Co., Ltd., Canton, USA). The tensile test was carried out on the rectangular specimens of 10 mm width×30 mm length×0.5 mm depth, with a gauge length was 10 mm, with a stretching speed of 20 mm min^{-1} at room temperature. The SEM images of the samples were measured by a scanning electron microscope (S-4300, HITACHI, Japan). The formulae for calculating the electrochemical properties of the electrode materials and the assembled AFSCs are detailed in the chapter 5.

6.3 Results and Discussion

6.3.1 Analysis of the preparation process

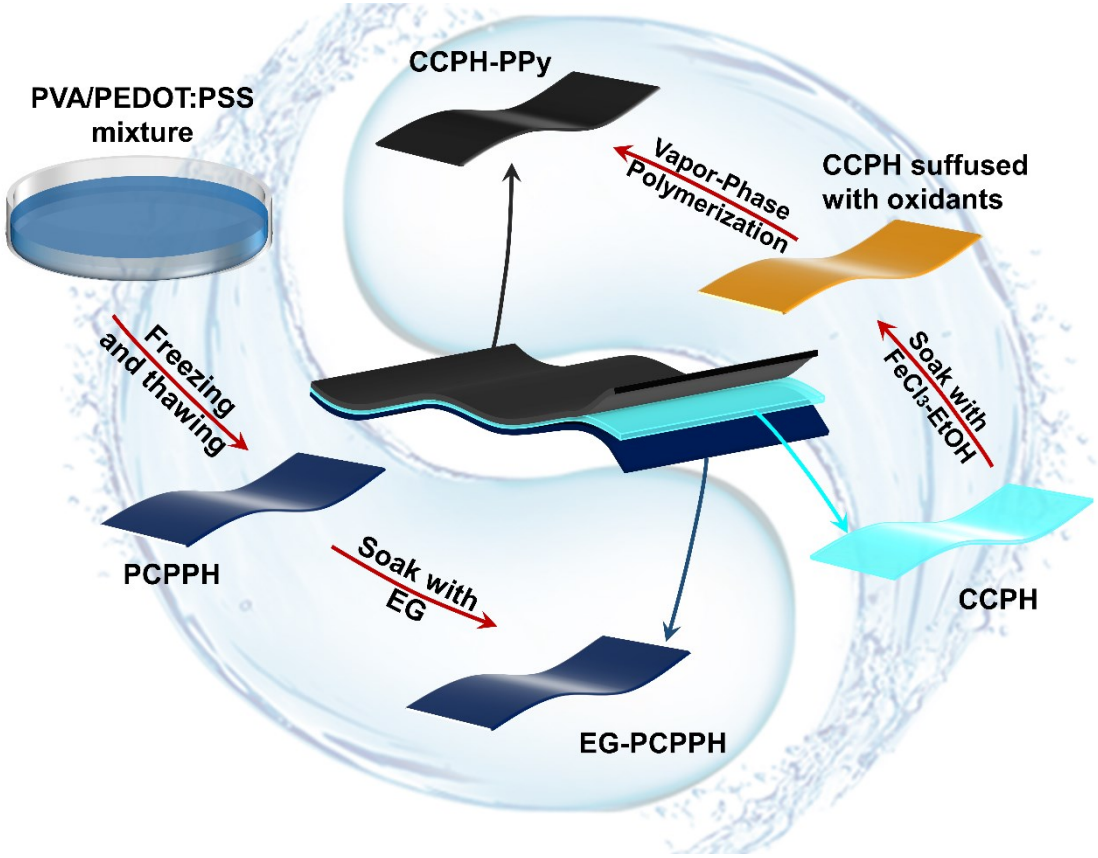

Fig. 6.1 Schematic illustration of the preparation process of the all-solid-state integrated AFSCs.

The schematic for the preparation of the solid-state integrated AFSCs based on free-standing conductive polymer hydrogel electrodes is illustrated in **Fig. 6.1**. The EG-PCPPH is fabricated by two steps of freeze-thaw crosslinking and EG immersion.

Repeated freezing and thawing are prompting physical cross-linking of the PEDOT:PSS/PVA mixture to form PCPPH with high mechanical strength. EG soaking treatment process is to obtain the higher conductivity EG-PCPPH composite electrode. After EG treatment, the resistance of PCPPH decreased from 877 Ω to 125 Ω, which was mainly due to the change of PEDOT chain structure by EG immersion. The configuration of the PEDOT chain in PEDOT:PSS changes from a benzol structure to a more conductive quinone structure, while the insulating PSS layer around PEDOT:PSS is partially detached, improving the contact between the conductive PEDOT components and enhancing carrier transport, thus increasing the conductivity.[34, 35] As for CCPH-PPy, the CCPH is obtained by chemical cross-linking with GA as the cross-linking agent and then vapor phase polymerization with ferric chloride as the oxidizing agent, so that PPy is uniformly embedded in CCPH to obtain CCPH-PPy composite electrode. Finally, an all-gel-state integrated AFSC was fabricated by sandwiching the EG-PCPPH, CCPH-PPy composite electrodes, and CCPH electrolyte together. CCPH plays two roles, serving as a flexible substrate for composite electrodes as well as an electrolyte for the final device.

6.3.2 Chemical composition and micromorphological characterization

FTIR and Raman spectroscopy are guiding tools for the study of chemical composition and bonding. To confirm the components and chemical bonds of the EG-PCPPH electrodes, Raman spectra were probed and the details are given in **Fig. 6.2a**. It can be observed that the characteristic peaks of PEDOT at 1505, 1442, 1365, and 1253 cm^{-1} and the bands at 989 and 1100 cm^{-1} for the PSS component appear in the Raman spectra of both PCPPH and EG-PCPPH.[36, 37] By comparison, the asymmetric stretching of $C_\alpha = C_\beta$ at 1442 cm^{-1} was red-shifted and narrowed after EG soaking, indicating that the PEDOT chain changed from the benzenoid structure to the quinoid structure.[29, 38] The band at 1575 cm^{-1} is associated with the doping-induced peak and represents the vibrational peak of the PSS, where the decrease in intensity implies partial removal of the PSS. The change of PEDOT conformation and partial removal of PSS contribute to the enhancement of the electrical conductivity of EG-PCPPH since the conformational change leads to easy delocalization of electrons, which increases the rate of electron migration, and the partial removal of PSS facilitates the aggregation of PEDOT to form a conductive pathway.[39-41] For CCPH-PPy, FTIR spectroscopy was used for

characterization, and the corresponding results are shown in **Fig. 6.2b**. Compared with pure PVA, the FTIR spectrum of CCPH shows a new absorption peak at 1192 cm^{-1}, which corresponds to the C-O-C group formed by the acetal reaction between -OH of PVA and -CHO of glutaraldehyde, confirming the cross-linking of PVA. The absence of the characteristic double peak of -CHO in the spectrum of CCPH indicates there is no glutaraldehyde residue and the cross-linking reaction is performed completely.[31] For CCPH-PPy, the characteristic peak of PPy (1554, 1430, 1329, 1172 cm^{-1}) appears in the FTIR spectrum, which indicates that PPy is successfully embedded in CCPH.[42]

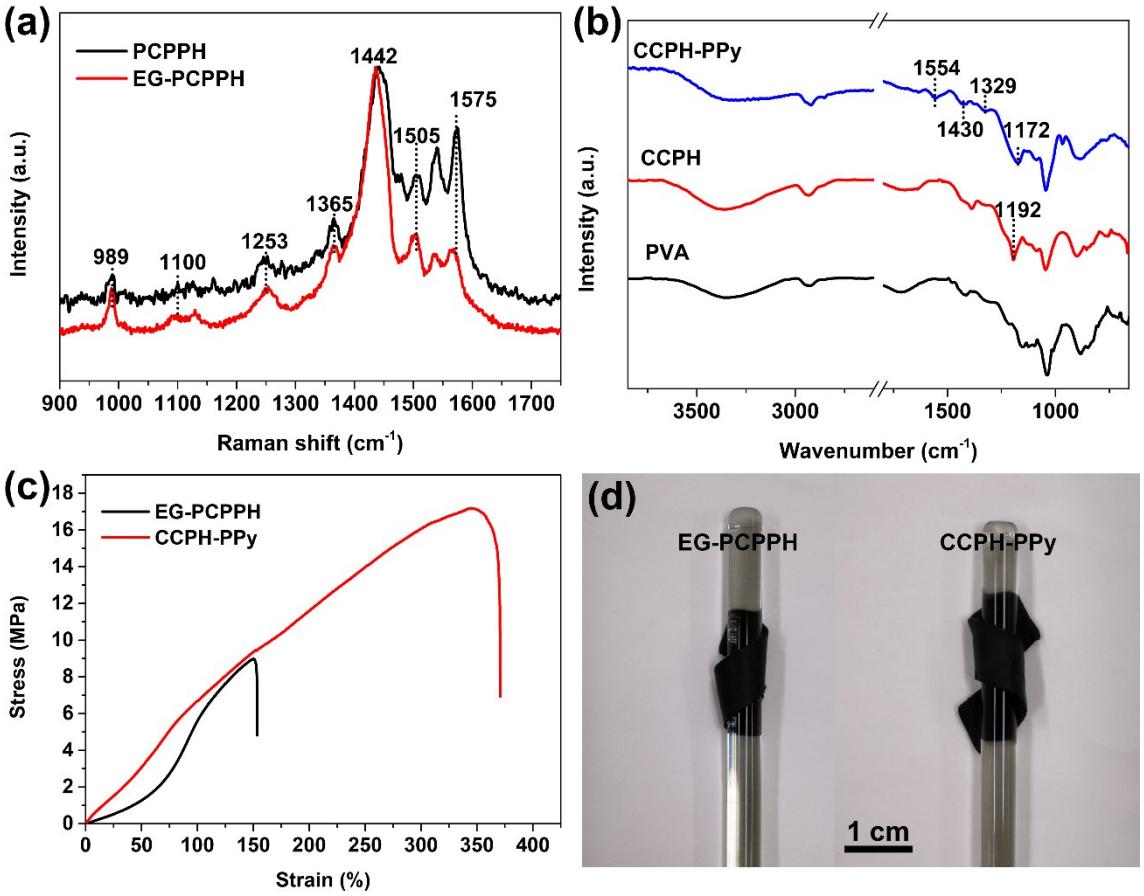

Fig. 6.2 Characterization of EG-PCPPH and CCPH-PPy. (a) Raman spectra of the PCPPH and EG-PCPPH; (b) FTIR spectra of CCPH-PPy, CCPH, and PVA; (c) Tensile stress-strain curves of the EG-PCPPH and CCPH-PPy; (d) Digital photos of EG-PCPPH and CCPH-PPy flexibility demonstration.

PVA-based gel electrolytes are widely used in supercapacitors because of their good solvent retention, high ion migration rate, and wide temperature window. Besides, the

hydrogel formed by PVA after cross-linking has excellent mechanical properties which is an excellent flexible substrate material. The distribution of electroactive substances in the flexible matrix affects not only the electrochemical properties but also the mechanical properties of the composite electrode material. The homogeneous dispersion of the electroactive material facilitates the construction of a conductive network to improve the electrical conductivity and also achieves interpenetration synergy with the substrate material to improve the mechanical properties. In this work, different methods were used to ensure the homogeneity of the dispersion in their composite electrode materials, according to the nature of the different electroactive materials. For the preparation of EG-PCPPH, since PEDOT:PSS is a suspension, the liquid phase blending method is used to mix uniformly with PVA before freeze-thaw cross-linking. For CCPH-PPy, the PPy is uniformly embedded in the matrix by the vapor phase polymerization method in the pre-crosslinked PVA film.

The stress-strain curve of EG-PCPPH, CCPH-PPy are shown in **Fig. 6.2c**. The EG-PCPPH is capable of achieving a tensile strength of 8.97 MPa and an elongation at break of 150.8%. The CCPH-PPy has a tensile strength of up to 17.18 MPa with an elongation at break of 346.2%. Moreover, EG-PCPPH and CCPH-PPy exhibit excellent mechanical flexibility (**Fig. 6.2d**) and can be easily wrapped around the glass rod. Compared to attaching the electroactive material to the surface of a flexible substrate, our method embeds the electroactive material in the flexible substrate ensuring that it would not fall off under large deformations, improving the durability of the composite electrode. In view of these advantages, the comprehensive performance of all-conducting polymeric solid-state AFSCs prepared based on EG-PCPPH and CCPH-PPy is highly anticipated.

Fig. 6.3 illustrates the microscopic morphology of the EG-PCPPH and CCPH-PPy cross-sections after freeze-drying. Because of the different fabrication processes, EG-PCPPH and CCPH-PPy show distinctly different morphologies. EG-PCPPH exhibits a three-dimensional (3D) porous network structure under the action of freezing and thawing, which similarly facilitates the transport of electrons. Moreover, it can be observed in SEM images of larger magnification that the pore walls have mountain-like folds, which not only increase the specific surface area but also provide more transmission channels (**Fig. 6.3a**). In contrast, the SEM images of the CCPH-PPy prepared by chemical cross-linking followed by gas-phase polymerization show that the

PPy particles are uniformly embedded in the CCPH matrix, forming a conductive pathway (**Fig. 6.3c**). Despite the differences in microscopic morphology, both are favorable for electrochemical performance.

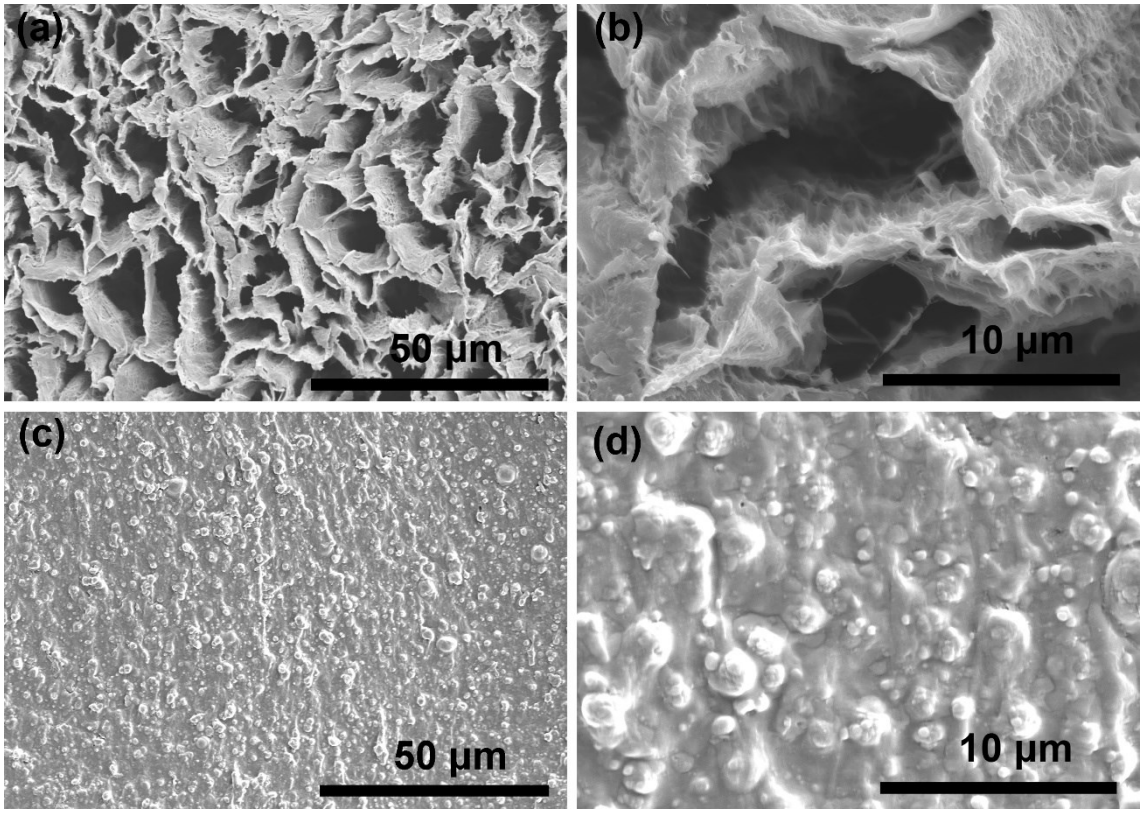

Fig. 6.3 SEM images of the cross-section of (a, b) EG-PCPPH and (c, d) CCPH-PPy.

6.3.3 Electrochemical properties and mechanical stability

The electrochemical properties of EG-PCPPH and CCPH-PPy were evaluated by CV, GCD, and EIS in a three-electrode system, with the results presented in the Supporting Information. A comparison of the CV curves of EG-PCPPH and CCPH-PPy at scan rates from 10 to 100 mV s^{-1} is shown in **Fig. 6.4**. The area enclosed by the CV curves of EG-PCPPH and CCPH-PPy at the same scan rate is not very different, implying that the electrochemical properties are at the same level. **Fig. 6.5** shows the comparison of the GCD curves of EG-PCPPH and CCPH-PPy at different current densities. The GCD curve of EG-PCPPH shows a better symmetry, which is characteristic of the charge-discharge curve of PEDOT. The volumetric specific capacitance calculated based on the GCD data is shown in **Fig. 6.6a**. The specific capacitance of CCPH-PPy is 12.4 to 10.5

F cm^{-3} at a current density of 40 to 320 mA cm^{-3}, while the value of EG-PCPPH is 10.5 to 9.5 F cm^{-3}. The current density is expanded to 8 times, the capacitance retention rate of EG-PCPPH is 90.5%, and that of CCPH-PPy is 84.7%, both showing good rate performance. As shown in **Fig. 6.5**b, the Nyquist plots of EG-PCPPH and CCPH-PPy have almost the same intercept on the horizontal axis and the curvature of the semicircular curvature in the high-frequency region is nearly the same, indicating that they have nearly the same equivalent series resistance and charge transfer resistance. The EG-PCPPH and the CCPH-PPy have similar specific capacitance, rate performance, and internal resistance, providing a basis for the subsequent assembly of asymmetric supercapacitors with interchangeable positive and negative electrodes.

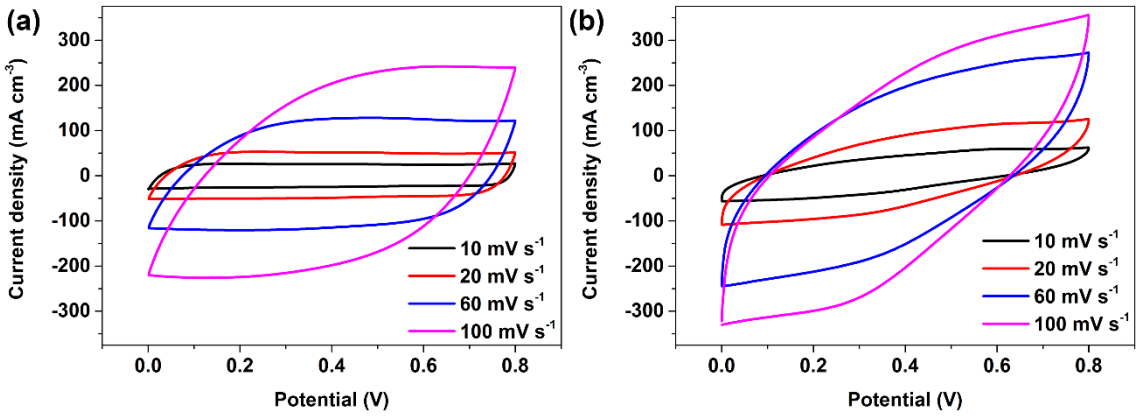

Fig. 6.4 The comparison of the CV curves of EG-PCPPH (a) and CCPH-PPy (b) at scan rates from 10 to 100 mV s^{-1} in a three-electrode system.

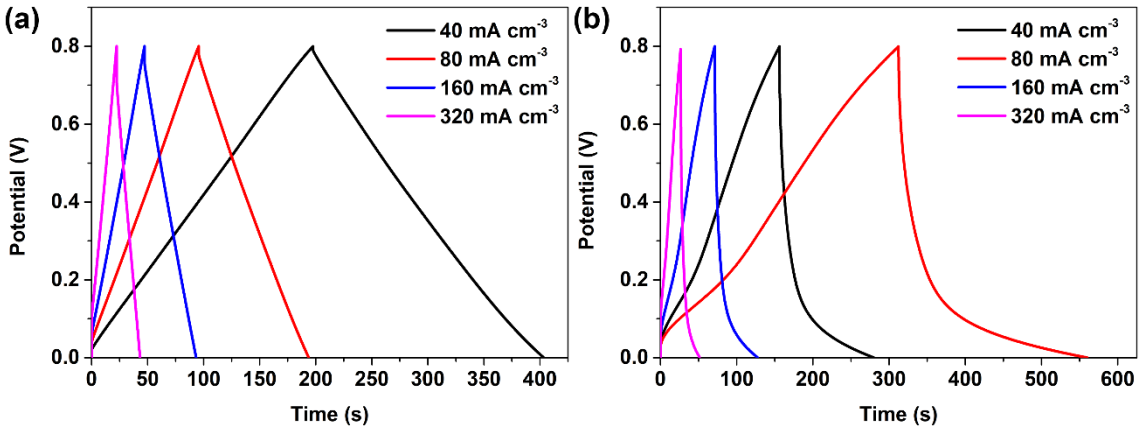

Fig. 6.5 The comparison of the GCD curves of EG-PCPPH and CCPH-PPy at scan rates from 40 to 320 mA cm^{-3} in a three-electrode system.

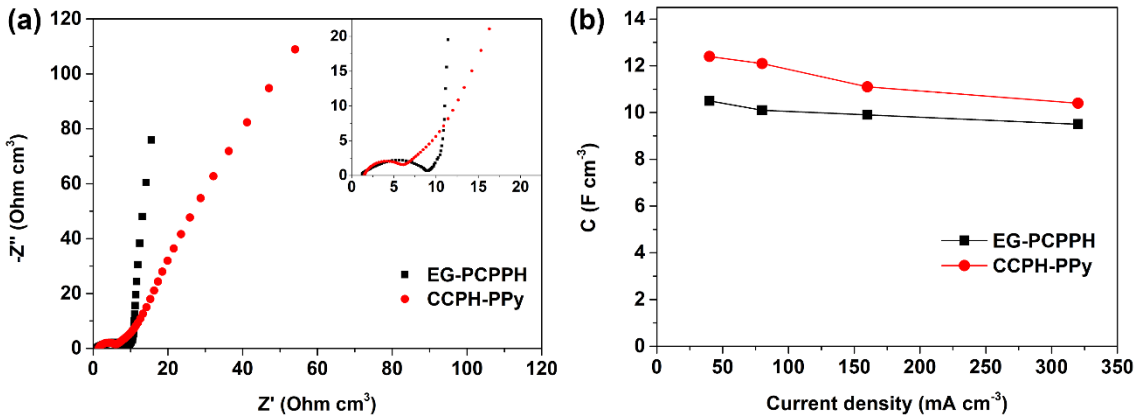

Fig. 6.6 The comparison of Nyquist plots(a) and specific capacitance(b) of EG-PCPPH and CCPH-PPy.

Compared with general asymmetric supercapacitors, our all-solid-state integrated AFSC has the following special features: (1) the design of all-conductive polymers without carbon materials and metal oxides/hydroxides; (2) independent self-supporting all-hydrogel combination; (3) same substrate material used for electrodes and electrolytes. The fully conductive polymer design is more conducive to the flexibility of the device, as shown in **Fig. 6.7a**, the assembled AFSC can be freely bent and can quickly recover its original shape after releasing the external force. The hydrogel substrate provides high strength flexibility and also ensures the uniform distribution of electroactive substances (PPy and PEDOT:PSS). Both positive and negative electrodes and electrolytes are based on PVA hydrogel, where there is a strong hydrogen bonding between layers, which is conducive to the integrated molding of the device, avoiding the delamination of electrodes and electrolytes during deformation and improving the mechanical properties of the whole device. **Fig. 6.7b** is the optical micrograph of the cross-section of the AFSC, which shows a clear three-layer structure with no gaps visible at the interface between electrode and electrolyte. The fusion of electrolyte and electrode not only reduces the interfacial resistance but also strengthens the mechanical properties of the device. As shown in **Fig. 6.7c**, AFSC exhibits ultra-high mechanical tensile properties with a tensile strength of 22.3 MPa and an elongation at break of 286%. The maximum tensile strength of AFSC was enhanced compared to that of CCPH-PPy electrode, and the elongation at break was also much better than that of EG-PCPPH electrode, indicating that the strong interaction between electrodes and electrolyte layers lead to a synergistic enhancement.

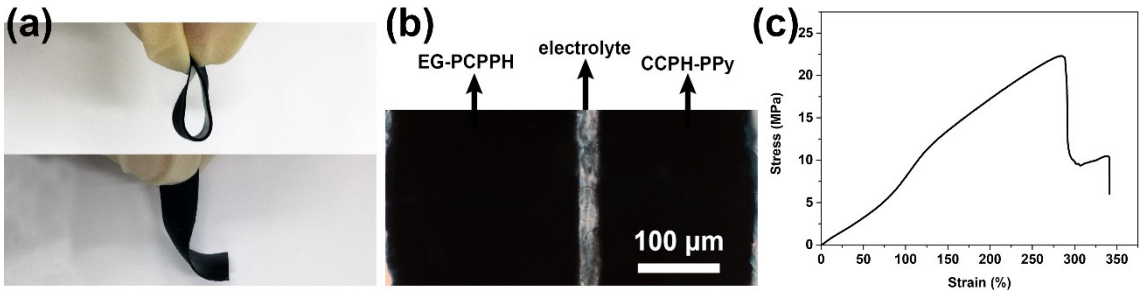

Fig. 6.7 (a) Digital photos of AFSC showing flexibility (b) Cross-section of the AFSC by optical microscopy. (c) Tensile stress−strain curve of the AFSC.

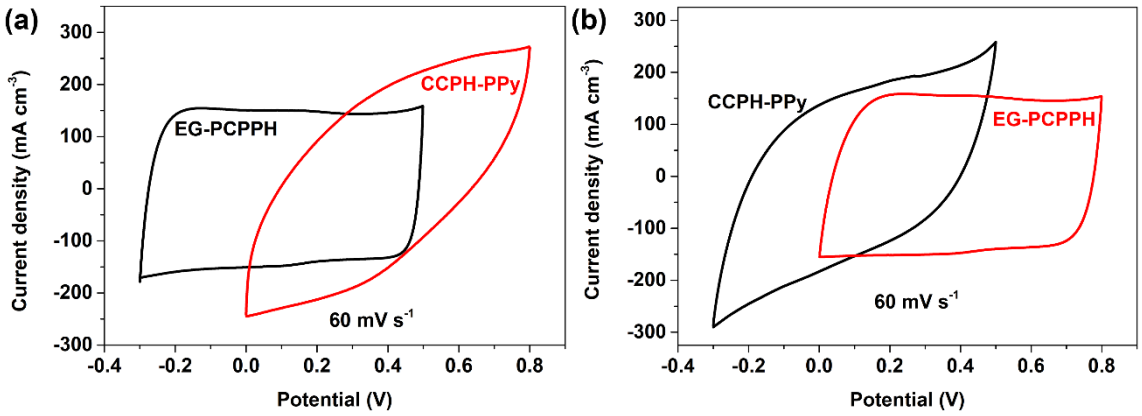

Fig. 6.8 CV curves of EG-PCPPH and CCPH-PPy in different potential windows with scan rate of 60 mV s^{-1}. (a) EG-PCPPH in the negative potential window, CCPH-PPy in the positive potential window; (b) CCPH-PPy in the negative potential window, EG-PCPPH in the positive potential window.

The individual potential windows of EG-PCPPH and CCPH-PPy were explored before assembly into devices. **Fig. 6.8a** shows the CV curves of EG-PCPPH and CCPH-PPy in the negative and positive potential windows at a scan rate of 60 mV s^{-1}. The ratio of the area enclosed by their CV curves was calculated by integration to be 1:1.04, which means that their volumetric capacitance is almost the same. The same conclusion is obtained when CCPH-PPy is in the negative voltage window and EG-PCPPH is in the positive voltage window, as shown in **Fig. 6.8b**. Due to the fabrication process, the electroactive material in CCPH-PPy cannot be precisely calculated to perform mass balance to match the charge of positive and negative electrodes. Fortunately, the volumetric capacitance of the EG-PCPPH and CCPH-PPy electrodes happened to be almost equal. Since the positive and negative electrodes have the same pair area, the

AFSC can be assembled with EG-PCPPH and CCPH-PPy of the same thickness to achieve charge balance.

To investigate the electrochemical performance of AFSC, a comprehensive evaluation was performed via CV, GCD, EIS, and circulating charge and discharge measurements. Considering that the volume of the assembled device is compressed compared with that of the single electrode, the performance of the single electrode in the three-electrode system is not sufficient to illustrate the performance of the device, thus we directly take the assembled device as the object of study. As shown in **Fig. 6.9a**, the optimal voltage window is explored at a scan rate of 60 mv s^{-1} with CCPH-PPy as the positive electrode and EG-PCPPH as the negative electrode. The CV curves of the device maintain a rectangular-like shape in the voltage range of 1.4 V. When the voltage window exceeds 1.5 V, the CV curve deviates from the original trajectory and becomes distorted, and the symmetry becomes poor, which is due to the electrode polarization and the decomposition of the electrolyte. To ensure stable electrochemical performance, we set the voltage window at 1.4 V. The CV curves of the AFSC at a voltage window of 1.4 V with scan rates range of 10-100 mV s^{-1} are shown in **Fig. 6.9b**. All of the CV curves can be observed with significant redox peaks, exhibiting excellent pseudocapacitance behavior. In addition, the current in the CV curves increased significantly with increasing scan rate, indicating that the device has a promising current-voltage response rate. [43] In the CV curves, a relationship exists between the current (i) and the scan rate (v) as a function of $i=av^b$.[44, 45] The value of b is approximately similar to 1 implies that the charge storage process at the electrode is almost not controlled by diffusion and is close to the surface process. After taking the logarithm, the function $i = av^b$ can be converted into a linear function $\lg i = \lg a + b \lg v$. The value of b is the slope of this function. To obtain more accurate b-values, the CV curves of AFSC were tested at low scan rates of 1~10 mV s^{-1}. The peak current (i) versus scan rate (v) in the scan rate range of 1~10 mV s^{-1} is shown in **Fig. 6.9c**. The b value of 0.91 was obtained from the slope of the fitted straight line, which indicates that the electrode redox process is fast and less limited by ion diffusion. This is attributed to the 3D porous network structure of EG-PCPPH and the conductive pathway formed by PPy in CCPH-PPy which facilitates the rapid embedding/detachment of electrolyte ions.

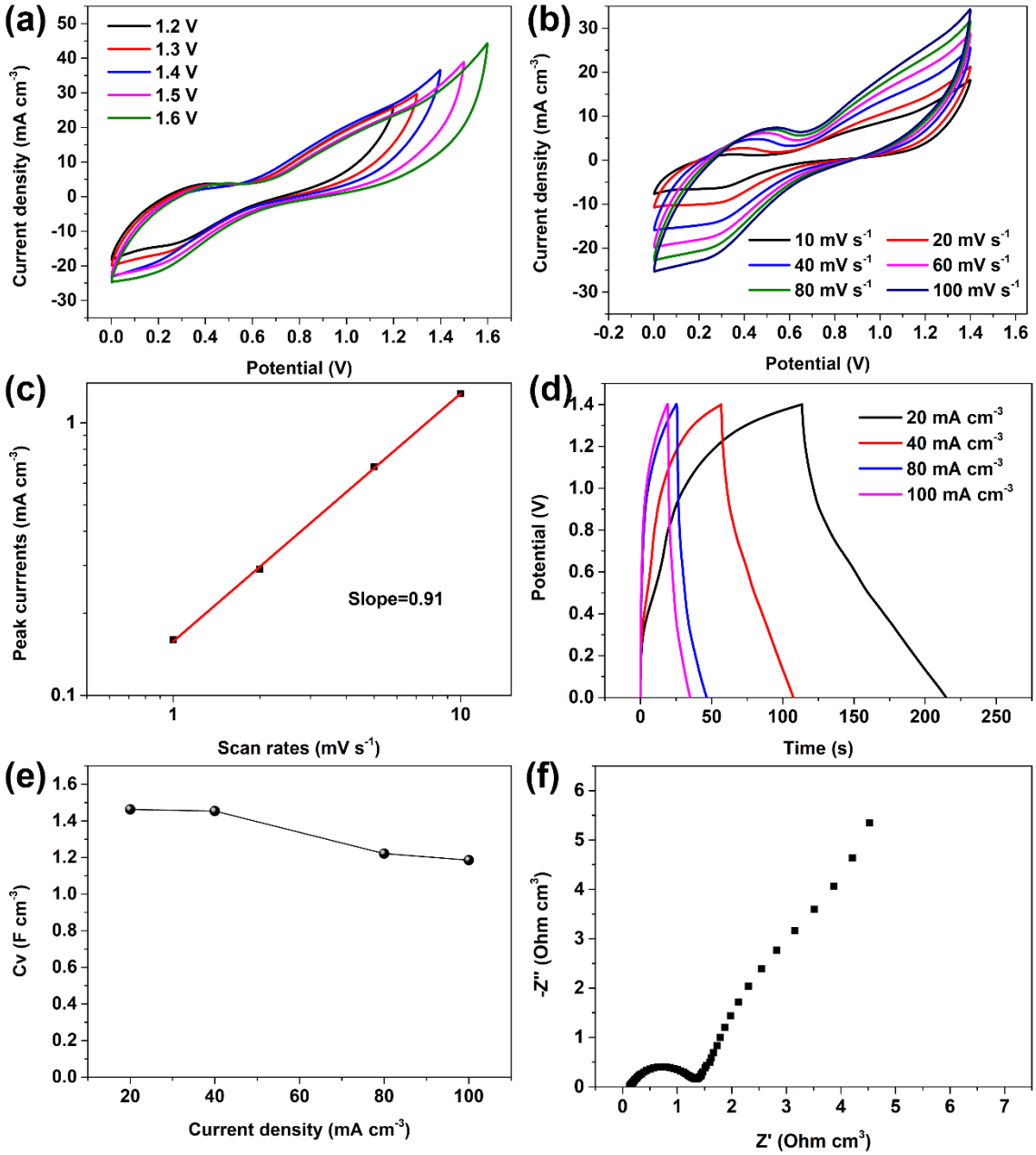

Fig. 6.9 The electrochemical performance of AFSC. (a) CV curves of AFSC at different voltages with a scan rate of 60 mV s^{-1}; (b) CV curves of AFSC at different scan rates with a voltage window of 1.4 V; (c) The dependence of peak currents on scan rates in the scan rate range of 1~10 mV s^{-1}; (d) GCD curves of AFSC at different current densities; (e) The volumetric specific capacitance of AFSC at different current densities; (f) Nyquist plots in the range of 10^6 Hz to 10^{-2} Hz.

The AFSC was further evaluated by GCD measurements and the details are shown in **Fig. 6.9d**. A clear curvature can be observed in the GCD curves which is characteristic of the Faraday contribution of the two conducting polymer electrodes. The volumetric

specific capacitances (Cv) at different current densities are calculated from the GCD curves and the results are shown in **Fig. 6.9e**. The AFSC exhibited a Cv of 1.462, 1.453, 1.221, and 1.185 F cm^{-3} at a current density of 20, 40, 80, and 100 mA cm^{-3}.The current density is expanded to 5 times, while the capacitance remains 81.1 % of the original capacity, demonstrating excellent rate performance. The electrochemical impedance spectrum of AFSC is shown in **Fig. 6.9f**. The equivalent series resistance (R_s) and charge transfer resistance (R_{ct}) of 0.13 and 1.29 Ohm cm^3 were obtained by fitting the Nyquist curve, indicating that the device has a very low cell resistance and a fast charge transfer rate. Such a low R_s of the device is attributed to the low interlayer interface resistance of the electrodes and electrolyte layers as well as the high conductivity of the electrodes themselves, indicating that the all-gel integrated design is a very promising strategy.

Subsequently, 10,000 cycles of charge/discharge at 100 mA cm^{-3} were carried out to evaluate the electrochemical stability of AFSC, and the results are shown in **Fig.6.10a**. The capacitance of AFSC decreases slowly as the number of cycles increases. After 10,000 charge/discharge cycles, the capacitance retention rate is 88.1%, which shows excellent electrochemical stability. Thanks to the good specific capacitance and the broadened voltage window of the asymmetric design, AFSC has an excellent volumetric energy density. The Ragone plots of the AFSC are presented in **Fig. 6.10b**. The maximum volumetric energy density (E_v) of the AFSC is 397.99 μWh cm^{-3} with a volumetric power density (P_v) of 14.13 mW cm^{-3}, and the E_v is 322.6 μWh cm^{-3} when the P_v is increased to 73.04 mW cm^{-3}, which is much better than the symmetrical supercapacitor prepared based on PPy/CPH (E_v was 138.3 μWh cm^{-3} with P_v of 60 mW cm^{-3})[31], and EG-PPPH (E_v was 64.13 μWh cm^{-3} with P_v of 18.13 mW cm^{-3})[41]. As shown in the Ragone plot, the energy density and power density of AFSC is comparable to that of other general water-based asymmetric supercapacitors, with no significant disadvantage, such as asymmetric supercapacitor based on $Ni(OH)_2$/NGP//Mn_3O_4/NGP (E_v = 350 μWh cm^{-3}, P_v = 7 mW cm^{-3})[46], MnO_2 Nanowires//Fe_2O_3 Nanotubes (E_v = 550 μWh cm^{-3}, P_v = 20 mW cm^{-3})[47], MnO_2//Fe_2O_3NRs (E_v = 410 μWh cm^{-3}, P_v = 55 mW cm^{-3})[48], PANI NRs//α-Fe_2O_3@PANI (E_v = 350 μWh cm^{-3}, P_v = 120.5 mW cm^{-3})[49]. However, since the AFSCs we prepared are based on an integrated all-gel state structure of all-conducting-polymer electrodes, they possess more excellent flexibility and mechanical durability.

To evaluate the stability of the electrochemical properties of AFSC under mechanical deformation, the CV curves of the devices were measured at 30°, 60°, 90°, and 180° bending states. As shown in **Fig. 6.10c**, the CV curves showed almost no change under small bending angles, and only a slight deformation when the bending angle increased to 180°, indicating that the AFSC has good mechanical stability. The bending cycle test is a universal evaluation method for evaluating the mechanical durability of flexible supercapacitors.[50] To study the durability of the electrochemical stability under long-term deformation, AFSC was bent to 90° with a bending radius of 5 mm, and CV testing was performed in the bending state. As shown in **Fig. 6.10d**, the capacitance retention rate of AFSC is 98.1% after 1000 times of bending, which indicates that the device possesses excellent mechanical durability.

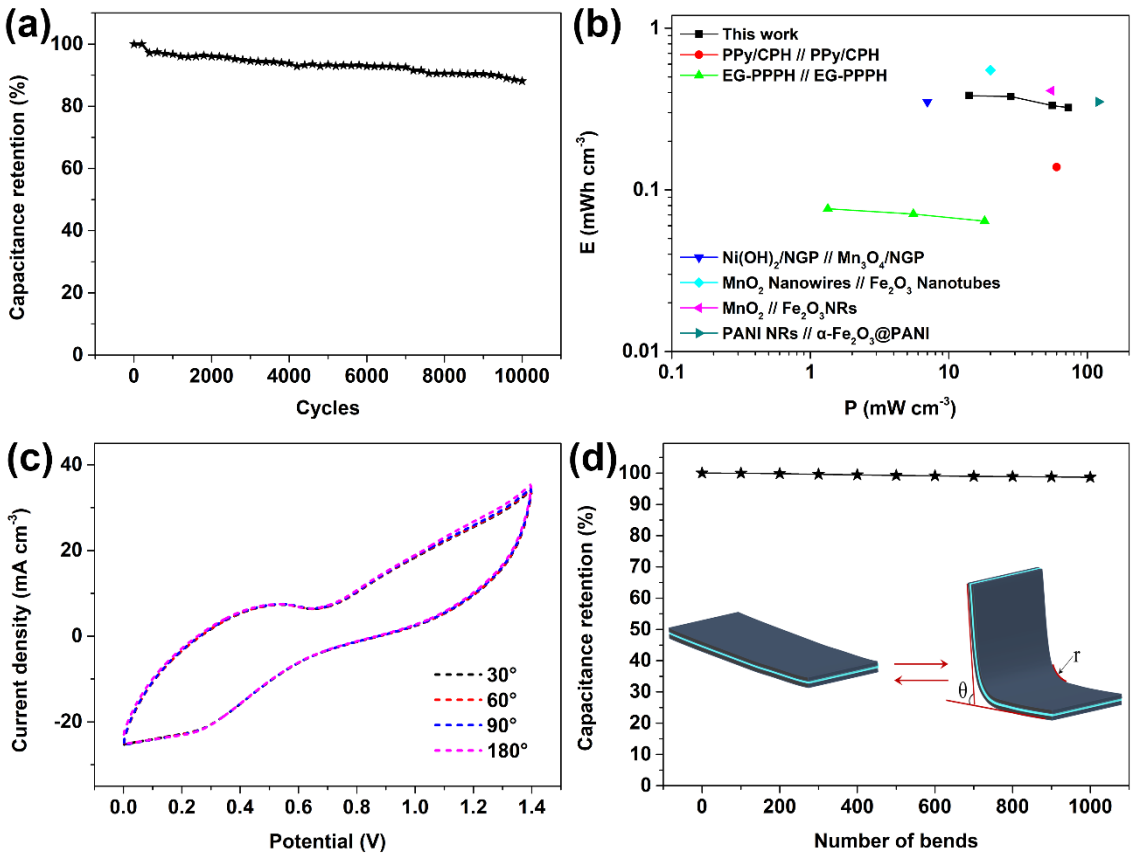

Fig. 6.10 The electrochemical performance of AFSC. (a) Charge/discharge cycle stability of AFSC with 10 000 cycles at 100 mA cm^{-3}; (b) Ragone plot of AFSC and the other reported asymmetric supercapacitors; (c) CV curves of AFSC under different bending states at a scan rate of 60 mV s^{-1}; (d) Capacitive stability of AFSC under 1000 bendings at a bending angle of 90°, Insets is the bending schematic of AFSC.

In general, the positive and negative electrodes of an asymmetric supercapacitor are stationary and need to be connected correctly. Incorrect connections could cause irreversible damage to the capacitor, with reduced capacity and reduced cycling stability. Here, we have tried to interchange the positive and negative electrodes of AFSC, with EG-PCPPH as the positive electrode and CCPH-PPy as the negative electrode, to test its electrochemical performance. Surprisingly, the electrochemical performance of the AFSC with interchanged positive and negative electrodes did not show any significant degradation. As shown in **Fig. 6.11a**, although the trajectory of the charge/discharge curve has changed somewhat, the discharge time remains almost unchanged from the original. The comparison of the CV curves also shows the same results, as shown in **Fig. 6.11b**, where the area enclosed by the CV curves is almost the same. To evaluate the cycling stability of AFSC after swapping positive and negative, the same 10,000 charge and discharge tests were performed (**Fig. 6.11c**). The final capacitance retention rate was 83 % without a significant drop, which indicates that the AFSC can be used normally after swapping positive and negative electrodes. The ability of AFSC to exchange positive and negative electrodes is attributed to the appropriate combination of conducting polymers and a suitable voltage window. Within a suitable voltage range, CPs provide stable and impressive electrochemical properties at both positive and negative working potentials.[28] In previous reports, it has been shown that PEDOT and PPy can exhibit stable electrochemical performance in sulfuric acid electrolytes at voltages no lower than -0.5 V.[29, 51] In addition, PEDOT: PSS has good electrochemical activity in a wide voltage window of 1.2~1.5 V.[29, 52] Therefore, under the voltage window of 1.4 V, both EG-PCPPH and CCPH-PPy can work stably as negative electrodes. For practical demonstration, we labeled the two electrodes of AFSC as A and B, where A is CCPH-PPy and B is EG-PCPPH. Then the two AFSCs were connected in series as schematically shown in **Fig. 6.11d**, **6.11e**, and **6.11f**. After charging, all three sets of schemes successfully lit a blue LED with a rated voltage of 2.4 V. This confirms that the device can be used in practice without differentiating between positive and negative electrodes. In commercial designs, a single supercapacitor is a module, and these modules can be externally connected in series and parallel to provide higher operating voltages and higher capacitance. Asymmetric supercapacitor modules that do not differentiate between positive and negative electrodes can greatly improve the assembly efficiency of power systems and avoid

safety issues caused by misconnections of positive and negative electrodes.

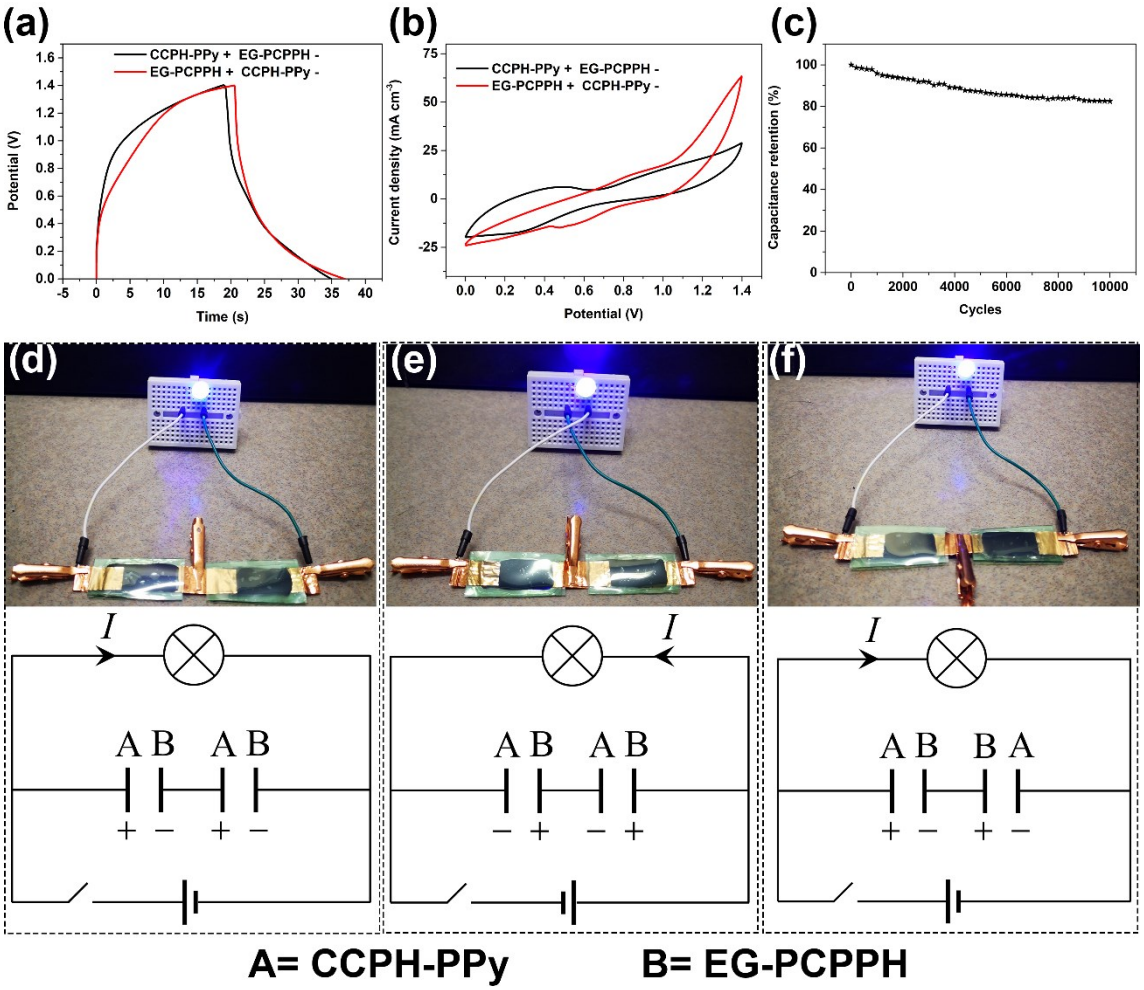

Fig. 6.11 The electrochemical performance of AFSC. (a) Comparison of GCD curves of AFSC and AFSC after exchanging positive and negative electrodes at 100 mA cm^{-3}; (b) Comparison of CV curves of AFSC and AFSC after exchanging positive and negative electrodes at 60 mV s^{-1}. (c) Cycling stability of AFSC after switching positive and negative electrodes; (d), (e), and (f) Schematic diagram of the connection of two AFSCs in series and electronic photo of the lit LEDs.

6.4 Conclusion

In summary, EG-PCPPH and CCPH-PPy composite electrodes were prepared by a green and efficient strategy, and then a novel all-conducting polymer-based integrated asymmetric flexible supercapacitor was successfully fabricated. The AFSC has excellent flexibility, can be freely bent, and quickly recovered after the release of external forces;

outstanding mechanical strength, tensile strength up to 22.3 MPa with elongation at break 286%. In addition, it has excellent electrochemical performance and stability, with a maximum volumetric energy density of 397.99 μWh cm^{-3} and a capacitance retention rate of 88.1% for 10,000 charge/discharge cycles. Impressively, as an asymmetric device, AFSC can be used as the symmetric device without differentiating between positive and negative. In a practical demonstration, it can be connected in any series to power the LEDs. The concept of asymmetric devices with interchangeable positive and negative may provide a direction for the design of asymmetric supercapacitors in the future. Accordingly, this strategy will open up a new trend in the design of flexible energy storage devices with high energy density.

Reference

[1] Z. Wang, M. Zhu, Z. Pei, Q. Xue, H. Li, Y. Huang, C. Zhi, Polymers for supercapacitors: boosting the development of the flexible and wearable energy storage, Mater. Sci. Eng. R Rep. 139 (2020) 100520.

[2] L. Liu, Y. Feng, W. Wu, Recent progress in printed flexible solid-state supercapacitors for portable and wearable energy storage, J. Power Sources 410 (2019) 69-77.

[3] D. Wang, C. Han, F. Mo, Q. Yang, Y. Zhao, Q. Li, G. Liang, B. Dong, C. Zhi, Energy density issues of flexible energy storage devices, Energy Storage Mater. 28 (2020) 264-292.

[4] R. Hou, G.S. Gund, K. Qi, P. Nakhanivej, H. Liu, F. Li, B.Y. Xia, H.S. Park, Hybridization design of materials and devices for flexible electrochemical energy storage, Energy Storage Mater. 19 (2019) 212-241.

[5] W. Lyu, W. Zhang, H. Liu, Y. Liu, H. Zuo, C. Yan, C.F. Faul, A. Thomas, M. Zhu, Y. Liao, Conjugated Microporous Polymer Network Grafted Carbon Nanotube Fibers with Tunable Redox Activity for Efficient Flexible Wearable Energy Storage, Chem. Mater. 32 (2020) 8276-8285.

[6] Z. Liu, H. Li, M. Zhu, Y. Huang, Z. Tang, Z. Pei, Z. Wang, Z. Shi, J. Liu, Y. Huang, Towards wearable electronic devices: A quasi-solid-state aqueous lithium-ion battery with outstanding stability, flexibility, safety and breathability, Nano Energy 44 (2018) 164-173.

[7] L. Han, H. Huang, X. Fu, J. Li, Z. Yang, X. Liu, L. Pan, M. Xu, A flexible, high-voltage and safe zwitterionic natural polymer hydrogel electrolyte for high-energy-density zinc-ion hybrid supercapacitor, Chem. Eng. J. 392 (2020) 123733.

[8] L. Dong, G. Liang, C. Xu, W. Liu, Z.-Z. Pan, E. Zhou, F. Kang, Q.-H. Yang, Multi hierarchical construction-induced superior capacitive performances of flexible electrodes for wearable energy storage, Nano energy 34 (2017) 242-248.

[9] Y. Wang, C. Chen, H. Xie, T. Gao, Y. Yao, G. Pastel, X. Han, Y. Li, J. Zhao, K. Fu, 3D‐printed all‐fiber li‐ion battery toward wearable energy storage, Adv. Funct. Mater. 27 (2017) 1703140.

[10] X. Wu, Y. Xu, Y. Hu, G. Wu, H. Cheng, Q. Yu, K. Zhang, W. Chen, S. Chen, Microfluidic-spinning construction of black-phosphorus-hybrid microfibres for non-

woven fabrics toward a high energy density flexible supercapacitor, Nat. Commun. 9 (2018) 1-11.
[11] J. Han, H. Wang, Y. Yue, C. Mei, J. Chen, C. Huang, Q. Wu, X. Xu, A self-healable and highly flexible supercapacitor integrated by dynamically cross-linked electro-conductive hydrogels based on nanocellulose-templated carbon nanotubes embedded in a viscoelastic polymer network, Carbon 149 (2019) 1-18.
[12] J. Qin, S. Wang, F. Zhou, P. Das, S. Zheng, C. Sun, X. Bao, Z.-S. Wu, 2D mesoporous MnO2 nanosheets for high-energy asymmetric micro-supercapacitors in water-in-salt gel electrolyte, Energy Storage Mater. 18 (2019) 397-404.
[13] N. Yu, H. Yin, W. Zhang, Y. Liu, Z. Tang, M.Q. Zhu, High‐performance fiber-shaped all‐solid‐state asymmetric supercapacitors based on ultrathin MnO2 nanosheet/carbon fiber cathodes for wearable electronics, Adv. Energy Mater. 6 (2016) 1501458.
[14] Y.-k. Ahn, B. Kim, J. Ko, D.-J. You, Z. Yin, H. Kim, D. Shin, S. Cho, J. Yoo, Y.S. Kim, All solid state flexible supercapacitors operating at 4 V with a cross-linked polymer–ionic liquid electrolyte, J. Mater. Chem. A 4 (2016) 4386-4391.
[15] X. Zhang, M. Kar, T.C. Mendes, Y. Wu, D.R. MacFarlane, Supported ionic liquid gel membrane electrolytes for flexible supercapacitors, Adv. Energy Mater. 8 (2018) 1702702.
[16] Y. Shao, M.F. El-Kady, J. Sun, Y. Li, Q. Zhang, M. Zhu, H. Wang, B. Dunn, R.B. Kaner, Design and mechanisms of asymmetric supercapacitors, Chem. Rev. 118 (2018) 9233-9280.
[17] G. Nagaraju, S.C. Sekhar, J.S. Yu, Utilizing waste cable wires for high‐performance fiber‐based hybrid supercapacitors: an effective approach to electronic‐waste management, Adv. Energy Mater. 8 (2018) 1702201.
[18] N. Choudhary, C. Li, J. Moore, N. Nagaiah, L. Zhai, Y. Jung, J. Thomas, Asymmetric supercapacitor electrodes and devices, Adv. Mater. 29 (2017) 1605336.
[19] Q. Jia, C. Yang, Q. Pan, Y. Xin, F. Xu, W. Qi, H. Wei, S. Yang, C. Zhou, N. Hu, High-voltage aqueous asymmetric pseudocapacitors based on methyl blue-doped polyaniline hydrogels and the derived N/S-codoped carbon aerogels, Chem. Eng. J. 383 (2020) 123153.
[20] Y. Zhao, X. Wang, T. Xin, N. Wang, J. Liu, Aqueous asymmetric supercapacitors

based on electrodeposited poly (1, 5-naphthalenediamine) and poly (4, 4′-oxydianiline), Sustain. Energy Fuels 3 (2019) 3603-3610.
[21] R. Nasser, G.-F. Zhang, J.-M. Song, Facile and low-cost synthesis of cobalt-doped MnO2 decorated with graphene oxide for high performance 2.3 V aqueous asymmetric supercapacitors, Electrochim. Acta 345 (2020) 136198.
[22] V. Khomenko, E. Raymundo-Pinero, F. Béguin, Optimisation of an asymmetric manganese oxide/activated carbon capacitor working at 2 V in aqueous medium, J. Power Sources 153 (2006) 183-190.
[23] J. Huang, P. Xu, D. Cao, X. Zhou, S. Yang, Y. Li, G. Wang, Asymmetric supercapacitors based on β-Ni (OH) 2 nanosheets and activated carbon with high energy density, J. Power Sources 246 (2014) 371-376.
[24] F. Su, M. Miao, Asymmetric carbon nanotube–MnO2 two-ply yarn supercapacitors for wearable electronics, Nanotechnology 25 (2014) 135401.
[25] M.F. Dupont, S.W. Donne, Separating the faradaic and non-faradaic contributions to the total capacitance for different manganese dioxide phases, J. Electrochem. Soc. 162 (2015) A5096.
[26] X. Li, X. Chen, Z. Jin, P. Li, D. Xiao, Recent progress in conductive polymers for advanced fiber-shaped electrochemical energy storage devices, Mater. Chem. Front. 5 (2021) 1140-1163.
[27] Y. Han, L. Dai, Conducting polymers for flexible supercapacitors, Macromol. Chem. Phys. 220 (2019) 1800355.
[28] J. Sun, C. Wu, X. Sun, H. Hu, C. Zhi, L. Hou, C. Yuan, Recent progresses in high-energy-density all pseudocapacitive-electrode-materials-based asymmetric supercapacitors, J. Mater. Chem. A 5 (2017) 9443-9464.
[29] N. Kurra, R. Wang, H.N. Alshareef, All conducting polymer electrodes for asymmetric solid-state supercapacitors, J. Mater. Chem. A 3 (2015) 7368-7374.
[30] G.M. Suppes, C.G. Cameron, M.S. Freund, A polypyrrole/phosphomolybdic acid｜poly (3, 4-ethylenedioxythiophene)/phosphotungstic acid asymmetric supercapacitor, J. Electrochem. Soc. 157 (2010) A1030.
[31] L. Zang, Q. Liu, J. Qiu, C. Yang, C. Wei, C. Liu, L. Lao, Design and Fabrication of an All-Solid-State Polymer Supercapacitor with Highly Mechanical Flexibility Based on Polypyrrole Hydrogel, ACS Appl. Mater. Interfaces 9 (2017) 33941-33947.
[32] W. Li, H. Lu, N. Zhang, M. Ma, Enhancing the properties of conductive polymer

hydrogels by freeze–thaw cycles for high-performance flexible supercapacitors, ACS Appl. Mater. Interfaces 9 (2017) 20142-20149.

[33] Z. Yang, J. Ma, B. Bai, A. Qiu, D. Losic, D. Shi, M. Chen, Free-standing PEDOT/polyaniline conductive polymer hydrogel for flexible solid-state supercapacitors, Electrochim. Acta 322 (2019) 134769.

[34] J. Cárdenas-Martínez, B.L. España-Sánchez, R. Esparza, J.A. Ávila-Niño, Flexibleand transparent supercapacitors using electrospun PEDOT: PSS electrodes, Synth. Met. 267 (2020) 116436.

[35] J. Ouyang, C.W. Chu, F.C. Chen, Q. Xu, Y. Yang, High‐conductivity poly (3, 4-ethylenedioxythiophene): poly (styrene sulfonate) film and its application in polymer optoelectronic devices, Adv. Funct. Mater. 15 (2005) 203-208.

[36] S. Xiong, L. Zhang, X. Lu, Conductivities enhancement of poly (3, 4-ethylenedioxythiophene)/poly (styrene sulfonate) transparent electrodes with diol additives, Polym. Bull. 70 (2013) 237-247.

[37] H. Park, S.H. Lee, F.S. Kim, H.H. Choi, I.W. Cheong, J.H. Kim, Enhanced thermoelectric properties of PEDOT: PSS nanofilms by a chemical dedoping process, J. Mater. Chem. A 2 (2014) 6532-6539.

[38] J. Ouyang, Q. Xu, C.-W. Chu, Y. Yang, G. Li, J. Shinar, On the mechanism of conductivity enhancement in poly (3, 4-ethylenedioxythiophene): poly (styrene sulfonate) film through solvent treatment, Polymer 45 (2004) 8443-8450.

[39] H. Okuzaki, Y. Harashina, H. Yan, Highly conductive PEDOT/PSS microfibers fabricated by wet-spinning and dip-treatment in ethylene glycol, Eur. Polym. J. 45 (2009) 256-261.

[40] S. Ashizawa, R. Horikawa, H. Okuzaki, Effects of solvent on carrier transport in poly (3, 4-ethylenedioxythiophene)/poly (4-styrenesulfonate), Synth. Met. 153 (2005) 5-8.

[41] Q. Liu, J. Qiu, C. Yang, L. Zang, G. Zhang, E. Sakai, High‐Performance PVA/PEDOT: PSS Hydrogel Electrode for All‐Gel‐State Flexible Supercapacitors, Adv. Mater. Technol. 6 (2021) 2000919.

[42] Z. Fan, J. Zhu, X. Sun, Z. Cheng, Y. Liu, Y. Wang, High density of free-standing holey graphene/PPy films for superior volumetric capacitance of supercapacitors, ACS Appl. Mater. Interfaces 9 (2017) 21763-21772.

[43] J. Yu, J. Zhou, P. Yao, J. Huang, W. Sun, C. Zhu, J. Xu, A stretchable high performance all-in-one fiber supercapacitor, J. Power Sources 440 (2019) 227150.
[44] Q. Liu, L. Zang, X. Qiao, J. Qiu, X. Wang, L. Hu, J. Yang, C. Yang, Compressible All-In-One Supercapacitor with Adjustable Output Voltage Based on Polypyrrole-Coated Melamine Foam, Adv. Electron. Mater. (2019) 1900724.
[45] J. Yan, C.E. Ren, K. Maleski, C.B. Hatter, B. Anasori, P. Urbankowski, A. Sarycheva, Y. Gogotsi, Flexible MXene/Graphene Films for Ultrafast Supercapacitors with Outstanding Volumetric Capacitance, Adv. Funct. Mater. 27 (2017) 1701264.
[46] J.-X. Feng, S.-H. Ye, X.-F. Lu, Y.-X. Tong, G.-R. Li, Asymmetric paper supercapacitor based on amorphous porous Mn3O4 negative electrode and Ni (OH) 2 positive electrode: a novel and high-performance flexible electrochemical energy storage device, ACS Appl. Mater. Interfaces 7 (2015) 11444-11451.
[47] P. Yang, Y. Ding, Z. Lin, Z. Chen, Y. Li, P. Qiang, M. Ebrahimi, W. Mai, C.P. Wong, Z.L. Wang, Low-cost high-performance solid-state asymmetric supercapacitors based on MnO2 nanowires and Fe2O3 nanotubes, Nano Lett. 14 (2014) 731-736.
[48] X. Lu, Y. Zeng, M. Yu, T. Zhai, C. Liang, S. Xie, M.S. Balogun, Y. Tong, Oxygen-deficient hematite nanorods as high-performance and novel negative electrodes for flexible asymmetric supercapacitors, Adv. Mater. 26 (2014) 3148-3155.
[49] X.-F. Lu, X.-Y. Chen, W. Zhou, Y.-X. Tong, G.-R. Li, α-Fe2O3@ PANI core–shell nanowire arrays as negative electrodes for asymmetric supercapacitors, ACS Appl. Mater. Interfaces 7 (2015) 14843-14850.
[50] H. Li, Z. Tang, Z. Liu, C. Zhi, Evaluating flexibility and wearability of flexible energy storage devices, Joule 3 (2019) 613-619.
[51] Y.-h. Chang, W. Zhou, G.-y. Han, Y.-z. Chang, Y.-m. Xiao, W.-h. Ma, Stabilities of flexible electrochemical capacitors based on polypyrrole/carbon fibers in different gel electrolytes, Chin. J. Polym. Sci. 35 (2017) 961-973.
[52] K.S. Ryu, Y.-G. Lee, Y.-S. Hong, Y.J. Park, X. Wu, K.M. Kim, M.G. Kang, N.-G. Park, S.H. Chang, Poly (ethylenedioxythiophene)(PEDOT) as polymer electrode in redox supercapacitor, Electrochim. Acta 50 (2004) 843-847.

Chapter 7 Summary

Wearable electronic devices are still hot after recent years of development, and with the development of artificial intelligence, the wearable device market has become even more frenetic. Many functions of current wearable devices are not perfect, not because the industrial design is not good enough, a large part of the reason comes from the indispensable energy storage devices of wearable electronic devices. Supercapacitors as the next generation of the most promising energy storage devices are expected to be applied to wearable devices, and the primary goal to solve this problem is supercapacitor flexibility. This thesis focuses on three aspects of electrode materials, design of device structures, and assembly methods, and is dedicated to the design and fabrication of a flexible all-solid-state supercapacitor. Using conductive polymers as the electroactive material, different flexible substrates are searched or prepared, made into flexible electrodes, and assembled into devices by simple and reasonable methods, and their mechanical properties, electrochemical properties, and stability under dynamic deformation are studied and analyzed, and the specific conclusions are as follows:

In chapter 3, a flexible fabric supercapacitor is designed and fabricated, which demonstrates excellent electrochemical performance, outstanding flexibility, robust mechanical performance, and reliable flame retardancy. The gas-phase polymerization method is applied to obtain the conductivity fiberglass cloth. Then, a PPy fabric composite electrode with a unique micro-morphology was derived from electrochemical polymerization and finally assembled into a supercapacitor. Due to the unique microstructure of PPy tentacles and the advantages of fiberglass cloth, the ultimate PPy/CFC supercapacitor possesses excellent electrochemical and mechanical properties, including excellent area-specific capacitance and energy density, outstanding cycle stability, and remarkable capacitance retention under repeated bending. As proved by the example of driving an LCD electronic watch, the device fabricated in this study has massive potential in the energy supply of electronics. Moreover, this study contributes an effective path for the application of insulating fabrics in the manufacture of wearable energy storage devices.

In chapter 4, a lightweight and compressible all-in-one flexible supercapacitor that can

easily extend voltage windows was designed and fabricated. The MF serves as the substrate for depositing PPy and the separator to avoid a short circuit. In addition, the MF can sufficiently absorb and lock in the electrolyte to make the electroactive material fully contact the electrolyte. The AFSC exhibits superior electrochemical performance, excellent electrochemical stability under different compressive strains, and outstanding capacitance retention for 1000 compression cycles. With the novel design, the AFSC can extend voltage windows without the connection of additional devices in series. In view of the abovementioned advantages, this novel strategy may potentially guide the development of all-in-one supercapacitors for portable and wearable electronics.

In chapter 5, a robust flexible electrode with special leaf-veinlike microstructure pore walls has been fabricated by freeze-thaw crosslinking the PVA/PEDOT:PSS hydrogel followed by a soaking process with EG solution. The immersion treatment of EG not only improves the conductivity of PPPH but also endows PPPH with good frost resistance. The EG-PPPH electrode has good mechanical properties and can be easily stretched, compressed, and customized into different shapes; it also has high conductivity, low internal resistance, and excellent specific capacitance. Owing to the fascinating characteristics of EG-PPPH electrode, the as-prepared AGSI-FSC has outstanding mechanical durability and excellent electrochemical performance and can successfully drive an LCD watch under deformation and even in low-temperature environments. It is foreseeable that this strategy can provide a feasible scheme for the large-scale manufacturing of all-gel-state integrated flexible energy storage devices.

In chapter 6, EG-PCPPH and CCPH-PPy composite electrodes were prepared by a green and efficient strategy, and then a novel all-conducting polymer-based integrated asymmetric flexible supercapacitor was successfully fabricated. The AFSC has excellent flexibility, can be freely bent, and quickly recovered after the release of external forces; outstanding mechanical strength, tensile strength up to 22.3 MPa with elongation at break 286%. In addition, it has excellent electrochemical performance and stability, with a maximum volumetric energy density of 397.99 μWh cm^{-3} and a capacitance retention rate of 88.1% for 10,000 charges/discharge cycles. Impressively, as an asymmetric device, AFSC can be used as the symmetric device without differentiating between positive and negative. In a practical demonstration, it can be connected in any series to power the LEDs. The concept of asymmetric devices with interchangeable positive and negative may provide a direction for the design of asymmetric supercapacitors in the

future. Accordingly, this strategy will open up a new trend in the design of flexible energy storage devices with high energy density.

In this thesis, we have thoroughly explored the overall structure design, preparation process, and energy storage mechanism of flexible supercapacitors creatively proposed a low-cost and universal method to prepare flexible electrode materials, and successfully prepared a series of flexible supercapacitors. We have prepared bendable fabric flexible supercapacitors (chapter 3), compressible integrated flexible supercapacitors (chapter 4) by selecting suitable flexible substrate materials, and all gel state flexible supercapacitors (chapter 5,6) with an excellent performance by optimizing the structure of supercapacitors. Some results have been achieved, but further optimization and improvement are still possible. The electroactive material in this thesis uses only a single conductive polymer material. In order to further improve the electrochemical performance, without affecting the flexibility, it is necessary to explore the composite of conductive polymer materials with carbon and metal oxide materials to complement each other and obtain flexible composite electrode materials with more excellent performance. In addition to flexible electrodes, the development of advanced flexible electrolytes is also necessary, since the performance of the electrolytes also affects the overall performance of the final flexible supercapacitor.

Publications

1. Periodical papers

(1) **Qifan Liu**, Jianhui Qiu, Chao Yang, Limin Zang, Guohong Zhang, Eiichi Sakai. High-Performance PVA/PEDOT:PSS Hydrogel Electrode for All-Gel-State Flexible Supercapacitors, Advanced Materials Technologies, 2021, 6(1), 2000919. (IF= 7.848)

(2) **Qifan Liu**, Jianhui Qiu, Chao Yang, Limin Zang, Guohong Zhang, Eiichi Sakai. High-performance textile electrode enhanced by surface modifications of fiberglass cloth with polypyrrole tentacles for flexible supercapacitors, International Journal of Energy Research, *International Journal of Energy Research*, 2020, 44(11), 9166-9176. (IF= 5.164)

(3) **Qifan Liu,** Limin Zang, Xuan Qiao, Jianhui Qiu, Xue Wang, Lei Hu, Jun Yang, Chao Yang. Compressible all-in-one supercapacitor with adjustable output voltage based on polypyrrole coated melamine foam*, Advanced Electronic Materials*, 2019, 5(12), 1900724. (IF= 7.295)

(4) **Qifan Liu**, Jianhui Qiu, Chao Yang, Limin Zang, Guohong Zhang, Eiichi Saka, Hong Wu, Shaoyun Guo. Robust Quasi-Solid-State Integrated Asymmetric Flexible Supercapacitors with Interchangeable Positive and Negative Electrode Based on All-Conducting-Polymer Electrodes，*Journal of Alloys and Compounds,* 2021, 887, 161362. (IF= 5.316)

(5) Zijie Zhao, **Qifan Liu**, Limin Zang, Hui You, Jing Zhang, Xue Wang, Chao Yang. In situ growth of submicron polypyrrole on NiTi alloy wire as electrodes for recoverable and flexible quasi-solid-state supercapacitors, *Journal of Alloys and Compounds,* 2021, 888, 161646. (IF= 5.316)

(6) Yongjie Xu, **Qifan Liu**, Hui You, Limin Zang, Yayue Xiao, Xue Wang, Chao Yang. A facile patterning preparation of barnacle-like polypyrrole on sandpaper for flexible electronics, *Journal of Materials Science,* 2021, 56, 18162-18173. (IF= 4.220)

(7) Hui Liu, **Qifan Liu**, Hui You, Limin Zang, Mingzhen Chen, Chao Yang. In-situ growth of sub-micron tentacle-like polypyrrole on wolfram carbide coated

fiberglass cloth for flexible quasi-solid-state supercapacitors, *Journal of Electroanalytical Chemistry,* 2021, 893, 115332. (IF= 4.464)

(8) Chao Yang, **Qifan Liu**, Limin Zang, Jianhui Qiu, Xue Wang, Chun Wei, Xuan Qiao, Lei Hu, Jun Yang, Ge Song, Chanjuan Liu. High-Performance Yarn Supercapacitor Based on Metal–Inorganic–Organic Hybrid Electrode for Wearable Electronics. *Advanced Electronic Materials* 2019, *5* (3), 1800435. (IF= 7.295)

(9) Hui You, Ge Song, **Qifan Liu**, Chao Yang, Jianhui Qiu, Limin Zang, Hui Liu, Jiucun Chen. A Facile Route for the Fabrication of a Superhydrophilic and Underwater Superoleophobic Phosphorylated PVA-Coated Mesh for both Oil/Water Immiscible Mixture and Emulsion Separation, *Applied Surface Science*, 2020,147986. (IF= 6.707)

(10) Limin Zang, Xuan Qiao, **Qifan Liu**, Chao Yang, Lei Hu, Jun Yang, Zihan Ma. High-performance solid-state supercapacitors with designable patterns based on used newspaper. *Cellulose*, 2020, 27(2), 1033-1042. (IF= 5.044)

(11) Lei Hu, Limin Zang, Wusheng Zuo, **Qifan Liu**, Chao Yang, Chunliu Liang, Jianhui Qiu. Enhanced electrochemical performance and high voltage window for supercapacitors based on fabric electrodes derived from tannin-Fe3+ complexes, *Synthetic Metals*, 2020, 269, 116566. (IF= 3.266)

(12) Wusheng Zuo, Limin Zang, Xue Wang, **Qifan Liu**, Jianhui Qiu, Chunliu Liang, Xin Liu, Chao Yang. Flexible Polypyrrole@ Fe2O3@ Stainless Steel Yarn Composite Electrode for Symmetric Thread-Like Supercapacitor with Extended Operating Voltage Window in Li2SO4-Based Aqueous Electrolyte, *Advanced Sustainable Systems,* 2020, 2000173. (IF= 6.271)

(13) Chao Yang, Lei Hu, Limin Zang, **Qifan Liu**, Jianhui Qiu, Jun Yang, Xuan Qiao. High-Performance All-Solid-State Supercapacitor Based on Activated Carbon Coated Fiberglass Cloth Using Asphalt as Active Binder. Journal of The Electrochemical Society, 2020, 167(2), 020540. (IF= 4.316)

(14) Lei Hu, Limin Zang, **Qifan Liu**, Jianhui Qiu, Chao Yang, Xu Xu , Jun Yang , Xuan Qiao. Effective and selective removal of cationic dye from aqueous solution using rosin derivative modified wheat straw. *Desalination and water treatment*, 2019, 153,349-356. (IF= 1.145)

(15) Lei Hu, Limin Zang, Jun Yang, **Qifan Liu**, Xuan Qiao, Jianhui Qiu, Chao Yang, Huihao Li. A scalable strategy for carbon derived from complex six-membered

ring-like tannin on glass fiber for 1D/2D flexible all solid state supercapacitors. *Journal of Electroanalytical Chemistry*, 2020, 856(1), 113693. (IF= 4.464)

(16) Xin Liu, Limin Zang, Yongjie Xu, **Qifan Liu**, Hui You, Mingzhen Chen, Chao Yang. Activated carbon fiber yarns with birnessite-type MnO2 and oxygen-functional groups for high-performance flexible asymmetric supercapacitors. *Diamond and Related Materials,* 2021, 115, 108371. (IF= 3.315)

(17) Chunyin Lu, Jianhui Qiu, Manxi Sun, **Qifan Liu**, Eiichi Sakai, Guohong Zhang. Simple preparation of carboxymethyl cellulose-based ionic conductive hydrogels for highly sensitive, stable and durable sensors. *Cellulose*, 2021, 28, 4253-4265. (IF= 5.044)

(18) Xin Liu, Limin Zang, Chunliu Liang, **Qifan Liu**, Yan Deng, Chao Yang, Jianhui Qiu. Design and fabrication of high performance flexible supercapacitor with polypyrrole@ carbon fiber yarn electrode and redox active dopants. *Synth. Met.* **2021,** *271*, 116654. (IF= 3.266)

(19) Chunliu Liang, Chao Yang, Limin Zang, **Qifan Liu**, Jianhui Qiu, Yuqi Li, Wusheng Zuo, Xin Liu. UV assisted one step synthesis of ternary graphene/polypyrrole/silver nanocomposites for supercapacitors. *Energy Technology,* 2021, 9, 2000966. (IF= 3. 631)

(20) Lei Hu, Chao Yang, Limin Zang, **Qifan Liu**, Jianhui Qiu, Jun Yang, Xuan Qiao, Xue Yang, Huihao Li. Effective and selective removal of anionic dye-based on wasted magnetic chitosan immobilized cellulase beads. *Desalination and water treatment,* 2020**,** *204*, 114-123. (IF= 1.145)

(21) Chao Yang, Jun Yang, Ge Song, Limin Zang, **Qifan Liu**, Jianhui Qiu, Xue Yang, Chun Wang. Facile fabrication of multifunctional superoleophobic and antifouling metal mesh by dip-coating polyanion for efficient oil/water mixtures as well as emulsions separation. *Desalination and water treatment*, 2020, 189, 165-178. (IF= 1.145)

注：博士論文研究関連：4 編（(1) ～ (4)），その他：17 編（(5) ～ (21)）

2. International conference

(1) **Qifan Liu**, Jianhui Qiu, Eiichi Sakai, Chao Yang, Limin Zang. Coaxial PPy/MnO2/Stainless Steel Yarn Supercapacitors for Wearable Electronics. The 1st

International Symposium on Advanced Materials Science and Engineering (AMSE-1). Akita, Japan, August 20-25th, (2019).

(2) **Qifan Liu**, Jianhui Qiu, Eiichi Sakai, Chao Yang, Limin Zang. A Flexible Supercapacitor Based on Ternary Composite Electrode Material for Wearable Electronic Devices. The 1st International Symposium on Advanced Materials Science and Engineering (AMSE-1). Akita, Japan, August 20-25th, (2019)

注：博士論文研究関連：2 編（(1）～（2)）

3. National conference

(1) 劉 啓凡, 邱 建輝, 楊 超, 臧 利敏, 張 国宏, 境 英一, 陸 春因, 張 康. PVA と PEDOT:PSS ハイドロゲル複合電極による全固体フレキシブルスーパーキャパシタの性能評価. M&M2021 材料力学カンファレンス. Zoom 会議, Japan, September 15-16th, (2021).

(2) 陸 春因, 邱 建輝, 劉 啓凡, 境 英一, 張 国宏.優れた力学特性をもつブルネットワーク PAA ヒドロゲルの設計と作製. M&M2021 材料力学カンファレンス. Zoom 会議, Japan, September 15-16th, (2021).

(3) 張 康, 邱 建輝, 境 英一, 張 国宏, 劉 啓凡, 山口 博之, 長南 安紀. 熱伝導フィラーの組み合わせによる熱伝導材料の開発. M&M2021 材料力学カンファレンス. Zoom 会議, Japan, September 15-16th, (2021).

注：博士論文研究関連：1 編（1）

Acknowledgments

Time flies and the years fly by. Three years of doctoral study are coming to an end. These three years of study abroad have been the most memorable period in my life. I am very glad to express my thanks to those who have given me help during this time.

I would firstly like to acknowledge the guidance and support of my supervisor Professor Jianhui Qiu, who works at the Department of Mechanical Engineering, Faculty of Systems Science and Technology of Akita Prefectural University. He imparted the knowledge of material science to me, and his elaborated guidance, considerable encouragement, and invaluable discussion make my research of great achievement and my study life unforgettable. Secondly, I would like to appreciate Prof. Teruo Bitoh in Department of Mechanical Engineering, Faculty of Systems Science and Technology at Akita Prefectural University for his guidance and advice, which helped me greatly in my research work.

My deepest appreciation goes to ASS. Prof. Eiichi Sakai in Department of Mechanical Engineering, Faculty of Systems Science and Technology at Akita Prefectural University and Prof. Noboru Nakayama in Department of Mechanical Systems Engineering, Faculty of Engineering at Shinshu University for the comments and suggestions, whose advice have inestimable value for my research.

I appreciate the technical support from ASS. Prof. Eiichi Sakai, Prof. Teruo Bitoh, Dr. Nobuhiro Kanazawa, and Dr. Takao Komiyama in Akita Prefectural University.

I am grateful to the professors in the College of Material Science and Engineering at the Guilin University of Technology, Dr. Chao Yang, and Dr. Limin Zang for the guidance and suggestions of my research.

And thanks also go to my peer research group members including Guohong Zhang, Haodao Mo, Hongjian Huang, Manxi Sun, Chunyin Lu, Wei Zhao, Haonan Wu, Kang Zhang, and Andong Pan, and fellow international students Zhaoxing Lin, Tingting Wu, and Xin Fang for assisting with my research as well as providing friendship and support. Thanks to Mrs. Qiu who has taken good care of me in three years.

A giant thank you also goes to my family for their support, encouragement, and patience throughout this Ph.D. and indeed for my entire life.